Functionalized Aramid Nanofibers for the Reinforcement of Thermosets and Rubber Nanocomposites

by

Jaehyun Jung

A dissertation submitted in partial fulfillment
of the requirements for the degree of
Doctor of Philosophy
(Macromolecular Science and Engineering)
in the University of Michigan
2022

Doctoral Committee:

    Professor Henry A. Sodano, Chair
    Professor Jinsang Kim
    Associate Research Scientist Kathleen Sevener
    Professor Alan I. Taub

Jaehyun Jung

jaehyunj@umich.edu

ORCID iD: 0000-0001-9592-9338

Dedication

This dissertation is dedicated to my family, without whom this would not have been possible.

Acknowledgements

I would like to first thank my advisor, Professor Henry Sodano. His expertise, scientific curiosity, exceptional guidance, and passion for research have inspired me and were very precious and important to me throughout my Ph.D. study. I am grateful for his effort, which allowed me to pursue my own research topics and build the necessary research skills to become an independent researcher. Furthermore, it has been a unique experience to explore various scientific fields besides the tire industry through an interdisciplinary approach under his guidance. I am also sincerely grateful to my dissertation committee members: Professor Jinsang Kim, Professor Alan Taub, and Dr. Kathleen Sevener, for their help and advice. Especially, Professor Kim helped and supported me throughout my Ph.D. journey not only as a director of the Macromolecular Science and Engineering program but also as a mentor.

I would like to express my sincere gratitude for the support from Hankook Tire and Technology. I could focus fully on the research throughout my Ph.D. study thanks to the financial support from Hankook.

I would like to also thank Dr. Jalal Nasser and Dr. Lisha Zhang for their valuable suggestions and advice, which allowed me to step into the right track of my Ph.D. life quickly. I want to thank my past lab mates, Dr. Jiajun Lin, Dr. Alireza Nafari, Dr. LoriAnne Groo, Mrs. Tianyu Yuan, and Dr. Kelsey Steinke, as well as my current colleagues, Mr. Ruowen Tu, Dr. Hyunchan Kim, Mr. Steven Mamolo, and Mr. Dijia Zou for their unwavering support, generous

Table of Contents

List of Tables

List of Figures

Abstract

Polymer nanocomposites have received attention for a wide range of applications over the past few decades due to their high mechanical properties. With the introduction of a relatively low weight fraction of nanofillers, polymer nanocomposites have shown superior properties to composites reinforced with macro- or micro-sized fillers. The properties and performance of polymer nanocomposites are affected by the morphology and dimensions of the nanofillers and the interfacial interactions between polymer matrices and nanofillers. Recently, aramid nanofibers (ANFs) have been obtained through the dissolution and deprotonation process of macroscale aramid fibers in a solution with dimethyl sulfoxide and potassium hydroxide. ANFs have shown great potential as a reinforcing filler for polymer nanocomposites due to their excellent mechanical properties, high aspect ratio, and large surface area. In addition to these unique characteristics, there are rich functionalities on the surface of ANFs that can be used to introduce surface modification agents or multifunctional nanomaterials on the ANFs. Therefore, the properties of polymer nanocomposites can be further increased through the introduction of functionalized ANFs that enhance their chemical and mechanical interaction.

In this work, ANFs are modified using various silane coupling agents to reinforce rubber nanocomposites for tire tread and epoxy nanocomposites. The silane coupling agent treatment improves the dispersion of ANFs in polymer matrices and chemical interfacial interaction between the matrices and ANFs through covalent linkages between them. The functionalization of ANFs is investigated using characterization techniques such as Fourier transform infrared spectroscopy

(FTIR), X-ray photoelectron spectroscopy (XPS), and atomic force microscopy (AFM). Rubber nanocomposites reinforced with functionalized ANFs exhibit improved mechanical properties and tire performance metrics, including an 11.3% increase in abrasion resistance and 14.7% improvement in fuel efficiency, without decreasing wet grip performance. As shown from the results of rubber nanocomposites, functionalized ANF reinforced epoxy nanocomposites also show enhanced tensile strength, elastic modulus, fracture toughness, and dynamic mechanical properties due to the improved interfacial interaction.

In addition, this work also considers the hybridization of ANFs using other strong nanomaterials such as graphene oxides (GOs) and cellulose nanocrystals (CNCs) for the reinforcement of tire tread rubber nanocomposites and epoxy nanocomposites. The novel hybrid materials based on ANFs are expected to contribute to improved chemical and mechanical interaction within nanocomposites through the extensive branching and network structure of the hybrid fillers and covalent bonding between the polymer matrix and fillers. The hybrid filler reinforced rubber nanocomposites and epoxy nanocomposites exhibit a synergetic effect of nanofillers on increasing mechanical properties and performance compared to the nanocomposites reinforced with ANFs or GOs or CNCs alone. Especially, the ANF/GO hybrid filler reinforced rubber compounds show an 18.2% improvement in abrasion resistance and 21.8% improvement in rolling resistance. Thus, the research presented in this dissertation provides novel reinforcement methods to improve the overall performance of tire tread rubber nanocomposites, including abrasion resistance and fuel efficiency, which can help overcome energy and environmental challenges. In addition, thermosetting polymers using functionalized ANFs are expected to have an impact in the field of structural polymer composites with improved properties.

Chapter 1

Introduction

1.1 Motivation

The motivation for this study lies in the functionalization of nano-sized aramid fibers to prepare novel nanofillers for polymer nanocomposites, especially for the reinforcement of cross-linked thermosetting polymers and tire tread rubber composites. Aramid fibers are commercial *p*-phenylene terephthalamides fibers (PPTA), which are widely used for protective gears, soft body armor, and high-performance tire reinforcement cords because of their high tensile strength and thermal stability.[1,2] The outstanding mechanical properties of aramid fibers originate from the unidirectional hydrogen bonding between the para-structured aramid polymer chains. Moreover, the aligned aramid chains form sheets, and the sheets are stacked by van der Waals bonds to form a highly crystalline structure.[3] The highly crystalline structure and excellent mechanical properties are beneficial for the conventional fiber-reinforced polymer composites. However, the application of aramid fibers for the preparation of polymer nanocomposites has been limited due to the chemically inert and smooth surface of aramid fibers and difficulties in the formation of nanoscale version of aramid fibers.[2]
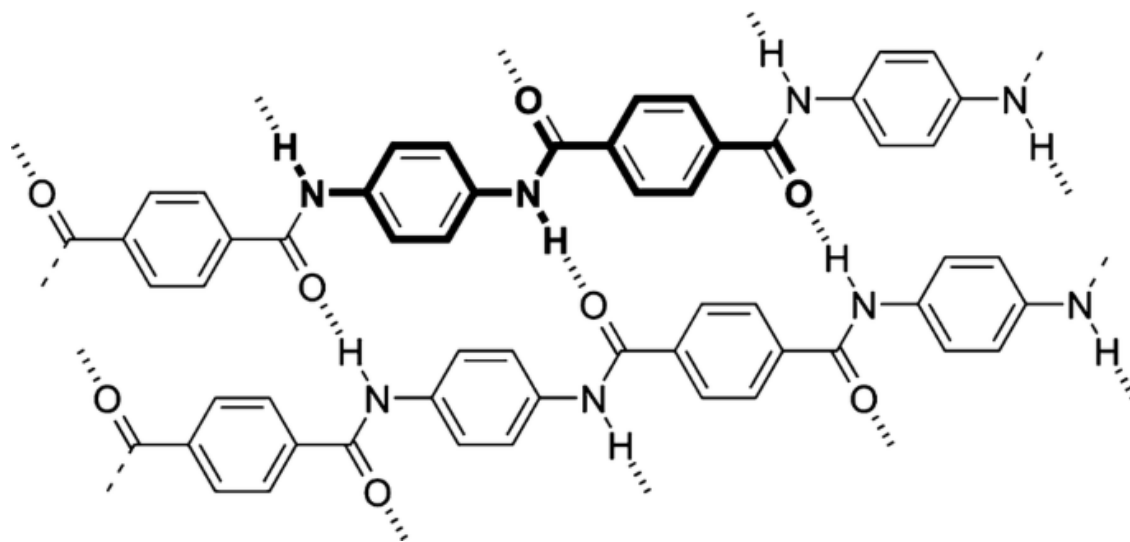
Figure 1.1. Chemical structure of aramid fibers and hydrogen bonding interaction between aramid chains.[3]

Recently, a new method to produce aramid nanofibers (ANFs) with a high aspect ratio was developed by Yang et al.[4] The authors proposed a dissolution and deprotonation process to reduce the strength of hydrogen bonding between the polymer chains and increase intermolecular electrostatic repulsion (Figure 1.2). The dissolution process yielded ANFs that range from 5 to 30 nm in diameter and 5 to 10 μm long. Even though the polymer chains are disintegrated into nanoscale fibers, complete dissolution was inhibited by hydrophobic attraction and π−π stacking in the polymer backbone so that the high strength and stiffness were maintained. Moreover, rich functionalities, including hydroxyl, carboxylic acid, amine groups, and carbonyl groups, are formed on the surface of the ANFs during the dissolution process due to hydrolysis.[5–7] These functionalities can provide opportunities for the modification of ANFs.
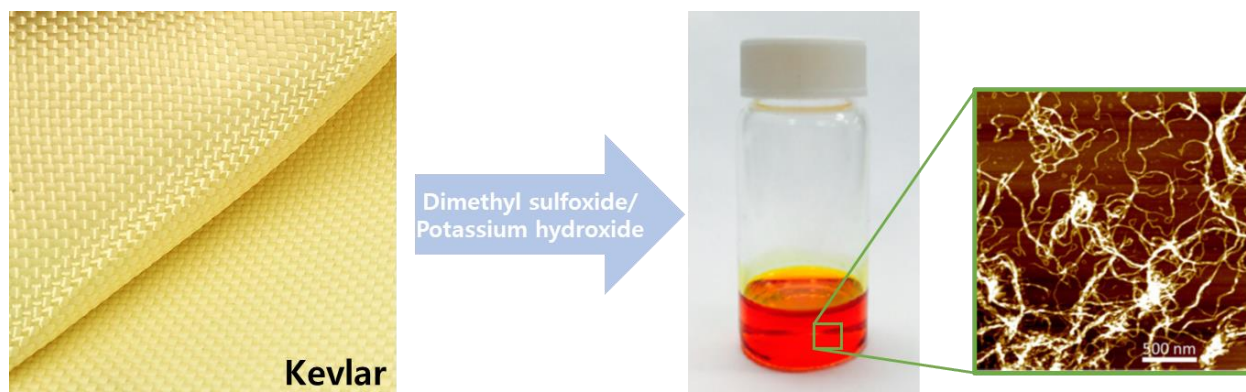
Figure 1.2. The preparation of ANFs using Kevlar, dimethyl sulfoxide, and potassium hydroxide.

In this research, thermosetting polymers and rubber composites will be reinforced using functionalized ANFs. Various types of silane coupling agents will be used to functionalize ANFs to improve the interfacial interaction between the matrices and nanofillers and the dispersion of nanofillers in the matrices. In addition to the surface modification using a silane coupling agent, the ANFs will be hybridized with other nanomaterials such as graphene and cellulose to further improve mechanical properties and performance of nanocomposites through enhanced chemical and mechanical interactions. For the thermosetting polymer nanocomposites, physical properties such as tensile strength, elastic modulus, fracture toughness, and dynamic mechanical properties will be examined and discussed. The effect of functionalized ANFs on the properties and tire performances of rubber composites will also be investigated through mechanical tests. The following sections will present a brief review of the previously reported thermosetting polymer composites and rubber nanocomposites for tire tread, followed by a review of the research regarding functionalization and hybridization of nanofillers that aim to improve the properties of polymer nanocomposites.

1.2 Polymer nanocomposites

Polymer nanocomposites have attracted substantial interest in the field of materials research due to their ability to enhance the mechanical properties of the polymer using relatively low weight filler fractions.[8] Compared to neat polymers, polymer nanocomposites demonstrate excellent properties, including improved storage modulus, tensile strength, Young's modulus, and thermal properties.[8–14] The nanofillers used in polymer nanocomposites allow for a considerably larger interfacial area than that of macro or micro-sized fillers of similar weight fractions, which typically leads to improve load and stress transfer between the polymer matrix and fillers.[15] Below is a brief review of the epoxy and rubber nanocomposites that will be focused on in this dissertation.

1.2.1 Epoxy nanocomposites

Among organic matrices for polymer nanocomposites, epoxy resins are widely used in the fabrication of nanocomposites due to their high rigidity, favorable adhesive properties, and excellent heat, moisture, and chemical resistance, among other outstanding characteristics. As a result, epoxy resin has been popular in a number of applications, including coatings,[16–18] adhesives,[19] electronic devices,[20,21] and aerospace parts.[22,23] Epoxy resins are usually composed of aliphatic, aromatic, or heterocyclic backbone structures with multiple epoxy groups at the end of the structures. Because of the different backbone chemical structures, epoxy resins exhibit different properties.[24] For instance, the epoxy resins with aromatic backbone structures show higher mechanical properties and thermal properties compared to the epoxy resins with aliphatic backbone structures. One of the examples of aromatic epoxy resins is liquid type Epon 862 resin (diglycidyl ether of bisphenol F epoxy), shown in Figure 1.3. The liquid epoxy resins

4

are cured with curing agents such as multifunctional amines or acids to form a hardened epoxy through a crosslinking process. The physical properties of cured epoxy are known to be affected by the types of epoxy resins and curing agents.
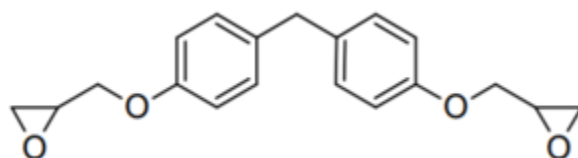
Figure 1.3. Molecular structure of Epon 862 epoxy resin.

The incorporation of nanomaterials in the epoxy matrices can provide them with multifunctional performance compared to the neat epoxy resin, thus further broadening the potential applications of the material. Various studies have been conducted with the aim of improving the properties of the epoxy nanocomposites using nanoscale materials such as nano clays,[25,26] carbon nanofibers,[27,28] carbon nanotubes (CNTs),[11,29–32] graphene,[33–36] silica,[16,17,37] metal oxide particles,[13] and cellulose nanofibers.[38] For example, Wang et al. prepared epoxy/clay nanocomposites using a slurry compounding process to improve thermal mechanical properties.[25] The epoxy nanocomposites exhibited 30% and 150% increase in storage modulus at 50 ℃ and 240 ℃, respectively, with 5 wt % of clay in the composites. In addition, Gojny et al. conducted a comparative study to compare the effect of single-wall CNTs, double-wall CNTs, and multi-wall CNTs on the mechanical properties of epoxy nanocomposites.[32] The 0.5 wt % double-wall CNT reinforced epoxy nanocomposites exhibited 10%, 15%, and 43% improvements in mechanical strength, stiffness, and fracture toughness, respectively. This study showed that the mechanical properties of thermosetting polymers could be enhanced by using a very low weight fraction of nanofillers such as 0.5 wt %. Moreover, Tang

et al. investigated the effect of graphene dispersion state on the mechanical properties of epoxy composites.[36] Higher mechanical strength, fracture toughness, and glass transition temperature were observed from the epoxy nanocomposites with highly dispersed graphene, while tensile and flexural moduli didn't show significant differences by the dispersion levels. Therefore, the physical properties of epoxy nanocomposites, such as mechanical and thermal properties, have been shown to be enhanced by the incorporation of nanofillers.

1.2.2 Rubber nanocomposites for tire tread

As interest in environmental protection and the reduction of energy consumption continue to grow within the industrial world, the automotive industry is steadily moving toward manufacturing more fuel-efficient vehicles. Currently, global transportation energy consumption accounts for over 20% of the total energy available, making the design of more efficient vehicles a necessity. Among the various vehicle components, tires provide the only point of contact between the vehicle and the road and account for approximately 6.6% of the total fuel energy consumed by a vehicle.[39] To address the environmental issues regarding the tire industry and inform end users, the European Union (EU) introduced legislation titled "Tire Labelling Regulation (EC NO. 1222/2009)" in 2009, which regulates and classifies three important parameters for tire performance: the rolling resistance, wet traction, and external rolling noise of tires.[40] Tire rolling resistance is defined as the force required to move the tire forward and is heavily dependent on the energy dissipated due to the deformation of the tire during driving. It is known that a 4% reduction in rolling resistance results in 1% fuel savings.[39] In addition to energy consumption, tires are known to generate wear particles, negatively affecting the environment, including air, water, and soil. It is assessed that the mass of tire wear particles in the European

6

Union is 1,327,000 tons annually, while that of the United States is 1,120,000 tons.[41] Therefore, decreasing both the rolling resistance and abrasion loss of tires can contribute to more environmentally friendly vehicle performance.
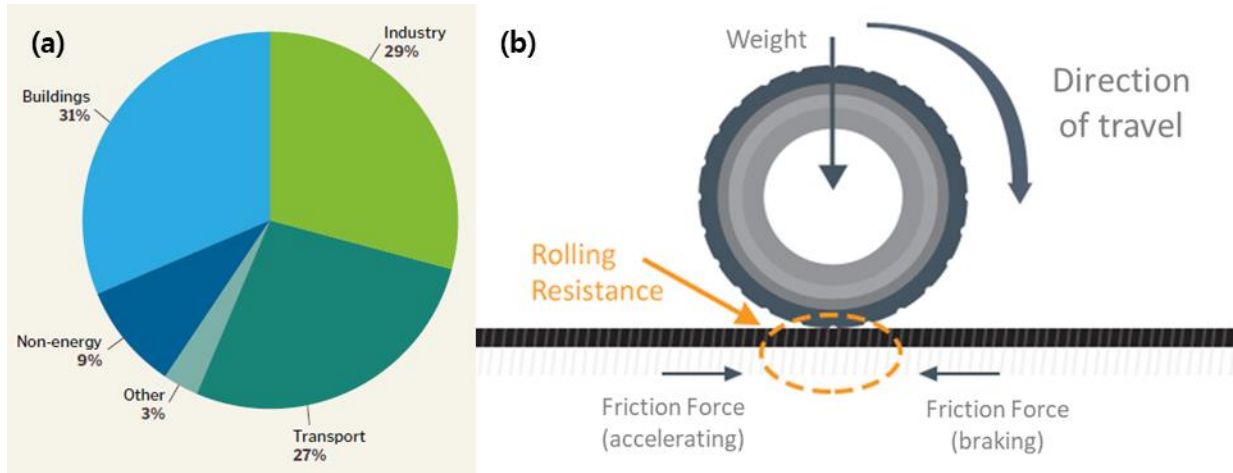
Figure 1.4. (a) Global total energy usages, and (b) forces related to tire rolling resistance.

Figure 1.5. The Tire Labeling Regulation label based on the EC No. 1222/2009.[40]

The three most important performance parameters for tire tread rubber compounds are wet-skid resistance, rolling resistance, and wear resistance, forming what is known as the "magic

7

triangle."[42,43] However, these three requirements are interrelated, making it difficult to improve all of them simultaneously. Therefore, simultaneously balancing and optimizing of these properties is a long-standing challenge that the tire industry aims to satisfy. The performance and characteristics of tire rubber compounds are influenced by the type of fillers used. To this end, rubber compounds have been reinforced by various types of fillers, including carbon black,[44] silica,[45,46] nano clays,[47,48] graphene oxides (GOs),[49–52] CNTs,[53–55] and short fibers,[56–60] for the enhancement of the mechanical properties. Specifically, carbon black and silica have been commonly used in the industry for reinforcing rubber compounds. However, increasing the amount of carbon black causes high rolling resistance, while silica-filled rubber compounds require well-controlled mixing processes to achieve a comparable abrasion resistance to the carbon black filled rubber.[61,62] Given the described disadvantages, recent research efforts have focused on exploring the role of novel nano-sized organic materials as promising fillers in rubber compounds and their potential in practical applications. Among the promising fillers, short fibers have attracted wide interest because of their reinforcing efficiency and high aspect ratio while requiring relatively low content to achieve the desired properties.

Figure 1.6. The internal structure of a passenger car tire. The orange circle indicates the tire tread. (photo provided by Hankook Tire and Technology).

Figure 1.7. Reinforcing fillers: carbon black, silica, nano clays, CNTs, GOs, and short fibers (from upper left to right).

Aramid short fibers are one of the most promising fillers for the reinforcement of rubber compounds because of their outstanding mechanical properties and thermal and chemical resistance. In a previous study by Kashani, aramid short fibers were used to reinforce tire tread composites. The resulting modulus at 300% strain was reported to increase by 6.3% along the longitudinal direction.[60] However, the final properties of rubber compounds reinforced with short fibers are largely dependent on the orientation of the fibers within the rubber compound, while the chemically inert surface of aramid fibers limits the interfacial load transfer properties within the compound. Alternatively, Nillawong et al. used aramid pulp for the reinforcement of styrene-butadiene rubber (SBR).[63] A carbon black/aramid pulp hybrid filler was prepared at various ratios, and the resulting compound was found to yield a high storage modulus over a range of temperatures up to 80 ℃. However, the tensile strength and abrasion properties of the resulting compound deteriorated with increasing aramid pulp loading because of the absence of significant chemical or mechanical interaction between the rubber and aramid fibers. Therefore, the macro-

scale size of fibers and lack of interfacial interaction between the aramid fibers and rubber matrix limit the application of aramid fibers for the reinforcement of rubber compounds.

1.3 Functionalized ANF reinforced polymer nanocomposites

1.3.1 ANF reinforced polymer nanocomposites

ANFs have shown great potential as a reinforcing filler in polymer matrices due to their outstanding mechanical properties, high surface area, and aspect ratio. Because of their excellent properties, ANFs have been used as nanoscale building blocks to reinforce polymer matrices, including poly(acrylic acid),[64] poly(vinyl alcohol),[65,66] polyurethane,[67] poly(methyl methacrylate),[68] epoxy resin,[7,69] natural rubber (NR),[70] styrene-butadiene rubber (SBR),[71–73] and butadiene rubber (BR).[72,73] Among those studies, Lin et al. reported the isolation of ANFs and subsequent dispersion into epoxy resins.[7] The dispersion of isolated ANFs into the epoxy matrix improved the tensile strength, Young's modulus, and toughness of the nanocomposites through physical interactions at the interface between the ANFs and polymer matrix. Yang et al. also prepared ANF/poly(acrylic acid) composite films using the vacuum-assisted flocculation method.[64] The prepared composite films exhibited improvement on elastic modulus up to 20 GPa, which is higher than that of CNT reinforced polymer nanocomposites. Kuang et al. reinforced polyurethane matrix using ANFs.[67] They reported Young's modulus of 5.3 GPa and ultimate strength of 98.0 MPa, which are the highest among all the reported polyurethane-based nanocomposites. In addition to the polar polymer matrices, Surya et al. mixed ANFs into NR latex and prepared NR composites to improve mechanical properties.[70] The NR nanocomposites showed increased tensile strength and modulus using 2 to 6 parts of ANFs, however, elongation at break and flexural fatigue properties decreased due to lack of interfacial

interaction between NR matrix and ANFs. Overall, the ANF reinforced polymer nanocomposites exhibited improved mechanical properties through physical interaction between the matrix and ANFs, while improvement of the interfacial chemical interaction between the polymer matrix and nanofillers and nanofiller dispersion within the matrix can provide further enhancement of the polymer nanocomposites properties.
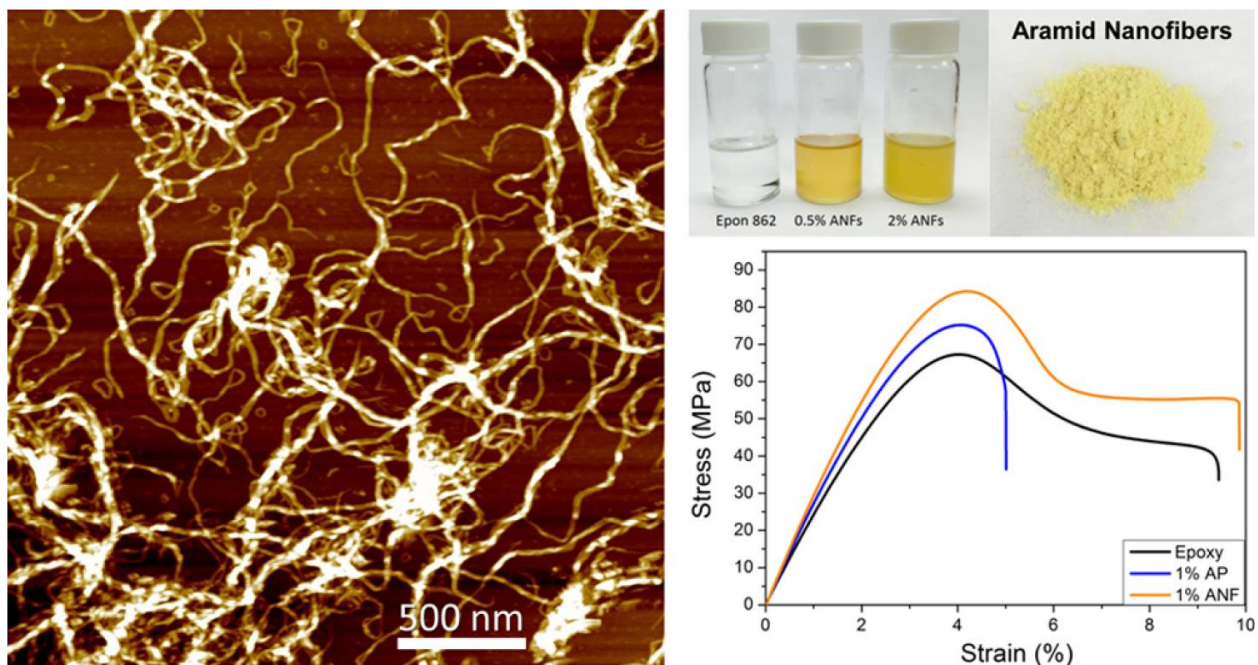
Figure 1.8. Epoxy nanocomposites reinforced with ANFs and stress-strain curves of neat epoxy resin, 1% aramid pulp (AP), and 1% ANF reinforced samples.[7]

1.3.2 Functionalization of nanofillers

Surface modification is one of the most widely used methods to improve the dispersion of nanofillers and enhance the interfacial interaction between the filler and the matrix in nanocomposites. For this reason, surface modifiers, including polymers, coupling agents, and surfactants, have been utilized to reinforce polymer matrices in several studies.[15,29,74,75]

Among these surface modifiers, silane coupling agents with at least two different functional groups at both ends are commonly used due to their ability to react with both the polymer matrix and the nanofillers. As a result, silane coupling agents provide chemical covalent linkages between the filler and matrix, which can transfer stress from the polymer to the filler. For example, Zhu et al. reported the surface functionalization of carbon nanofibers using an amine-functionalized silane coupling agent for carbon nanofiber-reinforced epoxy nanocomposites (Figure 1.9).[27] The results showed a 12.6% increase in tensile strength for the epoxy nanocomposites with surface-modified carbon nanofibers, and the glass transition temperature shifted to a higher temperature. Additionally, Ma et al. investigated the effect of silane functionalized carbon nanotubes on dispersion as well as the mechanical, thermal, and electrical properties of the resultant epoxy nanocomposites (Figure 1.10).[29] The silane functionalization of the carbon nanotubes was shown to improve dispersion in the epoxy matrix significantly, and the nanocomposites exhibited better thermal stability, flexural modulus, and fracture resistance. However, the electrical conductivity was decreased due to the wrapping of the non-conductive silane on the surface of the carbon nanotube. Drawing from the results shown from the previous studies, surface modification using a silane coupling agent can contribute to the reinforcement of polymer nanocomposites through the improved chemical interaction by covalent linkages between the polymer matrix and fillers.
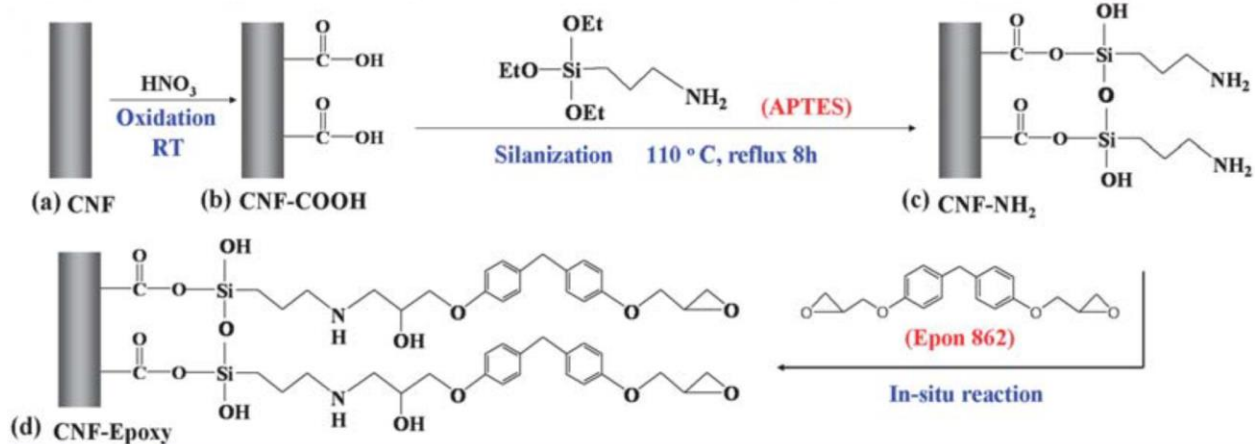
Figure 1.9. Preparation of epoxy nanocomposites using silane coupling agent treated carbon nanofibers.[27]
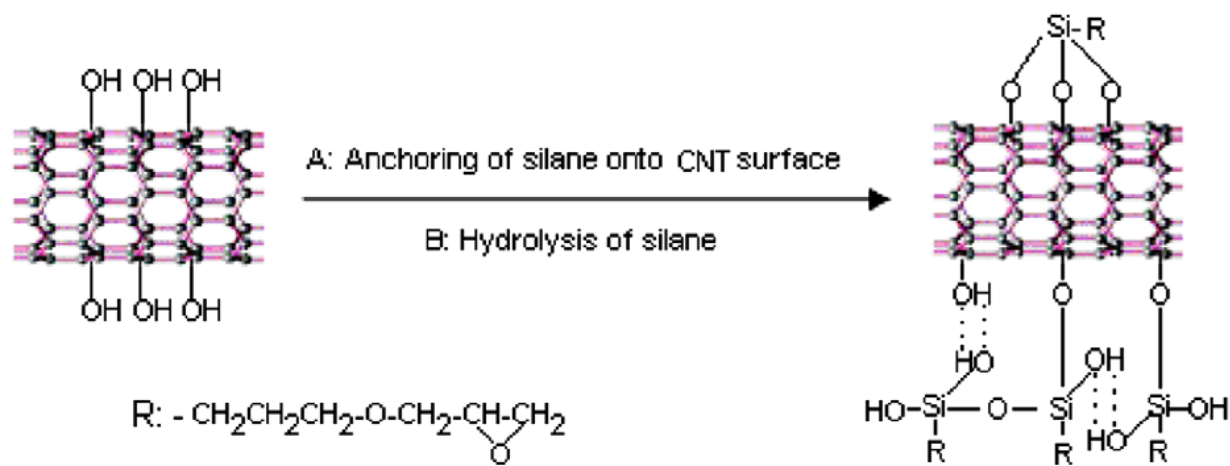
Figure 1.10. Scheme of the reaction between CNT and epoxy functionalized silane coupling agent.[29]

1.3.3 Functionalization of ANFs

As described in the previous section, there are abundant functionalities, including hydroxyl, carboxylic acid, and amine groups on the surface of ANFs, which are formed by hydrolysis during the dissolution process.[6,76,77] Patterson et al. reported increased COOH and C-OH functionalities on the ANFs, which indicate the partial hydrolysis of the polymer chain and

aromatic ring by the heavily basic solution to produce ANFs, as shown in Figure 1.11.[76] Additionally, Nasser et al. used X-ray photoelectron spectroscopy (XPS) and Fourier transform infrared spectroscopy (FTIR) to investigate the chemical structure of ANFs during the dissolution process (Figure 1.12).[77] In the study, an increase in the peaks corresponding to C=O stretching and Phenyl-N stretching was observed in FTIR, and the concentration of carboxylic acid increased in XPS as the time for dissolution increased (Table 1.1). The results confirm the presence of abundant functionalities on the surface of ANFs, which can be used to functionalize ANFs.
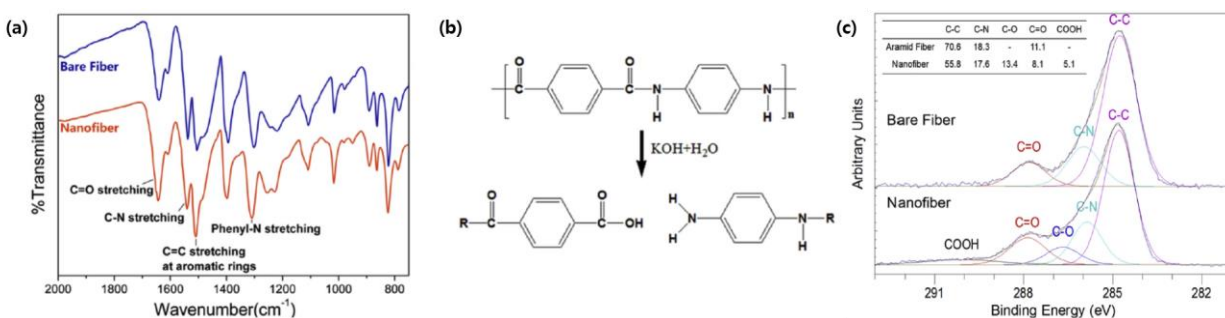
Figure 1.11. (a) FTIR spectra of ANFs and bare aramid fibers show that (b) hydrolysis takes place in the dissolution process and forms carboxylic acid and amine. (c) Normalized C1s XPS spectra of bare aramid fibers (top) and nanofibers (bottom) deconvoluted by the existing states of carbon on the surface. The inset table includes respective composition percentages of the various states of carbon.[76]
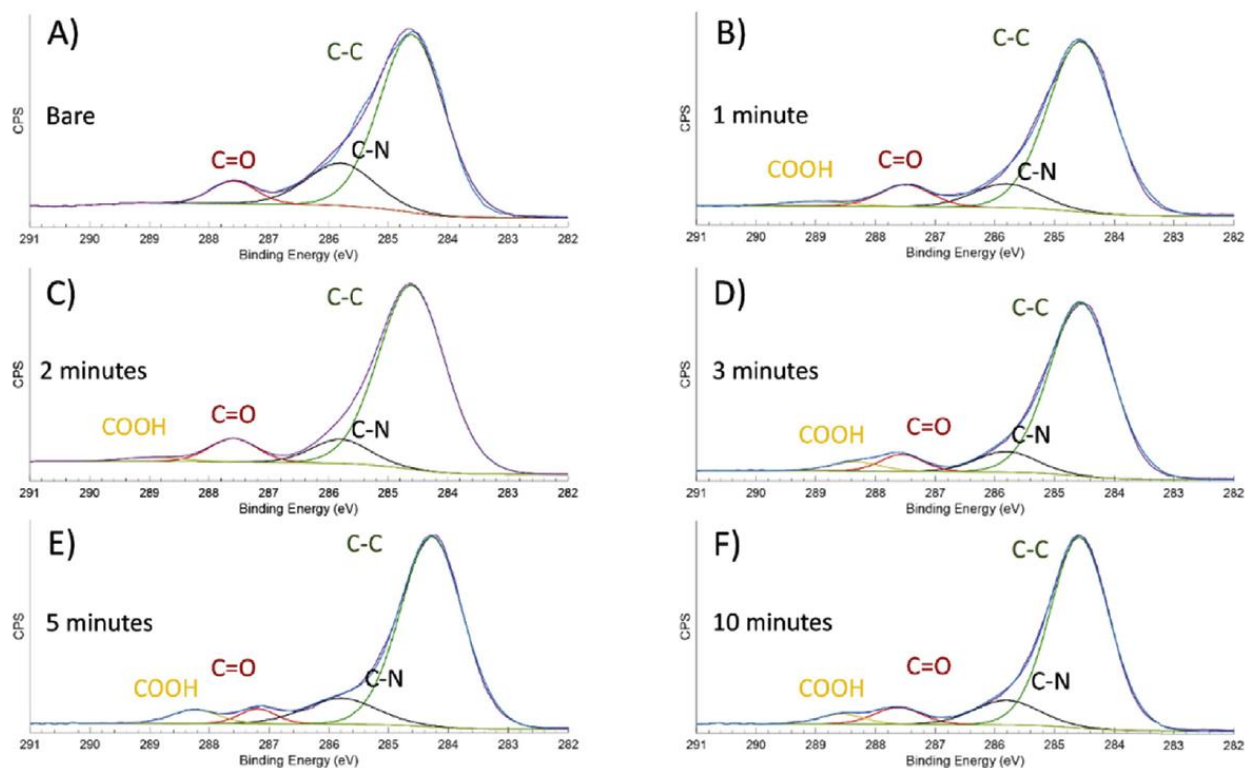
Figure 1.12. C 1s XPS spectra of ANF coated aramid fibers with varying durations.[77]

Table 1.1. Experimental bonding-state peak locations and concentrations of the decomposed C 1s energy state of bare and treated aramid fibers.[77]

Treatment	C-C (284.7 eV)	C-N (285.9 eV)	C=O (287.8 eV)	COOH (289.3 eV)
Bare fiber	81.11	10.25	8.64	0.00
1 min treated fiber	81.55	9.32	7.50	1.64
2 min treated fiber	79.06	11.04	7.75	2.16
3 min treated fiber	79.88	11.38	5.60	3.14
5 min treated fiber	78.99	12.22	5.35	3.43
10 min treated fiber	78.49	12.31	5.79	3.41

The untreated ANFs have been shown to improve the mechanical properties of polymer nanocomposites as described previously. However, a further enhancement of the polymer nanocomposites properties can be achieved through the improvement of the interfacial chemical

interaction between the polymer matrix and nanofillers by the functionalization of the ANFs. For example, Iijima et al. functionalized ANFs using surface-modified Ag nanoparticles by wet mixing process and dispersed them in epoxy resins to prepare transparent nanocomposites.[78] Additionally, Oh et al. and On et al. prepared modified ANF reinforced epoxy nanocomposites.[79,80] From the test results, the thermal expansion coefficient was reduced, and adhesion strength improved. Moreover, ANFs have been modified and used to reinforce rubber matrices by several researchers. Chen et al. modified Kevlar nanofibers (m-KNFs) using epichlorohydrin to reinforce an SBR matrix, and the reinforced SBR composites exhibited considerable improvement in their mechanical properties compared to pure SBR (Figure 1.13).[71] However, the application of the epichlorohydrin-modified KNFs is only limited to the rubber matrix having aromatic rings in the chemical structure because they are dispersed in the rubber matrix via π–π stacking of aromatic rings in the ANFs and the SBR, which is not applicable to BR. Xue et al. prepared hydrolyzed ANFs by acid-assisted hydrothermal treatment and used them to reinforce carboxylated acrylonitrile rubber (XNBR).[81] The mechanical strength improved through the hydrogen bonding interaction between the XNBR and the hydrolyzed ANFs, but this strategy is also limited to a rubber matrix with polar backbone structures.
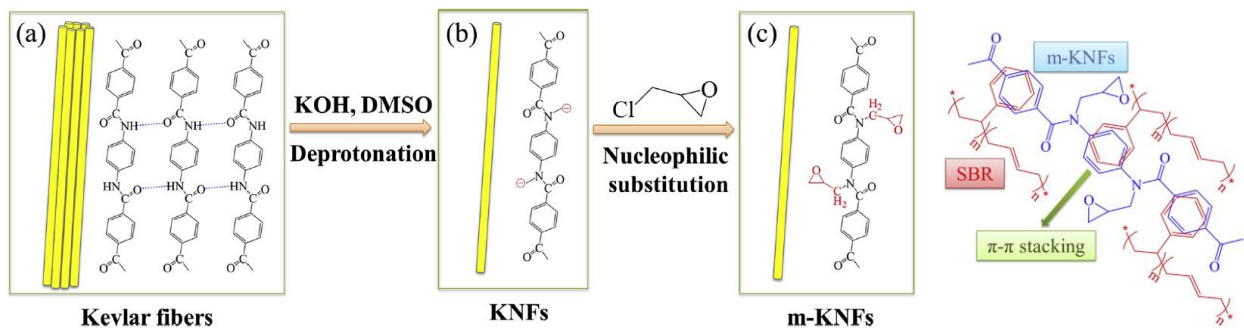
Figure 1.13. Synthetic mechanism of m-KNFs and schematic diagram of the interaction between m-KNFs and SBR.

The previously reported polymer nanocomposites reinforced with modified ANFs are mostly based on the physical interfacial interactions, such as hydrogen bonding or π–π stacking interaction between the modified ANFs and polymer matrices. Introducing covalent bonding between the polymer matrix and ANFs in the nanocomposite system using a silane coupling agent can improve the chemical interaction and increase mechanical properties for both polar and non-polar polymer matrices. For instance, ANFs can be used as a nanoscale building block for the nonpolar rubber matrices when they are functionalized using a silane coupling agent with polysulfide.[72,73] The sulfur moiety in the silane coupling agent can react with the double bond in the rubber molecule during the vulcanization process. The silane functionalization of ANFs not only improves the dispersion of ANFs in the rubber matrix but also provides covalent linkages between the rubber molecule and ANFs which enhance the mechanical properties. Moreover, covalent linkages between rubbers and fillers can reduce energy dissipation during the deformation of rubber composites compared to the rubber-filler system reinforced with physical interaction between them.[72] Thus, the silane coupling agent functionalized ANFs are expected to contribute to the improvement of performance for thermosetting polymers and rubber nanocomposites.

1.3.4 Hybrid fillers based on ANFs for polymer nanocomposites

Recently, researchers have shown that hybridized nanomaterials can be employed as reinforcing fillers for polymer composites, especially the combination of two strong nanomaterials. The use of nanofiller combinations with excellent mechanical properties has shown a synergetic effect on the properties of composites when compared to composites reinforced with only one class of nanofillers. For instance, Fan et al. functionalized graphene using ANFs through π–π stacking interaction and used them to reinforce poly(methyl methacrylate).[82] The tensile strength and

Young's modulus of nanocomposites increased by 84.5% and 70.6%, respectively, by the incorporation of 0.7 wt % of the hybrid fillers. The improvements were also greater than those of ANF or graphene alone reinforced nanocomposites with the same loading of nanofillers. Moreover, Wang et al. studied the effect of graphene oxide (GO)/CNT hybrid filler on the properties of shape memory epoxy nanocomposites.[83] From the test results, a synergetic effect of GO/CNT hybrid filler in improving tensile strength and thermal properties was observed. Song prepared hybrid fillers based on two geometrically dissimilar fillers, including clay platelets and carbon nanotubes, and then used them to fabricate SBR nanocomposites with improved tensile strength, elastic modulus, and both thermal and electrical conductivities.[84] Additionally, the synergistic effect of multi-walled carbon nanotubes and graphene nanofillers on the mechanical performance of silicone rubber was reported by Pradhan et al.[85] The hybrid filler reinforced nanocomposites exhibited 110% and 173% improvements in tensile strength and elastic modulus, respectively. Therefore, the reported studies have shown the potential of hybrid fillers for the reinforcement of polymer nanocomposites.

The effect of ANFs on the properties and performance of polymer nanocomposites can be further enhanced by the functionalization with other strong nanomaterials. Among the nanomaterials being used as reinforcing fillers, GOs and cellulose nanocrystals (CNCs) are chosen to prepare novel hybrid fillers based on the ANFs for the reinforcement of thermosetting polymers and rubber nanocomposites in this dissertation.

GOs have attracted wide interest due to their excellent mechanical properties and large surface area, along with their high thermal stability and electrical conductivity.[86–89] Because of their outstanding properties, GOs have been used as a nanoscale reinforcement in polymer matrices. For example, Mao et al. fabricated GO/SBR nanocomposites through the mixing of GO colloid

18

with SBR latex and butadiene-styrene-vinyl-pyridine rubber latex.[90] The 2 vol % GOs reinforced GO/SBR composites were found to exhibit comparable mechanical strength to that of SBR composites containing 13.1 vol % carbon black. Wu et al. also reported NR nanocomposites reinforced with surface functionalized GOs using bis(triethoxysilylpropyl)tetrasulfide (TESPT).[50] The functionalization of GOs with TESPT improved their dispersion in the NR matrix and contributed to a 100% and 66% increase in the ultimate strength and moduli of the resulting NR nanocomposites, in addition to a 48% reduction in their air permeability.

CNCs have also received substantial attention in the field of polymer nanocomposites because of their high mechanical properties, high aspect ratio, and low density.[91–94] Because of their excellent properties, CNCs have been used to reinforce polymers such as poly(vinyl alcohol),[95] poly(methyl methacrylate),[96] poly(lactic acid),[97] polyurethane,[98] and poly(acrylic acid).[99] For example, Kang et al. studied the effect of CNCs on the properties of thermally degradable polymeric adhesives based on epoxy resin.[100] From the test results, shear strength was improved by more than 30%, and thermal degradation temperature was reduced by 40 °C. Kupka et al. dispersed CNCs in polyurethane to improve mechanical properties.[98] The results showed that Young's modulus and tensile strength increased by up to 50% and 25%, respectively, and the glass transition temperature also increased. Additionally, Li et al. prepared CNC or cellulose fiber reinforced poly(acrylic acid) for the application of strong composite adhesives.[99] The nanocomposites exhibited an improvement in the adhesive strength on an aluminum substrate. Lin et al. studied the effect of CNCs on the mechanical and wear properties of SBR/NR compounds.[101] From their test results, the incorporation of CNCs was found to increase the elastic modulus and decrease hysteresis loss; however, its effect on wear properties was deemed insignificant. Singh et al. modified the surface chemistry of CNCs using organosilanes

to improve interfacial interaction in an NR matrix.[93] The NR composites reinforced with organosilanes modified CNCs yielded improved elastic modulus and tensile strength compared to unmodified NR composites. Additionally, Guo et al. used CNCs as a thickener for ANF/ acrylonitrile rubber (NBR) composites during solution mixing to obtain a uniform dispersion of ANF into NBR.[102] By adding 1 part of CNC to the composites, both the tear strength and tensile strength of the nanocomposites were observed to improve. However, the effect of CNC as a thickener was limited to polar rubber matrices such as NBR.

The novel hybrid fillers based on ANFs are functionalized using a silane coupling agent to further improve chemical interaction between polymer matrices and nanofillers. The functionalized hybrid filler reinforced polymer nanocomposites are expected to exhibit enhanced mechanical properties and performance through improved chemical and mechanical interactions.

1.4 Dissertation overview

In the following chapters, a detailed description of the research regarding the reinforcement of rubber composites and thermosetting polymers using functionalized ANFs is provided.

Chapter 2 investigates the effect of functionalized ANFs for the reinforcement of rubber compounds for tire tread applications. In this chapter, it is shown that ANFs can be functionalized with bis(triethoxysilylpropyl)tetrasulfide (TESPT), a silane coupling agent containing polysulfide, to improve the dispersion of the ANFs in rubber compounds and to form covalent linkages between the rubber molecules and the ANFs. The resulting functionalized ANFs (fANFs) are expected to be able to reinforce all types of diene rubber currently consumed in the industry due to the sulfur moiety in the TESPT. First, the fANFs are dispersed in water, and an fANF/water paste is obtained for the simple dry mixing with rubber. Then, rubber compounds containing a hybrid filler of carbon

20

black and fANFs are prepared at various ratios before performing tensile and abrasion resistance tests to investigate the role of the fANFs on the properties of the rubber compounds. Finally, dynamic mechanical analysis is conducted to predict the wet traction performance and fuel efficiency of the fANF reinforced rubber compounds. The findings in chapter 2 contribute to understanding the influence of functionalization of ANFs on the reinforcement of polymer matrices through the improved dispersion and enhanced interfacial interaction between the matrix and fillers.

Chapter 3 focuses on the reinforcement of epoxy nanocomposites using epoxy functionalized ANFs. In this chapter, epoxy functionalized silane coupling agents are introduced to the ANFs through the surface functionalities of the ANFs formed during the dissolution process of the aramid fibers. The prepared epoxy functionalized ANFs (EANFs) are then used to fabricate EANF reinforced epoxy nanocomposites with different filler weight fractions for analysis. The EANFs are predicted to induce further mechanical improvements to the epoxy nanocomposites when compared to conventional ANF reinforced epoxy nanocomposites as a result of increased interfacial chemical bonding between the ANFs and the supporting matrix. To confirm the surface functionalization of the ANFs, chemical analysis is conducted using characterization techniques. Finally, tensile tests, fracture toughness tests, and dynamic mechanical analysis are performed to investigate the effect of the epoxy functionalized ANFs on the mechanical properties and dynamic mechanical properties of the epoxy nanocomposites. The findings in this chapter are instrumental in ensuring chemical interfacial interactions between the polymer matrix and reinforcing nanofillers in order to improve the static and dynamic mechanical properties of the resulting polymer nanocomposites.

Building on the findings of the previous chapters, chapter 4 of this dissertation develops functionalized ANF/GO hybrid fillers (fANF/GOs) for reinforcing tire tread rubber compounds with enhanced tire performances. In this chapter, ANFs and GOs are modified using TESPT and then combined to prepare fANF/GO hybrid fillers. The fANF/GOs are predicted to yield greater improvements in the mechanical performance of rubber compounds compared to the reference compound, as well as ANF or GO reinforced rubber compounds. These improvements are attributed to the covalent bonding between fANF/GOs and rubber matrix and the noncovalent interaction between the ANFs and GOs. The prepared fANF/GO hybrid filler is characterized using various characterization techniques, while the mechanical performance of the fANF/GO reinforced rubber compound is assessed using tensile and abrasion resistance testing. Finally, dynamic mechanical analysis (DMA) is performed in order to predict the wet skid resistance, and rolling resistance of the fANF/GO reinforced rubber compounds. The findings of this chapter result in enhanced mechanical properties, fuel efficiency, and abrasion resistance of tire tread rubber compounds without deterioration of wet grip performance.

Chapter 5 focuses on the development of CNC functionalized ANFs reinforced rubber compounds for tire tread with high abrasion resistance and fuel efficiency. In this work, CNCs are modified using thionyl chloride to prepare chlorinated CNCs (CNC-Cl), which are then used to functionalize ANFs. Then, CNC functionalized ANFs are modified with TESPT to yield functionalized ANF/CNC hybrid fillers (fACs) that exhibit better dispersion in an SBR/BR matrix and improved interfacial interaction between fACs and rubber chains. The fAC hybrid fillers are prepared at various ratios of ANFs and CNCs to determine the optimum ratio between the two nanofillers. Finally, rubber compounds are prepared using new hybrid fillers to replace regions of carbon black. Samples are then examined via tensile test, abrasion resistance test, and dynamic

mechanical analysis to investigate the role of the novel fillers on the properties and tire performance of rubber compounds. The developed fAC reinforced rubber compounds are expected to exhibit enhanced mechanical properties and tire performances compared to compounds reinforced with ANF or CNC alone and ANF/CNC hybrid filler without covalent bonding through a combination of improved chemical and mechanical interaction between fACs and the SBR/BR matrix.

Chapter 6 investigates the effect of CNC functionalized ANFs on the mechanical strength and toughness of epoxy nanocomposites. In this study, CNCs are attached to the surface of ANFs through covalent bonding to improve the chemical and mechanical interaction in an epoxy matrix. The chemically attached CNCs on the ANFs are expected to provide an additional mechanical interlocking effect when the epoxy nanocomposites are subjected to mechanical stresses. To prepare CNC functionalized ANFs (fACs), CNCs are chlorinated using thionyl chloride and reacted with ANFs, followed by modification with an epoxy functionalized silane coupling agent. Prior to the preparation of epoxy nanocomposites, the fACs are analyzed using various techniques to characterize the CNC functionalization on the ANFs. Finally, epoxy nanocomposites are prepared and tested to investigate the role of fACs on the mechanical properties and fracture properties of nanocomposites. To prove the effect of the chemical covalent interaction between ANFs and CNCs on the properties of nanocomposites, hybrid fillers without covalent linkages are also prepared to fabricate epoxy samples and tested to compare the performance between them. The findings of this chapter present new solutions for the reinforcement of epoxy nanocomposites using novel hybrid nanofillers based on the covalent linkages between the nanofillers.

The final chapter of this dissertation presents a summary of key findings and contributions discussed throughout the dissertation to the field of polymer nanocomposites. Particular emphasis

is given to the results regarding silane coupling agent modified ANFs, and hybrid nanofillers based on ANF reinforced thermosetting polymers and rubber nanocomposites. Additionally, the last section of this chapter provides some suggestions for potential future work to further expand the obtained and reported findings.

Chapter 2

Aramid Nanofiber Reinforced Rubber Compounds for the Application of Tire Tread with High Abrasion Resistance and Fuel Saving Efficiency

2.1 Chapter introduction

This chapter presents aramid nanofiber reinforced rubber compounds for tire tread applications. Tire performance plays a significant role in the safety of vehicles and fuel efficiency and is thus a critical vehicle technology that is driven by the materials used. The characteristics of tires are largely dependent on the properties of the tread rubber compound, which are significantly affected by the type and amount of fillers used for static and dynamic reinforcement. In this work, a silane coupling agent is used to functionalize aramid nanofibers (ANFs), and the effect of a carbon black/ANF hybrid filler on the properties of tire tread rubber compounds is investigated. A functionalized ANF (fANF)/water paste mixture is prepared and uniformly dispersed in the conventional dry rubber without using a solution mixing method, therefore avoiding latex co-coagulation, and the uniform dispersion of ANFs in the rubber matrix is confirmed through scanning electron microscopy. The properties of the carbon black/ANF hybrid filler reinforced rubber compounds at various weight fractions are then evaluated using tensile testing, dynamic mechanical analysis, and abrasion resistance testing. The rolling resistance and abrasion resistance of rubber compounds with 1 part of ANFs are found to improve over the baseline neat rubber samples by 14.7% and 11.3%, respectively, all while maintaining the wet-skid resistance. Thus, this study establishes that the addition of ANFs in the tread rubber compound enhances the overall performance requirements of tires, known as the "magic triangle."

2.2 Preparation and characterization of fANFs

2.2.1 Preparation of fANFs

ANFs were prepared by the method presented by Yang et al.[4] Specifically, a dark red solution of 1 g of Kevlar® KM2+ aramid fibers (style 790 scoured, CS-800), 1.5 g of finely ground potassium hydroxide (KOH) (ACS certified, Fisher Scientific), and 500 ml of dimethyl sulfoxide (DMSO) (ACS certified, Fisher Scientific) was prepared by mixing them with constant stirring for 7 days at room temperature. To prepare the fANFs, 2 g of bis(triethoxysilylpropyl)tetrasulfide (TESPT, Si69®, received from Evonik) was mixed with the ANF solution, followed by stirring at 80 °C for 1 day (Figure 2.1a).

500 ml of deionized water was poured to the solution in order to isolate and precipitate the fANFs. The precipitated fANFs were then collected by vacuum filtering, after which the product was washed with deionized water and acetone (ACS reagent, Sigma-Aldrich) to neutralize the high pH of the solution. Finally, the collected fANFs were re-dispersed in water using horn sonication (Branson Ultrasonics™ sonifier™ Q500). The water was then evaporated to obtain a fANF paste with a small water content.

(a)

ANF   Bis(triethoxysilylpropyl)tetrasulfide   Functionalized ANF (fANF)

(b)

Functionalized ANF

Rubber Molecule

Sulfur Crosslink

fANF Reinforced Rubber Compound
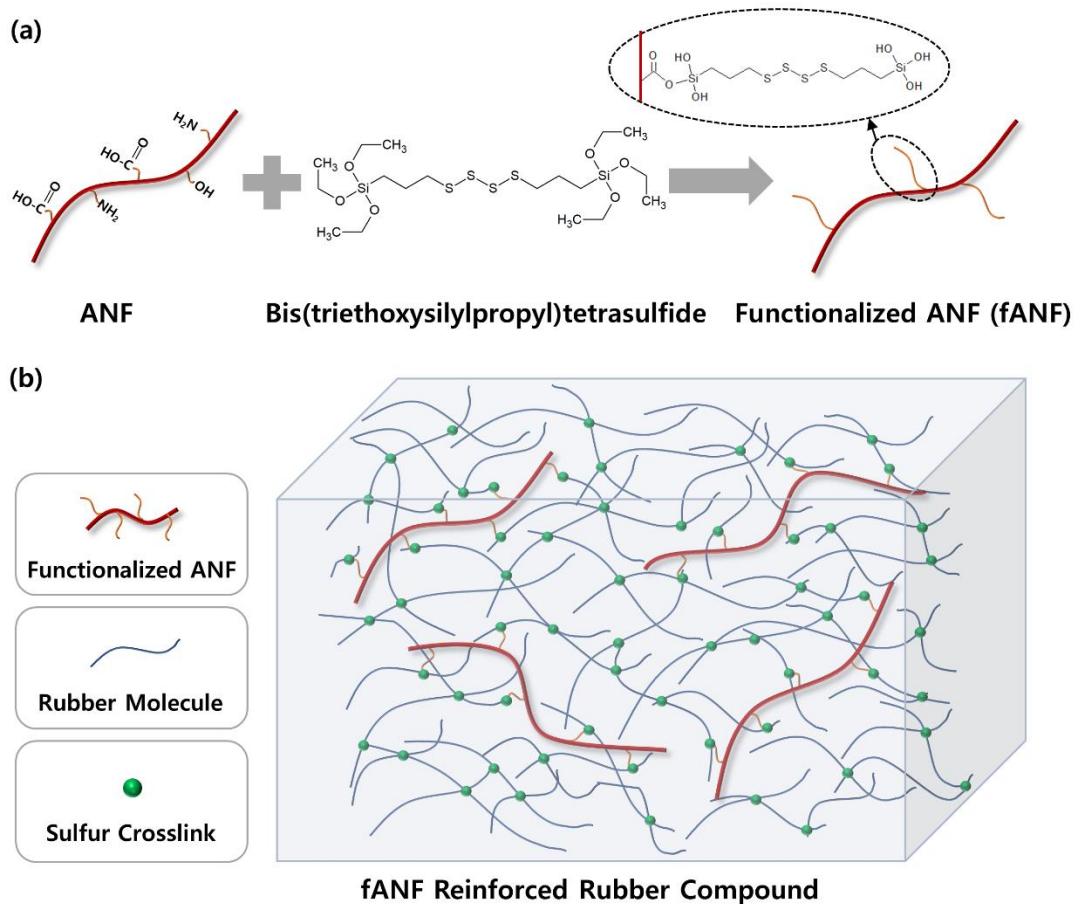
Figure 2.1. Illustration of (a) the reaction to prepare the fANFs, and (b) the fANF reinforced rubber compound.

2.2.2 Characterization of fANFs

The fANF reinforcement agent was characterized in detail to clarify its role in the reinforcement of rubber compounds. In order to determine any changes following the silane functionalization, atomic force microscopy (AFM) was performed using a Park Systems XE-70 to characterize the morphology and dimension of nanofibers. Figure 2.2a and 2.2b show AFM images of ANFs and fANFs after isolation and prior to dispersion in rubber compounds. As seen the AFM images, fANFs display similar morphology and dimensions to that of ANFs as the ANFs and fANFs are found to have diameters ranging between 4-10 nm and 4-12 nm, respectively. In

27

addition to similarities in the morphology and dimension, both ANFs and fANFs images show little agglomeration of nanofibers. ATR-FTIR was then used to investigate the alteration of the aramid chemical structure after the dissolution and deprotonation process of the ANFs and functionalization of ANFs using TESPT (Figure 2.2c). The FTIR spectra were obtained using a Nicolet iS50 spectrometer (Thermo Scientific) with a SMART diamond iTR accessory. When inspecting the FTIR spectra of ANFs, an increase in peak intensity of the phenyl-N stretching (1309 cm^{-1}) and C=O stretching (1642 cm^{-1}) is observed after using the dissolution process. These results confirm that ANFs contain more surface functional groups including carboxylic acid and amine, compared to macroscale aramid fibers resulting from the dissolution and hydrolysis process. Such findings are consistent with those previously reported by Nasser et al. and Patterson et al.[5,6] ANF functional groups are also indicative of the potential for the functionalization of ANFs. Therefore, the FTIR spectra of ANFs and fANFs were also compared to investigate any change to the chemical composition of the ANFs after TESPT treatment. When examining the spectra of ANFs and fANFs, previously absent peaks at 2940 and 2875 cm^{-1} attributed to the methylene nonsymmetric stretching vibration and methylene symmetric stretching vibration in silane coupling agent, respectively, are observed to appear. The Si-CH$_2$-R stretching vibration, Si-O stretching vibration, Si-O-C stretching vibration, and Si-O asymmetric stretching vibration peaks were also observed at 1199, 1100, 1017, and 950 cm^{-1}, respectively, after the treatment. The introduction of sulfur moieties on the fANFs is confirmed by the slight increase of the peak at 1246 cm^{-1}, which indicates the CH$_2$ wagging in -CH$_2$-S-. Thus, the alteration of the chemical structure investigated by FTIR indicates the introduction of TESPT on the ANF surface. This new fANF surface chemistry is useful for efforts to improve the interfacial chemical interaction between the rubber molecules and fANF reinforcement through covalent bonding.
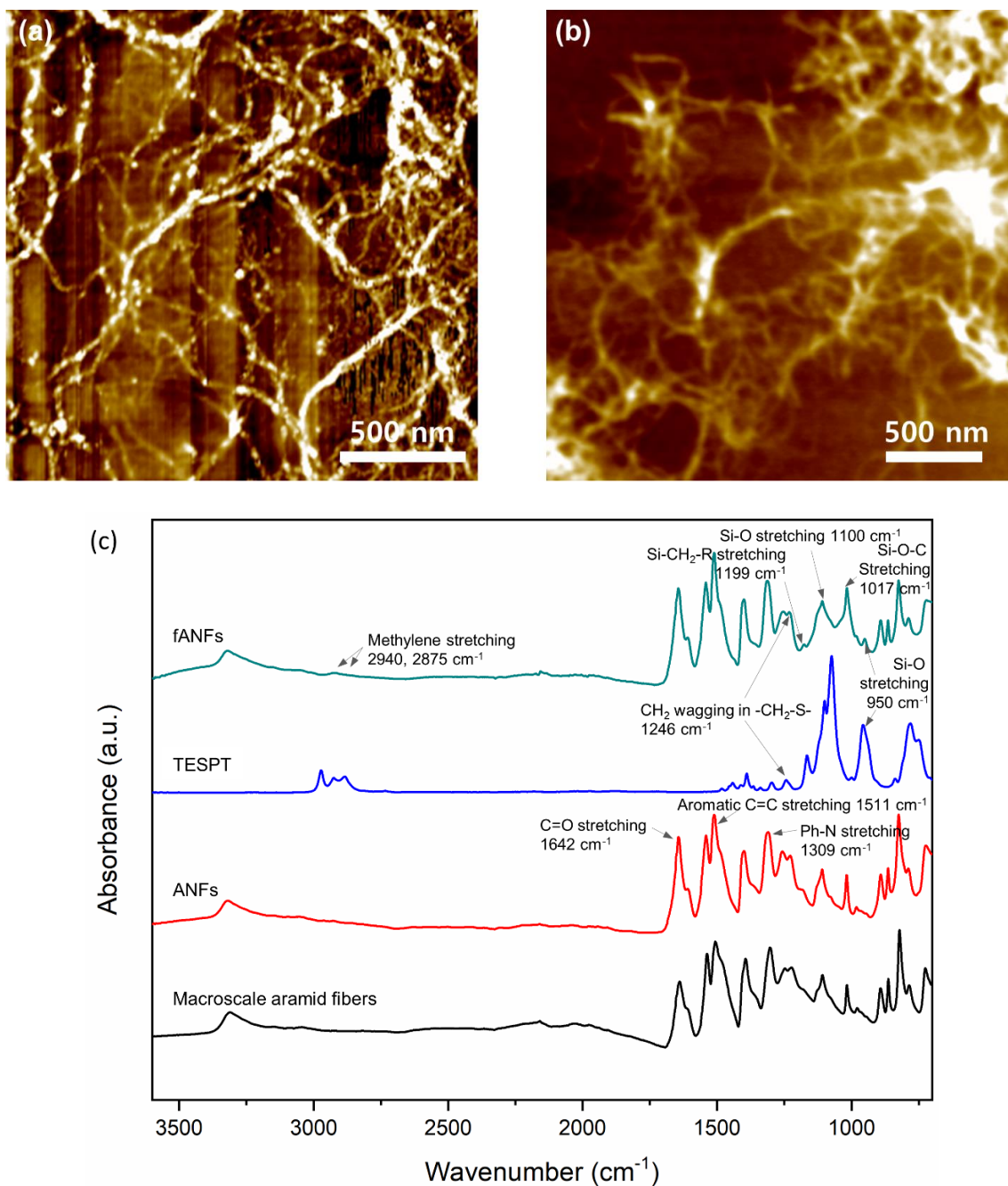
Figure 2.2. Microscopic images of (a) ANFs and (b) fANFs using AFM. (c) FTIR spectra of macroscale aramid fibers, ANFs, TESPT, and fANFs.

In addition, X-ray photoelectron spectroscopy (XPS) was used to characterize the chemical compositional changes of both the ANFs and fANFs. The XPS was conducted on a Kratos Axis Ultra XPS system. Given the importance of the fANF surface chemistry to the interfacial

interaction in composites, an element analysis summary is presented in Table 2.1. The tabulated element concentrations show considerable changes between the chemical composition of the macroscale aramid fibers and ANFs. Post-deprotonation, the oxygen content is found to increase in ANFs, relative to that of the macroscale aramid fibers, indicating that functionalities including hydroxyl groups and carboxylic acid are introduced onto the ANF surface. The C 1s XPS was performed on the macroscale aramid fibers and ANFs, with the results shown in Figure 2.3a and 2.3b, respectively. From the results, a new peak at 290.2 eV corresponding to COOH functionalities is detected from the C 1s spectra of the ANFs. The new peak is the result of the dissolution and hydrolysis process, which cleaves the amide bond in the macroscale aramid fibers into a carboxylic acid and an amine.[5,6,103] Therefore, ANFs are found to be more reactive than macroscale aramid fibers because of the additional functionalities on the surface.

After the TESPT treatment of the ANFs, 1.00% of the S element and 1.31% of the Si element were detected when performing an elemental analysis of fANFs (Table 2.1). The presence of the S and Si elements indicates the introduction of TESPT on the surface of the fANFs. In addition, the functionalization of the ANFs using TESPT resulted in other significant chemical composition changes, such as additional peaks corresponding to the S-OH (102.8 eV) and Si-O-C (103.7 eV), which can be seen in Figure 2.4b. When inspecting the O 1s XPS spectra displayed in Figure 2.5, new peaks assigned to the Si-OH or COOR (532.8 eV), and C-O-Si (533.9 eV) were shown in the fANFs. As for the untreated ANFs, the changes in binding energy at 531.4 eV and 533.1 eV represent the C=O and C-OH functionalities, respectively. In addition to the detailed Si 2p and O 1s XPS spectra, a new peak at 282.5 eV attributed to the C-Si was also observed in C 1s XPS spectra, indicating the presence of TESPT on the fANFs. With the introduction of TESPT to the nanoscale aramid surface, the fANFs are expected to be more reactive, as the interfacial

interaction between the rubber matrix and the fANFs can be further improved through the chemical covalent bonding.

Table 2.1. The XPS elemental survey results of macroscale aramid fibers, ANFs and fANFs.

	C 1s (%)	O 1s (%)	N 1s (%)	S 2p (%)	Si 2p (%)
Macroscale aramid fibers	84.75	7.90	7.35	-	-
ANFs	83.30	10.63	6.07	-	-
fANFs	78.15	10.04	9.50	1.00	1.31
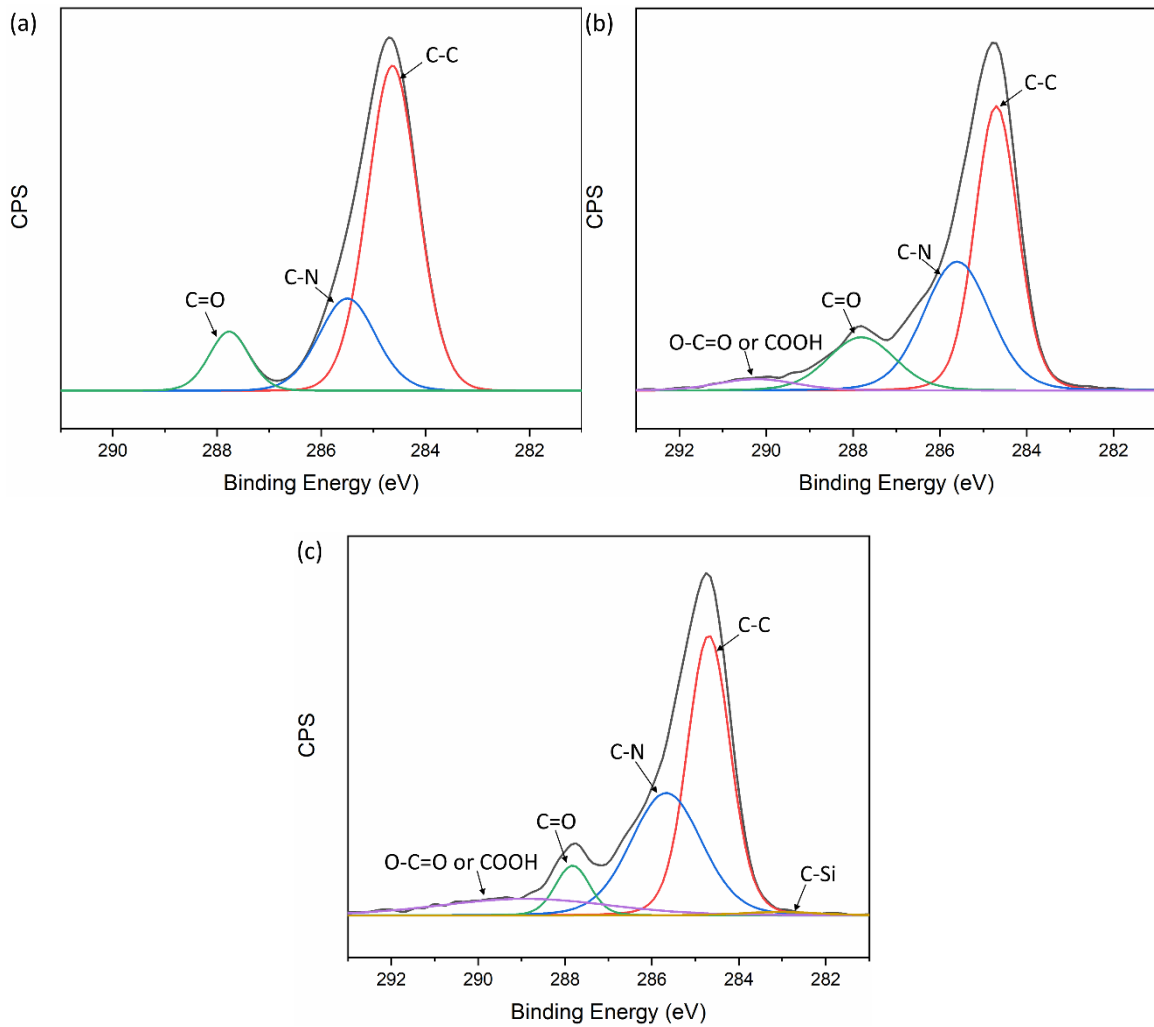
Figure 2.3. C1s XPS spectra of (a) macroscale aramid fibers, (b) ANFs and (c) fANFs.

31
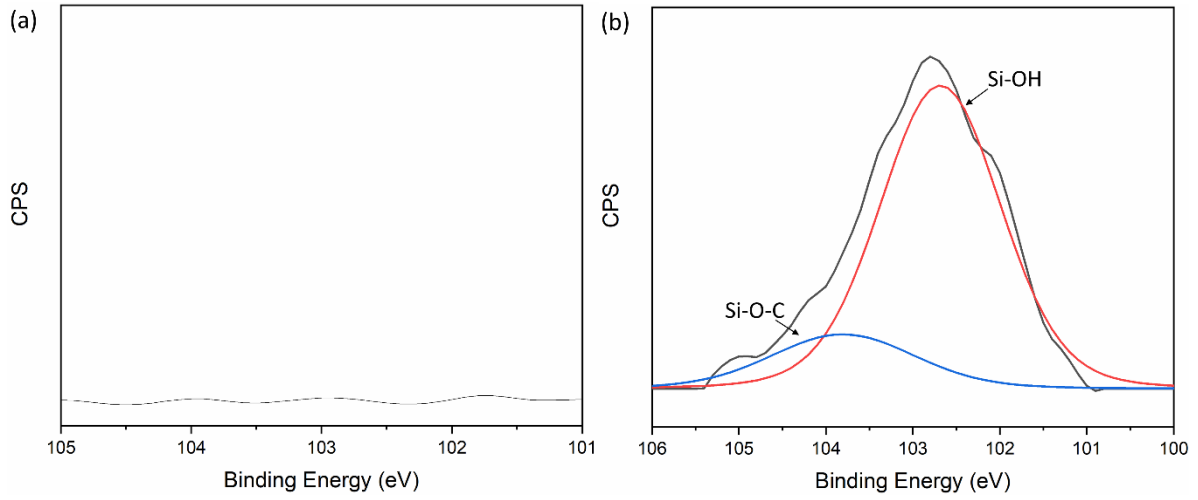
Figure 2.4. Si 2p XPS spectra of (a) ANFs and (b) fANFs.
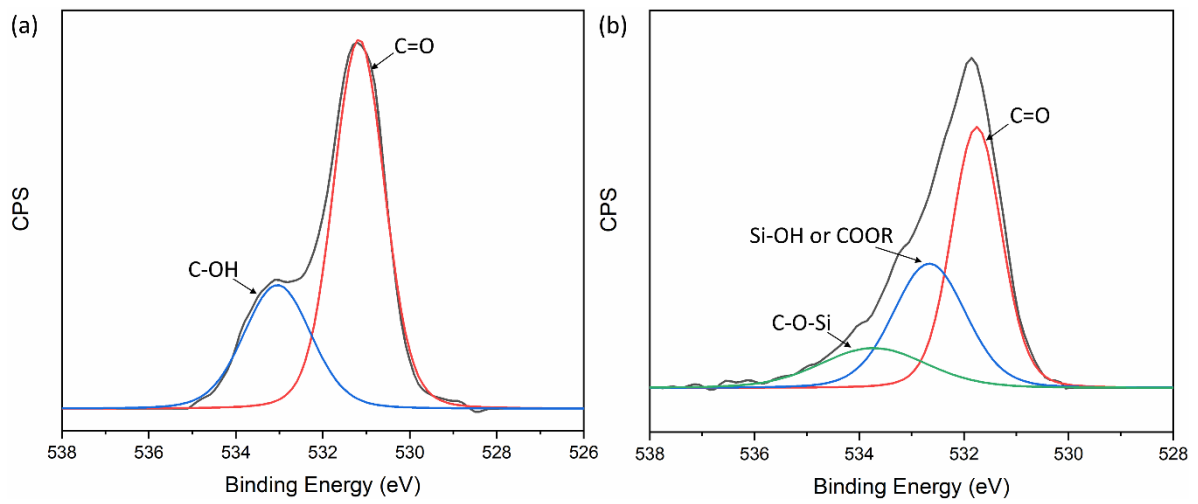
Figure 2.5. O 1s XPS spectra of (a) ANFs and (b) fANFs.

2.3 Preparation and characterization of fANF reinforced rubber compounds

2.3.1 Preparation of fANF reinforced rubber compounds

The fANF reinforced rubber compounds were prepared using an internal mixer (C. W. Brabender Plasti-corder) with a chamber size of 60 ml based on the recipes presented in Table 2.2. A schematic illustration of the fANF reinforced rubber compound is shown in Figure 2.1b for reference. The rubber compounding was performed in two stages with fill factors of 70%, and the internal mixing temperature was maintained at 140 to 150 °C. In the first stage, styrene-butadiene rubber SOL-6270M (MV 1+4 at 100 °C = 51, received from Kumho Petrochemical Co., Ltd) containing 37.5 phr (parts per hundred parts of rubber) of treated distillate aromatic extract oil content and butadiene rubber KBR 01 (MV 1+4 at 100 °C = 44, received from Kumho Petrochemical Co., Ltd) were combined and masticated for 1 min in the mixer, before adding carbon black (N339 grade, received from Birla Carbon), zinc oxide, stearic acid (provided by Akrochem Corporation), and naphthenic oil (provided by R.E. Carroll, Inc). After mixing for 1 min, the fANF paste was introduced and mixed for 5 min. The water in the fANF paste was evaporated during the mixing, as confirmed by measuring the weight of the mixed rubber compounds. In the next stage, the rubber compounds were subsequently mixed with sulfur and n-cyclohexyl-2-benzothiazole sulfonamide (CBS, provided by Akrochem Corporation) for 3 min, and then passed through a two-roll mill prior to vulcanization. Samples were vulcanized in a hot press at 168 °C for 10 min to fabricate the tensile testing and dynamic mechanical analysis specimens at 2 mm thickness, and 160 °C for 20 min for the abrasion test specimens at 8 mm thickness. The vulcanization conditions were determined by the cure characteristics obtained using a Rheometer MDR 2000 (Monsanto) at 160 °C for 30 min.

Table 2.2. Recipes of the fANF reinforced rubber compounds and the reference compound (unit: phr). (#A and #R stand for # part of fANF was added and # part of carbon black was replaced by fANF, respectively.)

Ingredients	Reference	0.5A	1A	3A	6A	0.5R	1R	3R	6R
SOL-6270M	96.25	96.25	96.25	96.25	96.25	96.25	96.25	96.25	96.25
KBR01	30	30	30	30	30	30	30	30	30
Carbon black, N339	50	50	50	50	50	49.5	49	47	44
fANF	-	0.5	1	3	6	0.5	1	3	6
Naphthenic oil	3.75	3.75	3.75	3.75	3.75	3.75	3.75	3.75	3.75
Zinc oxide	3	3	3	3	3	3	3	3	3
Stearic acid	1	1	1	1	1	1	1	1	1
Sulfur	1.5	1.5	1.5	1.5	1.5	1.5	1.5	1.5	1.5
CBS	2.2	2.2	2.2	2.2	2.2	2.2	2.2	2.2	2.2

2.3.2 Characterization and testing of fANF reinforced rubber compounds

The fracture surfaces of tensile testing samples were inspected using a field-emission scanning electron microscope (SEM, JEOL JSM-7800FLV). The crosslink density of the fANF reinforced rubber compounds was measured by the toluene swelling method as follows: In order to extract organic additives, the samples were soaked in tetrahydrofuran (THF) for 3 days and n-hexane for 2 days. They were dried at 25 °C for 2 days after which the weights of the obtained samples were measured. The samples were then immersed in toluene for 2 days before measuring the weights of the samples. The following equation was used to calculate the percentage of swelling ratio (Q):

$$Q = \frac{W_s - W_u}{W_u} \tag{2.1}$$

where W_s and W_u are weights of the swollen and dried samples, respectively. The crosslink density was then calculated using the following Flory-Rehner equation:[104,105]

$$\nu_e = -[\ln(1 - \nu_r) + \nu_r + \chi\nu_r^2]/[\nu_t \left(\nu_r^{\frac{1}{3}} - \frac{\nu_r}{2} \right)] \tag{2.2}$$

where ν_e is the network chain density (mol/cm^3), ν_r is the volume fraction of rubber, χ is the Flory-Huggins parameter representing the toluene-rubber interaction (0.391), and ν_t is the molar volume of toluene (106.3 cm^3/mol).

In order to evaluate the role of the fANFs on the mechanical properties of the rubber compound, both tensile tests and dynamic mechanical analysis were conducted. An Instron load frame (5982 series) using a 100 kN load cell was used to perform the tensile tests. Standard ASTM D412 type C specimens were tested at a strain rate of 500 mm/min according to ASTM D412. Additionally, dynamic mechanical properties were obtained using a TA Q800 dynamic mechanical analyzer (DMA) with temperature sweep. Test specimens which were length of 40.0 mm, width of 6.0 mm, and thickness of 2.0 mm were tested in tensile mode with a heating rate of 3 °C/min from -65 °C to 65 °C at 10 Hz and 0.5% strain. The abrasion resistance was then tested using an AF02 DIN Abrasion Tester (Aveno Technology Co., Ltd) following the DIN 53516 standard. Cylindrical shaped specimens with diameter of 16 mm and thickness of 8 mm were prepared and abraded for a distance of 40 m on a drum covered with abrasive paper rotating at 40 rpm. The weight of the sample was measured before and after the abrasion and the abrasion loss was obtained using the following equation:

$$A_A = \frac{\triangle m_t \times S_0}{d_t \times S} \tag{2.3}$$

where A_A is the abrasion loss (mm^3), Δm_t is the mass loss (mg), d_t is the density of the compound (g/cm^3), S is the abrasive grade (mg), and S_0 is the nominal abrasive grade (200 mg). The calculated

abrasion loss was converted to an abrasion resistance index by dividing the average abrasion loss of the reference compound by the average abrasion loss of the sample.

2.3.3 Tensile properties

Tensile tests were performed on the fANF reinforced rubber compounds to investigate the role of the fANFs on the mechanical properties. The average modulus, tensile strength, and elongation at break of the fANF reinforced rubber compounds are summarized in Table 2.3, while the stress-strain curves of the reference and fANF reinforced rubber compounds are presented in Figure 2.6. When compared to the reference compound, the mechanical properties of fANF reinforced rubber compounds are found to be improved after adding only 0.5 phr of fANFs. As more fANFs were added to the rubber compound, or more carbon black was replaced by fANFs, the moduli at 100% and 300% strain were simultaneously improved. Specifically, the moduli at 100% and 300% strain of the 6A samples were observed to be 65.3% and 27.1% higher, respectively, than those of the reference samples. The tensile strength of the fANF reinforced rubber compounds is also increased when up to 3 phr of fANFs is used in the rubber compounds. Drawing from the results of the 0.5R, 1R, 3R, and 6R samples, it can be concluded that the fANFs contribute to a more significant improvement of the mechanical properties of rubber compounds in comparison to the more traditional carbon black. On the other hand, bare ANF reinforced rubber compounds showed similar average modulus and tensile strength to the reference compound (Table 2.4). These results can be attributed to the physical characteristics of the fANFs, and the introduction of the covalent interface between the rubber molecules and fANFs. As previously stated, the fANFs maintain the inherent high strength and stiffness of macroscale aramid fiber, while gaining additional features such as a high aspect ratio and large specific area which are

beneficial for the reinforcement of the polymer matrix.[7] Moreover, the introduction of the silane coupling agent inhibits the polar functionalities on the surface of ANFs that usually complicate the dispersion of ANFs into non-polar rubber molecules, while inducing covalent linkage with the rubber matrix.[106] The crosslink density of the fANF reinforced rubber compounds also shows a similar trend to that of tensile test results. For reference, a summary of the swelling ratio and crosslink density is shown in Table 2.3. As the amount of fANFs added in the rubber compounds increases, the swelling ratio is decreased, while crosslink density is increased. The crosslink density is also increased when carbon black is replaced with fANFs, despite the samples having the same filler loading as the reference compound. The observed behavior in crosslink density and swelling ratio can be attributed to the covalent linkages between the rubber molecules and fANFs. In addition to the physical interaction between carbon black and rubber molecules, the chemical interaction induced by the fANFs can effectively improve the crosslink density and allow easier transfer of the load and stress from the rubber matrix to ANFs, leading to improved tensile strength and modulus of rubber compounds.

Table 2.3. Tensile test results and crosslink density of fANF reinforced rubber compounds.

	Reference	0.5A	1A	3A	6A	0.5R	1R	3R	6R
100% Modulus (MPa)	1.71 ± 0.01	1.94 ± 0.06	2.06 ± 0.11	2.33 ± 0.12	2.82 ± 0.20	1.96 ± 0.01	2.03 ± 0.29	2.26 ± 0.03	2.68 ± 0.13
300% Modulus (MPa)	7.48 ± 0.21	7.99 ± 0.07	8.40 ± 0.57	8.87 ± 0.24	9.51 ± 0.32	8.26 ± 0.05	8.56 ± 0.75	8.28 ± 0.08	8.23 ± 0.21
Tensile Strength (MPa)	13.40 ± 1.94	15.08 ± 0.44	15.30 ± 0.38	16.01 ± 0.51	15.65 ± 0.49	13.85 ± 0.52	13.98 ± 0.77	14.31 ± 0.48	14.26 ± 0.15
Elongation at Break (%)	451.9 ± 22.1	469.5 ± 7.3	462.1 ± 24.6	476.4 ± 21.4	462.2 ± 4.5	429.1 ± 12.4	428.4 ± 24.8	454.9 ± 13.9	480.0 ± 5.3
Swelling Ratio, Q	2.38	2.35	2.31	2.14	2.06	2.37	2.36	2.30	2.22

Crosslink Density, ν_e (10^{-4} mol/cm³)	2.89	2.97	3.07	3.52	3.77	2.93	2.95	3.10	3.30

Table 2.4. Comparison of tensile test results of bare ANF and fANF reinforced rubber compounds (1 part of nanofibers was added to the reference compound).

	Reference	Bare ANF 1	fANF 1A
100% Modulus (MPa)	1.71 ± 0.01	1.78 ± 0.05	2.06 ± 0.11
300% Modulus (MPa)	7.48 ± 0.21	7.69 ± 0.21	8.40 ± 0.57
Tensile Strength (MPa)	13.40 ± 1.94	13.28 ± 0.43	15.30 ± 0.38
Elongation at Break (%)	451.9 ± 22.1	431.3 ± 10.8	462.1 ± 24.6
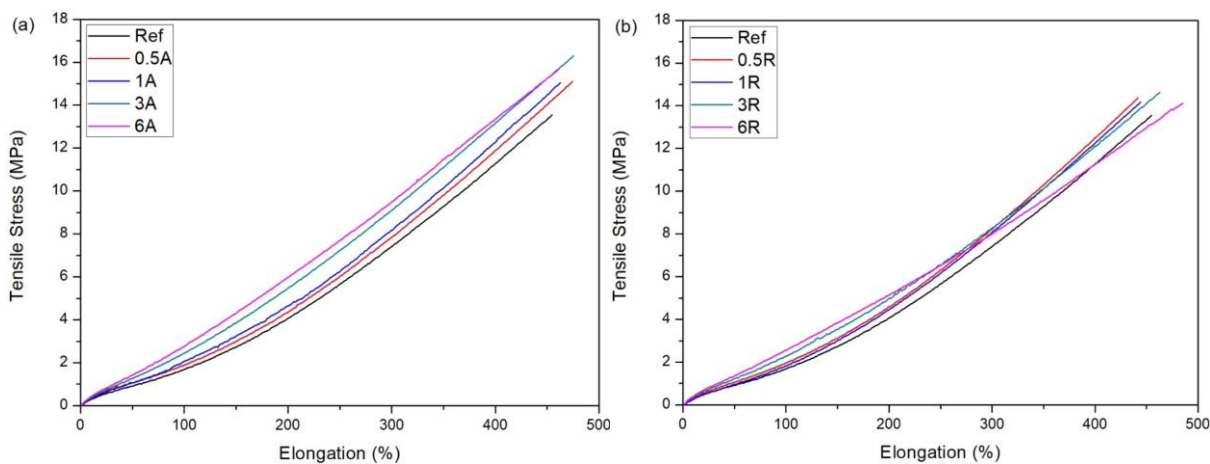
Figure 2.6. Stress-strain curves of fANF reinforced rubber compounds (a) when fANFs were added and (b) when carbon black was replaced with fANFs.

2.3.4 Fracture surface analysis

The compatibility between the matrix and filler, along with the proper dispersion of the reinforcing filler into the matrix, are essential parameters to obtain a high-performance

nanocomposite. In order to observe the dispersion of the fANFs in the rubber compounds, the fracture surfaces of tensile testing samples were examined post-testing using SEM as shown in Figure 2.7. While the fracture surface of the reference compound displays a flat and smooth texture (Figure 2.7a-b), the surface of samples with 1 part of fANFs clearly shows a considerable increase in roughness (Figure 2.7c-d). Additionally, further increase in the fANF content results in rougher fracture surfaces as can be seen in Figure 2.7e-h where the high magnification images show the presence of fANFs on the fracture surfaces. It is observed that the fibrous fANFs are well-dispersed within the rubber matrix, and the density of the nanofibers shown in the images increases with increased fANF loading. Partial fANF agglomerations are observed when incorporating 6 parts of ANFs in the rubber compound, however, 6A and 6R samples still displayed an improved modulus during tensile testing. The displayed high compatibility and homogeneous dispersion of the fANFs into the rubber matrix explain the improved mechanical performance discussed in the previous section. Moreover, the performed fracture surface analysis indicates that the ANFs can be uniformly dispersed in rubber compounds by simple dry mixing using a fANF/water paste.
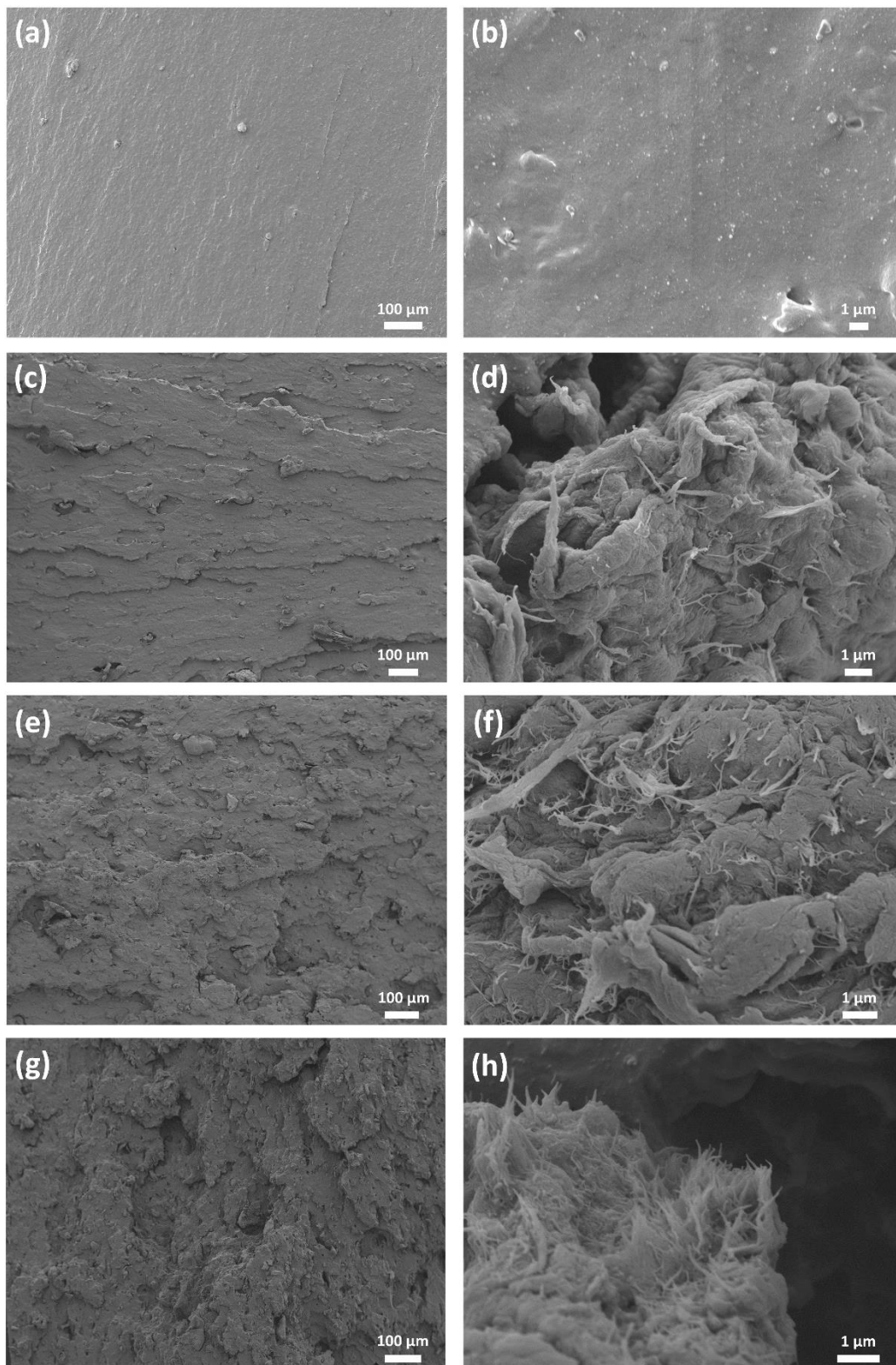
Figure 2.7. SEM images of the tensile test fracture surface. (a-b) Reference compound sample, (c-d) 1R sample, (e-f) 3R sample, and (g-h) 6R sample.

2.3.5 Dynamic mechanical properties

In addition to tensile testing, dynamic mechanical analysis was conducted to investigate the effect of the fANFs on the viscoelastic characteristics of the rubber compounds. The resulting tan δ curves of the fANF reinforced rubber compounds with various fANF concentrations are shown in Figure 2.8. The peak value of tan δ is reflective of the dissipated energy at the polymer matrix and filler interface and the mobility of the polymer molecules.[69] The introduction of fANFs into the rubber compounds is found to reduce the tan δ peak, with higher fANF content yielding a larger decrease of the peak tan δ value. The reduced tan δ peaks indicate that the incorporation of fANFs restricts the movement of the rubber molecules resulting in increased interfacial energy dissipation between the rubber and filler.[105] Moreover, the covalent bonds formed between the fANFs and rubber molecules further limit the mobility of the crosslinked rubber structure, thus increasing the rigidity of the rubber compounds.

Tire performance parameters such as wet skid resistance and fuel saving efficiency are usually predicted using the viscoelastic characteristics of rubber compounds. In particular, values of tan δ near 0 °C and 60 °C are widely utilized to predict the wet skid resistance and rolling resistance, respectively, of tire tread rubber compounds.[107–109] A higher tan δ value at 0 °C usually represents better wet grip performance on roads, while a lower tan δ value at 60 °C indicates lower rolling resistance, signaling an improvement in fuel saving efficiency. From the DMA results summarized in Table 2.5, the fANF reinforced rubber compounds demonstrated comparable or improved fuel saving efficiency, relative to the reference compound, except for the 6A sample. Specifically, the 1R rubber sample is found to display the lowest tan δ value at 60 °C, indicating a 14.7% reduced rolling resistance relative to the reference compound, all while preserving the wet skid resistance shown by the tan δ value at 0 °C. These results can be explained

41

by the characteristics of rubber-filler network. The rubber-filler network of traditional carbon black reinforced rubber compounds relies on the van der Waals forces between the rubber and filler.[110] The breakdown and reformation of the rubber-filler and filler-filler interactions dissipate energy during the deformation of the rubber sample that increase the rolling resistance.[111] However, the covalent bonding between the rubber molecules and fANFs prevents and reduces the breakdown and reformation of the interaction which leads to energy dissipation and contributes to the reduced rolling resistance.

Table 2.5. DMA results of fANF reinforced rubber compounds

	Reference	0.5A	1A	3A	6A	0.5R	1R	3R	6R
tan δ at 0 °C	0.393	0.386	0.404	0.385	0.398	0.420	0.395	0.392	0.388
tan δ at 60 °C	0.116	0.117	0.108	0.117	0.142	0.106	0.099	0.108	0.115
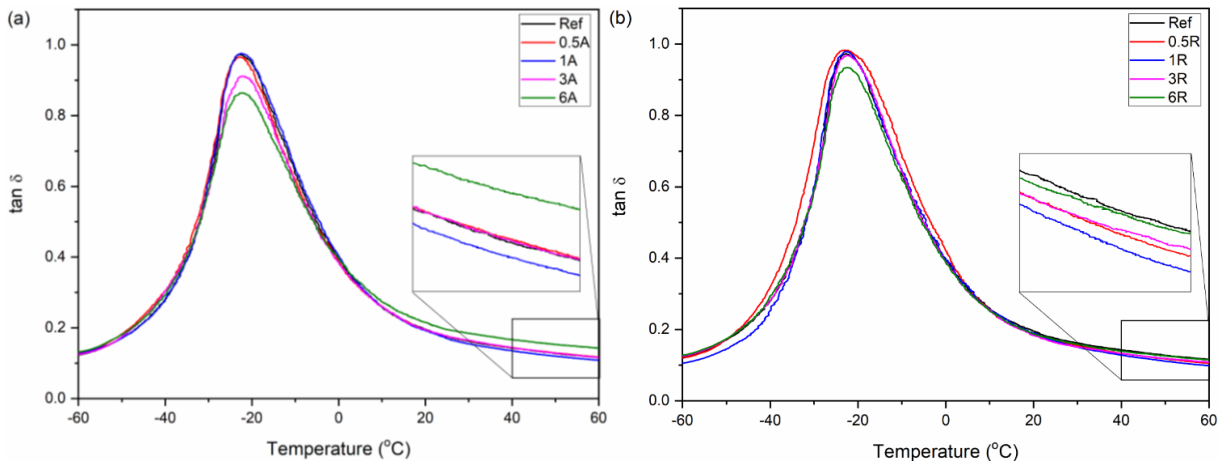
Figure 2.8. Resulting tan δ curves of fANF reinforced rubber compounds (a) when fANFs were added and (b) when carbon black was replaced with fANFs.

2.3.6 Abrasion resistance

Abrasion resistance is one of the most significant tire performance metrics because it is related to tire tread wear. Thus, the abrasion resistance of the fANF reinforced rubber compounds was evaluated using a DIN abrasion tester to evaluate their performance relative to the baseline. Figure 2.9 shows the average abrasion resistance indexes of the fANF reinforced rubber compounds with various filler concentrations relative to the reference rubber compound. For reference, a higher abrasion resistance index indicates better abrasion resistance of the rubber sample. From the figure, the abrasion resistance is found to increase as the amount of fANFs is increased up to 1 part in both the case where fANFs were added and the case where carbon black was replaced with fANFs. The abrasion resistance is observed to increase up to 14.0% when 1 part of fANFs was added to the rubber matrix, while an 11.3% increase in abrasion resistance was observed when 1 part of carbon black was replaced with fANFs. These results conclusively indicate the positive effect of the fANFs on the abrasion resistance of rubber compounds. It is known that the abrasion resistance can be enhanced by improving the dispersion of the filler, or increasing the rubber-filler interaction.[112,113] In addition to the beneficial features of ANFs, such as excellent mechanical properties and a high specific area, the functionalization using the silane coupling agent allows for covalent bonding between the fANFs and rubber matrix. The TESPT functionalized ANF surface also improves the dispersion of the fANFs, which have a hydrophilic chemical nature, in the hydrophobic rubber matrix. In addition to the improved dispersion of fANFs, the enhanced chemical interaction between the fANFs and rubber matrix improves reinforcement efficiency, which leads to an enhanced abrasion resistance in the modified rubber compounds. Drawing from the test results, the effect of fANFs on the "magic triangle" of tire performance is shown in Figure 2.10. Considering the performance predicted by the viscoelastic properties and abrasion test results

of the fANF reinforced rubber compounds, fANFs can be considered as a promising nanofiller that improves the fuel saving efficiency and abrasion resistance at the same time, without sacrificing the wet traction performance.
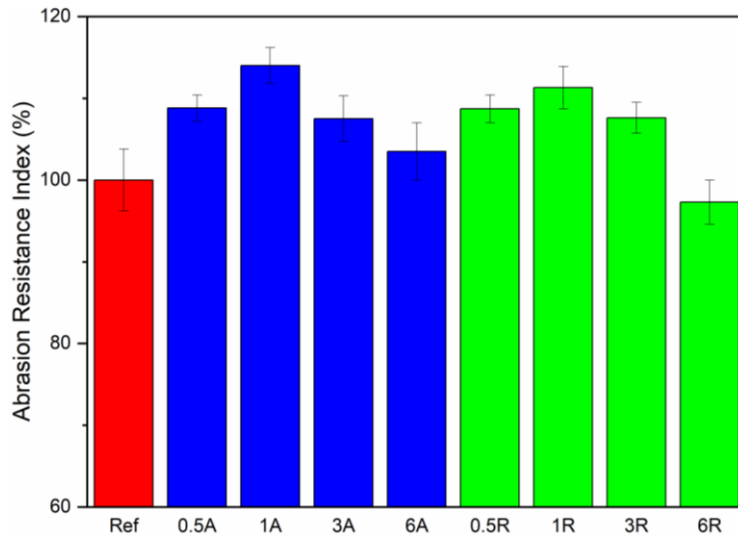
Figure 2.9. Abrasion resistance indexes of fANF reinforced rubber compounds.
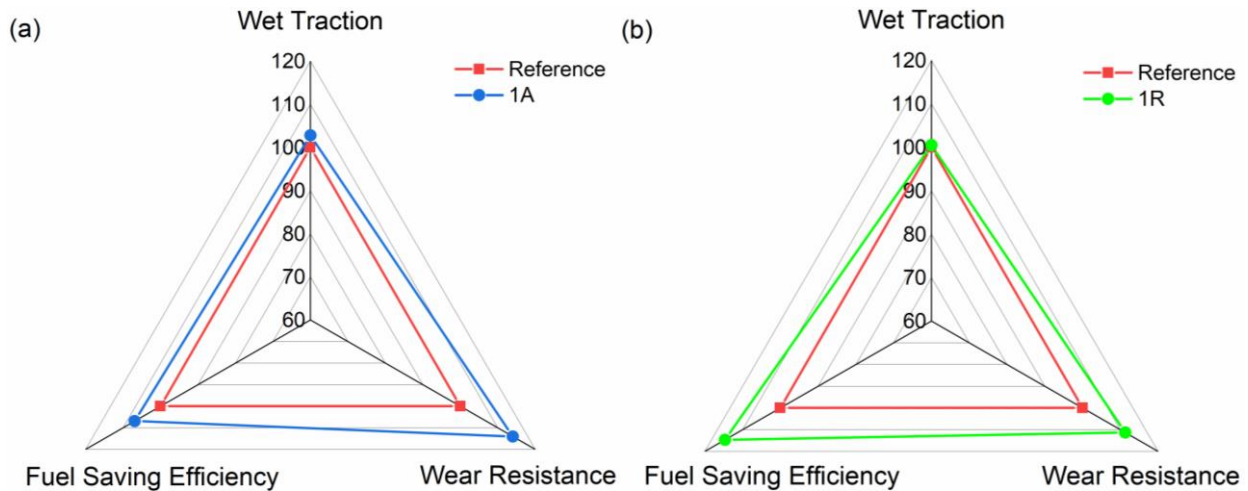
Figure 2.10. The "magic triangle" of tire performances for the fANF reinforced rubber compounds (a) 1A sample and (b) 1R sample predicted by viscoelastic properties and abrasion resistance test results.

2.4 Chapter summary

In this chapter, ANFs were functionalized with a silane coupling agent, and the resulting fANFs were used to prepare a fANF/water paste mixture that can be easily dispersed in a rubber matrix using conventional dry mixing. Following the simple dry mixing and curing process, the fANF reinforced rubber samples were mechanically tested using multiple methods to evaluate the effect of the fANFs on the mechanical properties and viscoelastic properties necessary to assess the performance of tire tread. Tensile testing, dynamic mechanical analysis, and abrasion resistance testing were conducted, and the results were compared to that of the reference rubber compounds. The tensile test results showed that moduli at 100% and 300% strain were increased by 65.3% and 27.1%, respectively, when 6 parts of fANFs were added to the rubber compounds. It was also observed that the fANFs provided superior filler performance to carbon black when using the same amount. The contribution of the TESPT treatment to both the uniform dispersion of nanofibers in the matrix and the reinforcement of compounds was confirmed by a fracture surface analysis of tensile specimens and crosslink density measurement. Additionally, the rolling resistance predicted by the viscoelastic properties was found to be improved by 14.7% when 1 part of carbon black was replaced with fANFs, and 6.9% when 1 part of fANFs was added to the compound. In each case the increase was achieved without deteriorating the wet traction performance. Moreover, the abrasion resistance of the rubber compounds was enhanced by 14.0% and 11.3% for 1A and 1R samples, respectively. This work thus conclusively demonstrates that fANFs are a promising nanofiller that offers overall improvement to the "magic triangle" performances of tire tread.

Chapter 3

High Strength Epoxy Nanocomposites Reinforced by Epoxy Functionalized Aramid Nanofibers

3.1 Chapter introduction

The focus of chapter 3 is the use of epoxy functionalized aramid nanofibers (ANFs) for the reinforcement of thermosetting polymers, especially epoxy nanocomposites. Thermosetting polymers have been demonstrated over the past couple of decades to exhibit improved mechanical properties when nanofillers are introduced. These improvements can be further increased through the introduction of covalent linkages between the polymer matrix and nanofillers that enhances the chemical interaction between them. In this work, ANFs are functionalized using a glycidyl ether silane coupling agent and their effect on the mechanical strength and dynamic mechanical properties of epoxy resin are investigated. Static and dynamic mechanical properties of the epoxy functionalized ANFs (EANFs) reinforced epoxy nanocomposites with different weight fractions are evaluated by conducting tensile testing and dynamic mechanical analysis. The results show that Young's modulus and tensile strength of 1 wt % EANFs reinforced nanocomposites increase by 16.8% and 14.0%, respectively, and fracture toughness increases by 4.4 times with the addition of 1.5 wt % EANFs. Additionally, both an increase in storage modulus and glass transition temperature are observed during dynamic mechanical analysis with increasing percentage of EANFs. Thus, this work demonstrates that the EANFs can further enhance the mechanical and viscoelastic properties of epoxy nanocomposites through chemical crosslinking between the epoxy matrix and ANFs.

3.2 Preparation and characterization of EANFs

3.2.1 Preparation of EANFs

The ANF solution was prepared using the method first demonstrated by Yang et al.[4] Here, 1.0 g of KM2+ aramid fibers (style 790 scoured, CS-800, received from JPS Composite Materials) and 1.5 g of potassium hydroxide (KOH) (ACS certified, Fisher Scientific) were added to 500 mL of dimethyl sulfoxide (DMSO) (ACS certified, Fisher Scientific). The mixture was stirred using a magnetic stirrer at room temperature for seven days, until a dark red solution of evenly dispersed ANFs was obtained. In order to functionalize the ANFs, 2 g of 3-glycidoxypropyltrimethoxysilane (received from Sigma-Aldrich) was added to the ANF/DMSO solution, and the mixture was stirred at 80 ℃ for 24 h (Figure 3.1a). Both ANFs and EANFs solutions were prepared for comparison.

The ANFs and EANFs were precipitated out of the solution and isolated by adding 500 ml of deionized water. Vacuum filtration was then used to collect the precipitate, after which the high pH of the solution was neutralized by washing with deionized water several times. Finally, the ANFs and EANFs were washed again with acetone (ACS reagent, Sigma-Aldrich) and dried in a vacuum oven at room temperature.
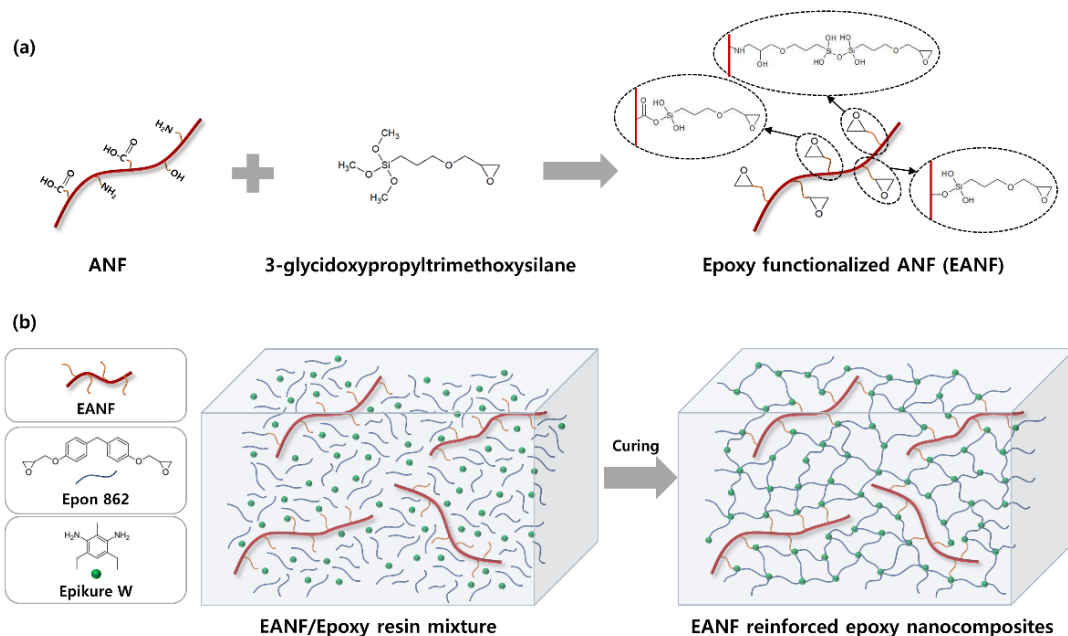
Figure 3.1. Schematic illustration of the reactions for (a) the preparation of EANFs, and (b) the EANF reinforced epoxy matrix.

3.2.2 Characterization of EANFs

The nanofibers' surface was imaged using an atomic force microscopy (Park AFM XE-70) to characterize the dimension and morphology of the ANFs and EANFs and determine any alterations due to the silane functionalization. The AFM images of the ANFs and EANFs are shown in Figure 3.2a and 3.2b, respectively. The AFM images were taken after spin coating and drying of isolated ANFs and EANFs dispersed in acetone on silicon wafers. From the figure, the EANFs maintained the fibrous shape observed in the untreated ANF image after treatment with the epoxy functionalized silane coupling agent. Additionally, little agglomeration of nanofibers was observed for both ANFs and EANFs images even after drying the nanofibers. The AFM images indicate that the ANFs have diameters in the range of 3 to 10 nm and the EANFs have diameters in the range of 4 to 10 nm. Thus, it can be observed that the morphology and dimension

of epoxy functionalized ANFs are similar to those of ANFs and they can be dispersed well in polymer matrices.
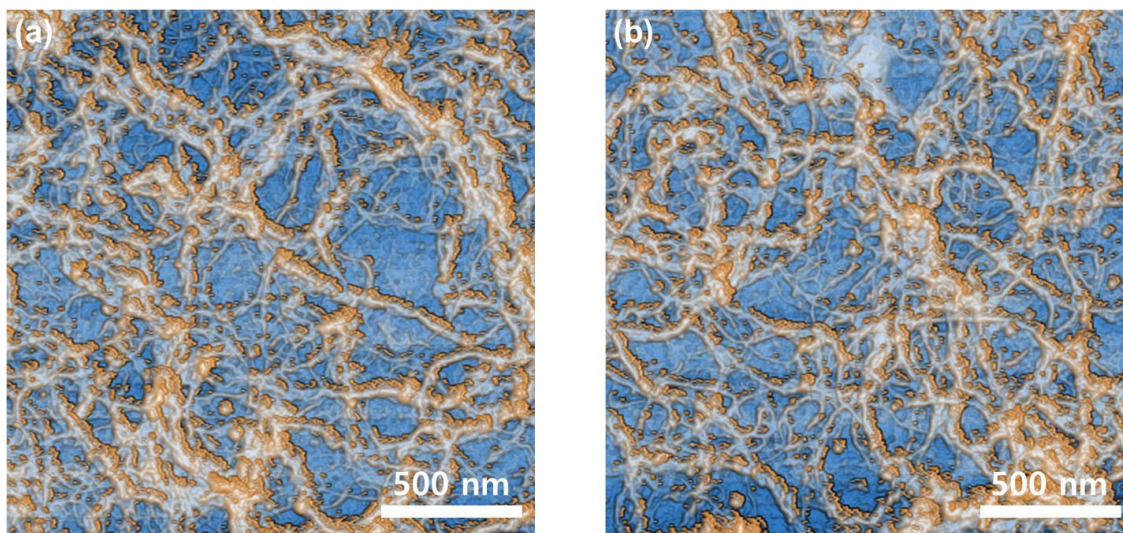
Figure 3.2. Enhanced color AFM images of (a) ANFs and (b) EANFs.

The chemical compositional change of the ANFs before and after the dissolution process was characterized by attenuated total reflection (ATR) Fourier transform infrared spectroscopy (FTIR) using a Nicolet iS60 spectrometer (Thermo Scientific) equipped with a SMART iTR accessary. Figure 3.3a and 3.3b show the FTIR spectra of the bare aramid fibers and untreated ANFs respectively. By examining these spectra, the chemical structures of ANFs are observed to exhibit an increase in the C=O stretching peak at 1642 cm^{-1}, and a slight increase of phenyl-N stretching peak at 1309 cm^{-1} compared to those of bare fibers, as indicated by Patterson et al. and Nasser et al.[5,6,103] The increase of these peaks indicates that functional groups like carboxylic acid and amine were increased on the surface of ANFs compared to the bare aramid fibers during the dissolution and hydrolysis process. ANFs are thus more reactive than bare aramid fibers due

to the presence of additional functional groups on the surface while retaining their original aromatic amide structure.[5,114]

Chemical characterization of the EANFs was also performed through ATR-FTIR after the ANFs were treated with the epoxy functionalized silane coupling agent. Figure 3.3c shows the FTIR spectra of epoxy functionalized silane and Figure 3.3d shows that of EANFs. After the treatment of the ANFs with epoxy functionalized silane, the absorption peaks at 2940 and 2875 cm^{-1} corresponding to the methylene asymmetric and symmetric stretching vibration from the alkyl chains assigning to silane moieties, respectively, were observed. The Si-CH$_2$-R stretching vibration peak at 1199 cm^{-1}, Si-O stretching vibration peak at 1100 cm^{-1}, and Si-O-C stretching vibration peak at 1017 cm^{-1} were also observed after the treatment. The introduction of the epoxy functional group on the ANFs was confirmed by the peak at 910 cm^{-1} which indicates the asymmetric stretching vibration of the epoxy group. These above results show that the ANFs could react with the epoxy functionalized silane coupling agent.

The EANFs containing epoxide end-groups like those in the epoxy resin can improve the compatibility with the epoxy matrix and provide covalent crosslinking through the reaction with amine groups in the curing agent, Epikure W (diethyltoluenediamine, received from Hexion). To confirm a contribution to the reinforcement of epoxy resin by the EANFs, curing agent Epikure W was reacted with the EANFs and characterized using ATR-FTIR. As shown in Figure 3.3f, the R-NH$_2$ peak at 1610 cm^{-1} and ring C=C stretching at 1480 cm^{-1} were observed, and the absorption peak at 910 cm^{-1} which correspond to the epoxy group was not seen after the reaction. These changes indicate that the EANFs can be reacted with the curing agent Epikure W and provide a direct contribution to the reinforcement by covalent bonding between the crosslinked epoxy resin network and the ANFs.
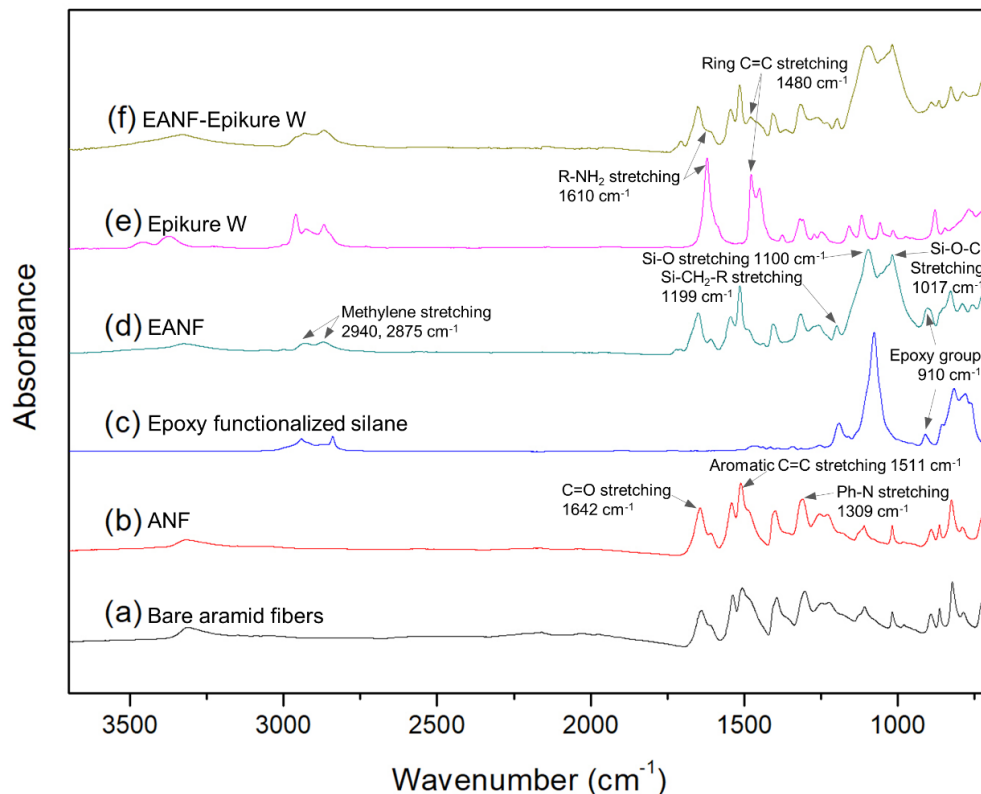
Figure 3.3. FTIR spectra of (a) bare aramid fiber, (b) ANF, (c) epoxy functionalized silane, (d) EANF, (e) curing agent Epikure W, and (f) reactant of EANFs and Epikure W.

The chemical composition changes were also investigated using a Kratos Axis Ultra X-ray photoelectron spectroscopy (XPS) system under high vacuum ($< 1\times10^{-8}$ Torr) with a monochromatic Al Kα source, 20 eV pass energy, and 0.05 eV step size. XPS spectra of bare aramid fibers, untreated ANFs, and EANFs were obtained for comparison. The results are shown in Table 3.1, and Figure 3.4 to 3.6. From the element analysis summarized in Table 3.1, the content of O element increased from 7.90 to 10.63% after the dissolution process of aramid fibers which yields ANFs. The increase of O element in the ANFs indicates that functional groups like carboxylic acid and hydroxyl group were increased on the surface of ANFs compared to the bare aramid fibers during the dissolution and hydrolysis process. In addition to the increased O element content, the C 1s XPS spectra in Figure 3.4a and 3.4b show the chemical compositional changes

between the bare aramid fibers and the ANFs. The C1s binding energy at 290.3 eV represents newly created COOH functionalities and verifies cleavage of the amide bond of the aramid fibers during the dissolution and hydrolysis process.[5,6,103] Due to the increase of functional groups on the surface, the ANFs can be more reactive than the original aramid fibers.

After the ANFs were treated with the epoxy functionalized silane coupling agent, 1.70% of Si element was observed on the surface of EANFs from the element analysis shown in Table 3.1. Figure 3.5 also shows the peaks at 102.8 eV and 103.7 eV which correspond to the binding energy of S-OH and Si-O-C, respectively, after the treatment of ANFs. The presence of C-O-Si bond and Si element indicates the formation of the coupling reaction between the ANFs and the silane coupling agent. The XPS spectra of O 1s on the surface of ANFs and EANFs are shown in Figure 3.6a and 3.6b. For the untreated ANFs, there are only two peaks at 531.2 eV and 533.1 eV which can be attributed to C=O and C-OH. However, new peaks at 530.8 eV, 532.8 eV and 534.0 eV which are assigned to Si-O-Si, Si-OH or COOR, and C-O-Si were observed from the O 1s XPS spectra of EANFs. Moreover, the C 1s XPS spectra show new C-Si peak at 282.1 eV and an increase of the peak at 285.7 eV which corresponds to C-N or C-O-C after the treatment of ANFs. The increase of the peak at 285.7 eV can be attributed to the epoxide group in the epoxy functionalized silane coupling agent. From the O 1s and C 1s XPS spectra, the functionalization of ANFs and the introduction of epoxy functional groups on the surface of ANFs were further confirmed.

Table 3.1. The element content analysis of bare aramid fibers, ANFs and EANFs using XPS.

Sample	C 1s (%)	O 1s (%)	N 1s (%)	Si 2p (%)
Bare aramid fibers	84.75	7.90	7.35	-
ANFs	83.30	10.63	6.07	-
EANFs	78.60	12.72	6.98	1.70
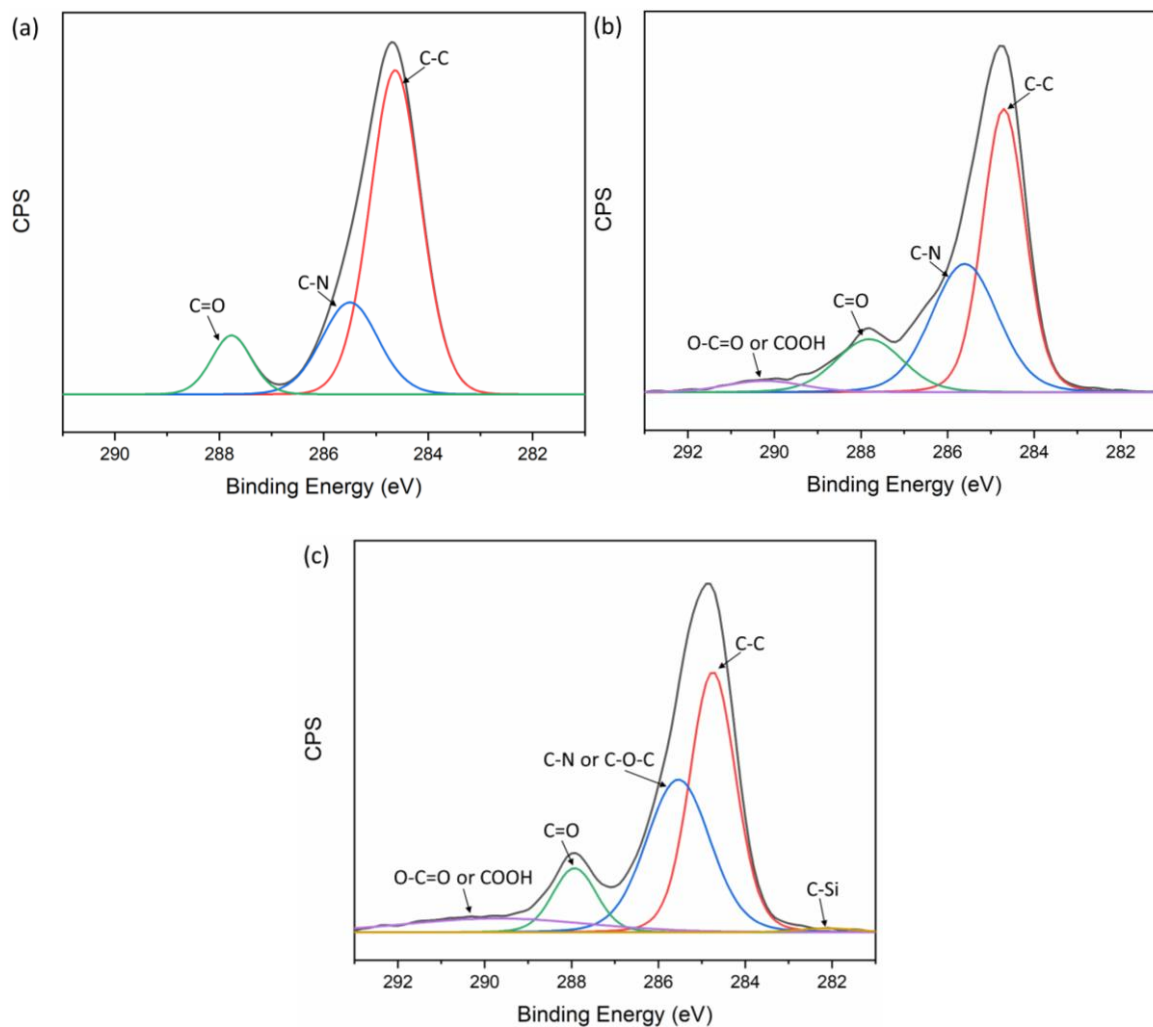
Figure 3.4. Normalized C 1s XPS spectra of (a) bare aramid fibers, (b) ANFs and (c) EANFs.
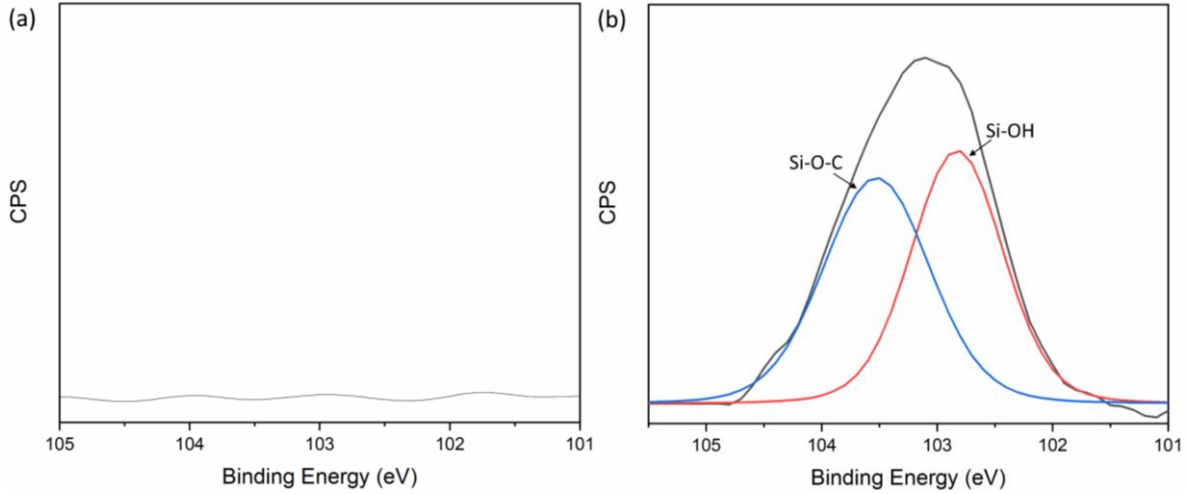
Figure 3.5. Normalized Si 2p XPS spectra of (a) ANFs and (b) EANFs.
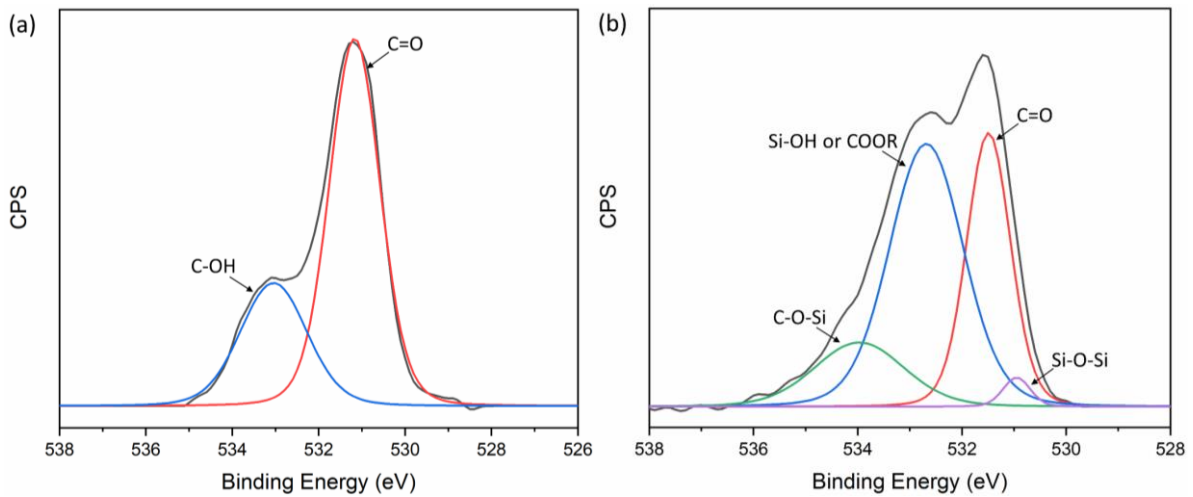
Figure 3.6. Normalized O 1s XPS spectra of (a) ANFs and (b) EANFs.

3.3 Fabrication and characterization of EANF reinforced epoxy nanocomposites

3.3.1 Fabrication of EANF reinforced epoxy nanocomposites

Epoxy nanocomposite specimens were prepared by adding varying weight fractions of EANFs, ranging from 0.2% to 2.0%, to the EPON 862 epoxy resin (diglycidyl ether of bisphenol-

F epoxy, received from Hexion) (Figure 3.1b). The EANFs were dispersed into the epoxy resin through horn sonication (Fisher Scientific Model 500) for 20 min and they were further mixed using shear mixer (FlackTek Speedmixer DAC 150.1 FVZ) for 15 min at 3000 rpm. Then 26.4 phr (part per hundred resin) of curing agent Epikure W was added to the mixture via centrifugal mixing for another 10 min. The final mixture was thoroughly degassed at 70 °C in a vacuum oven before it was cast into molds. After which a four-step curing procedure was used: first, room temperature to 121 °C for 30 min, followed by 121 °C for 120 min, 177 °C for 30 min, and finally 177 °C for 120 min. Epoxy specimens reinforced with untreated ANF and neat epoxy resin were also prepared using the same procedure described above.

3.3.2 Tensile properties

Tensile tests were conducted to investigate the effect of epoxy functionalization on the ANF reinforcement of the epoxy nanocomposites. The tensile tests were conducted at room temperature using an Instron universal load frame (Model 5982) with a 100 kN load cell. Standard type V dumbbell-shaped specimens were tested for the tensile tests at a crosshead speed of 1 mm/min following ASTM standard D638. Figure 3.7 shows the average tensile strength and Young's modulus of the EANF reinforced nanocomposites. From the figure, the Young's modulus was increased even with a nanofiber concentration as low as 0.2 wt %. However, the nanocomposite with 1 wt % nanofiber concentration showed the highest Young's modulus, 3.00 ± 0.11 GPa, which is approximately 16.8% higher than that of neat epoxy resin. The tensile strength of the nanocomposites was also observed to increase up to 88.9 ± 0.9 MPa at 1.0 wt %, displaying approximately 14.0% higher strength than that of the neat epoxy resin. When more than 1.0 wt % of the nanofibers was incorporated into the nanocomposites, the tensile strength and

Young's modulus were slightly decreased. This decrease with higher concentrations of ANFs is likely due to micro voids in the nanocomposites which are present even after the degassing process. The addition of the epoxy functionalized ANFs into the epoxy resin mixture resulted in a significant increase in viscosity, which causes micro void defects in the crosslinked nanocomposites.[115,116] However, despite the increased number of defects, the Young's modulus of 1.5 and 2.0 wt % nanocomposites were 14.7 and 13.0% higher than that of the neat resin, respectively, and the tensile strength of those nanocomposites were 12.4 and 12.9% higher compared to the neat resin, respectively.
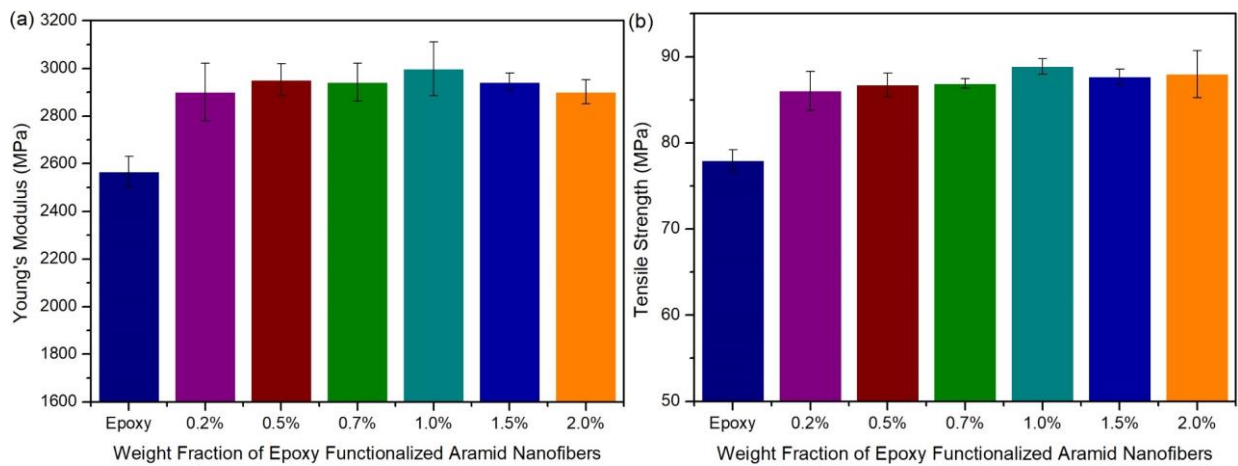
Figure 3.7. (a) Young's modulus and (b) tensile strength of EANF reinforced epoxy nanocomposites.

The introduction of chemical linkage between the epoxy resin matrix and the ANFs by the epoxy functionalization of the ANFs can lead to improved mechanical strength in comparison to conventional ANF reinforced epoxy nanocomposites. To prove this, epoxy nanocomposites reinforced with ANFs were prepared and tested using the same Instron load frame and testing conditions. Figure 3.8 shows the average Young's modulus, tensile strength and representative

stress-strain curves of the epoxy nanocomposites reinforced with ANFs and EANFs with concentrations up to 1.0 wt %. The untreated ANF reinforced epoxy resin specimens showed improved Young's modulus and tensile strength compared to the neat epoxy resin when the concentration of ANFs increased up to 1.0 wt %. However, the lowest average Young's modulus and tensile strength of EANF reinforced epoxy nanocomposites were found to be higher than the highest average Young's modulus and tensile strength of ANF reinforced samples. The 1.0 wt % EANF reinforced epoxy nanocomposites showed a 5.8% improved Young's modulus and a 4.3% improved tensile strength compared to the epoxy resin reinforced at the same weight fraction of untreated ANFs. These results confirm the effect of the epoxy functionalization on the mechanical properties of polymer nanocomposites. In addition to the characteristics of ANFs that are beneficial for the reinforcement of nanocomposites such as abundant polar functional groups on the surface and a large surface area, the epoxy functionalization produces covalent bonding between the ANFs and the epoxy matrix. The improved chemical interaction through the silane coupling agent between the ANFs and the polymer matrix improved their stress transferring efficiency which leads to enhanced mechanical properties of epoxy nanocomposites.[29,35,117]
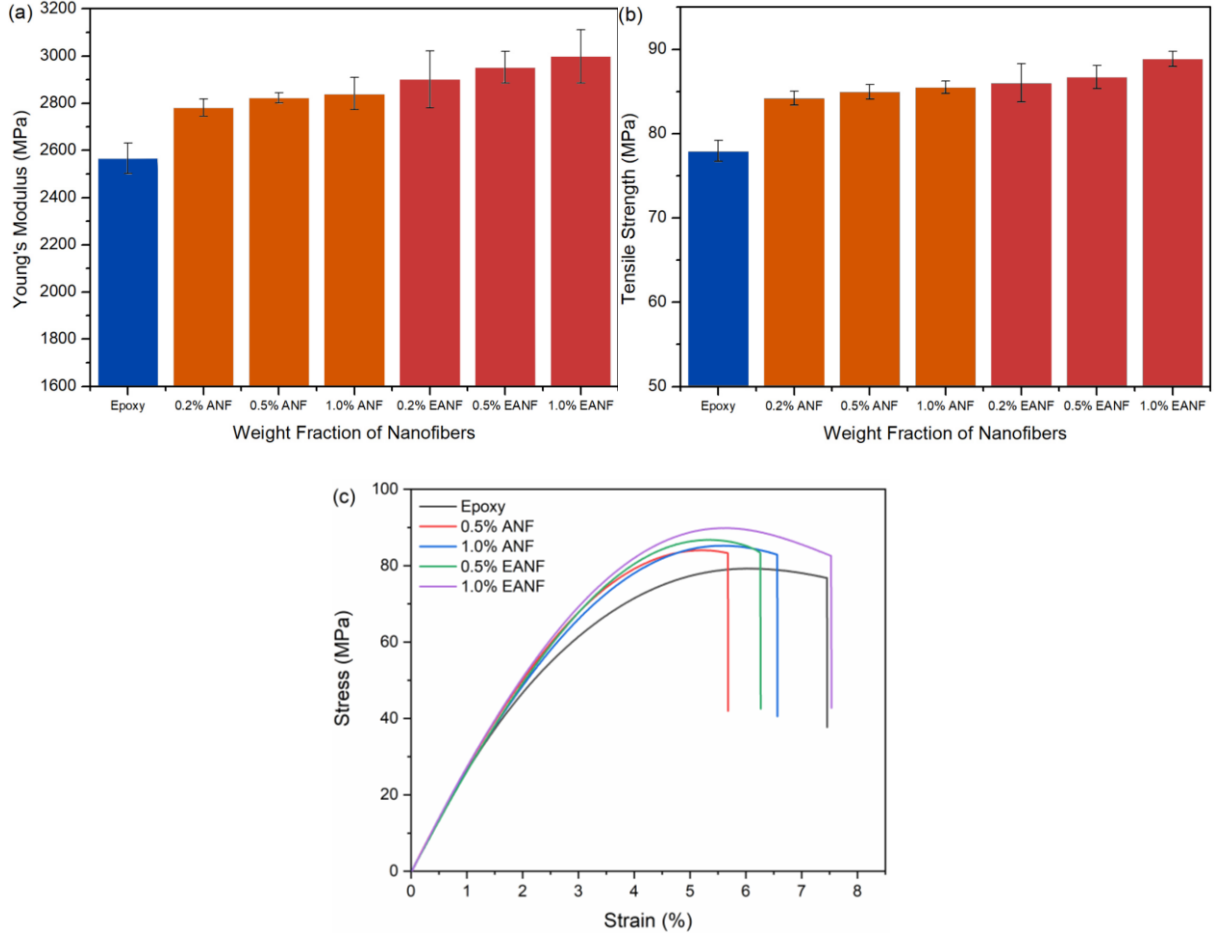
Figure 3.8. (a) Young's modulus, (b) tensile strength and (c) stress-strain curves of epoxy nanocomposites reinforced with ANFs and EANFs.

3.3.3 Fracture properties

Three-point bending tests using Single edge notch bend (SENB) specimens were performed to evaluate the fracture properties of the epoxy nanocomposites according to the requirements of ASTM D5045-99. The critical stress intensity factor (K_{Ic}) and fracture toughness (G_{Ic}) of the specimens were calculated using equation (3.1) and (3.3), respectively.

$$K_{Ic} = \frac{P_{max}}{BW^{\frac{1}{2}}} f(x) \tag{3.1}$$

$$f(x) = 6x^{1/2} \frac{[1.99 - x(1-x)(2.15 - 3.93x + 2.7x^2)]}{(1+2x)(1-x)^{3/2}}, x = a/W \tag{3.2}$$

58

$$G_{Ic} = \frac{K_{Ic}^2}{E}(1 - v^2) \tag{3.3}$$

where P_{max} is the peak load, B is the thickness of the specimen, W is the width of the specimen, a is the crack length, E is the Young's modulus measure from the tensile tests, and v is Poisson's ratio (assumed to be 0.353 for all samples). The average critical stress intensity factor, K_{Ic}, and fracture toughness, G_{Ic}, of nanocomposites reinforced with ANFs and EANFs are compared and shown in Figure 3.9a and 3.9b, respectively. Both ANF and EANF reinforced composites showed higher K_{Ic} and G_{Ic} than those for the neat epoxy resin. However, the highest K_{Ic} and G_{Ic} for the untreated ANF reinforced epoxy samples were lower than those for the EANF reinforced nanocomposites. Moreover, the K_{Ic} and G_{Ic} increased with increasing EANFs loading up to 1.5 wt % but those for the ANF reinforced epoxy nanocomposites slightly decreased at 1.5 wt % ANFs loading. The test results demonstrate that the nanocomposites reinforced with 1.0 wt % EANFs can improve the critical stress intensity factor by 139% and the fracture toughness by 376% compared to the neat epoxy resin. The samples with 1.5 wt % EANFs showed the highest enhancement in the critical stress intensity factor by 152% and the fracture toughness by 437%. The enhanced fracture toughness of the epoxy nanocomposites can be related to the role of ANFs and covalent bonding between the epoxy matrix and ANFs.[7] Energy can be dissipated at the interphase region because of the sliding of ANFs which can impede the crack propagation. The ANFs can also contribute to the crack bridging due to the high aspect ratio of the ANFs. The test results indicate that the crack bridging can be further enhanced by the improved chemical interaction between the matrix and ANFs based on the covalent linkages. Considering the tensile and fracture properties of the EANF reinforced epoxy nanocomposites, the EANFs can be considered as promising nanofillers that simultaneously improve the mechanical strength and fracture resistance.
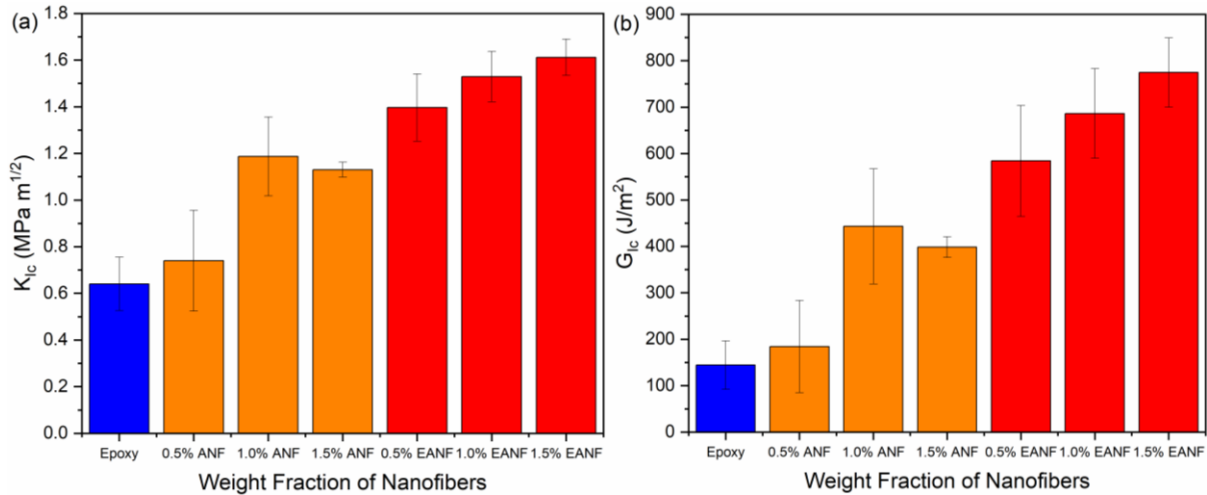
Figure 3.9. (a) Critical stress intensity factor, K_{Ic}, and (b) fracture toughness, G_{Ic}, of ANF and EANF reinforced epoxy nanocomposites.

3.3.4 Dynamic mechanical analysis

In addition to the tensile tests and fracture toughness tests, dynamic mechanical analysis was performed in tensile mode using a dynamic mechanical analyzer (TA DMA 800) to investigate the effect of the EANFs on the dynamic mechanical properties of epoxy nanocomposites. Specimens cut to dimensions 20.0 mm long x 4.0 mm wide x 2.0 mm thick were tested at 1 Hz with a constant heating rate of 3 °C/min starting from room temperature up to 200 °C in air. The storage modulus (E') and tan δ measured at 1 Hz frequency are plotted as a function of temperature and are shown in Figure 3.10 and 3.11, respectively, for both untreated ANF reinforced nanocomposites as well as EANF reinforced nanocomposites. The storage modulus was observed to decrease with increasing temperature for every sample and exhibited a relaxation around 130 °C, which is associated with the glass transition. Epoxy nanocomposites reinforced with ANFs and EANFs showed improved storage modulus both below and above the glass transition temperature.

Both ANF reinforced epoxy resins and EANF reinforced samples showed a maximum storage modulus at 1.0 wt % and slightly decreased storage modulus at 1.5 wt % which is a similar trend as the tensile testing. The addition of 1.0 wt % EANFs yielded a 13.4% increase in storage modulus at 40 °C over the neat epoxy resin while the same weight fraction of ANFs showed a similar storage modulus compared to the neat epoxy resin. The EANFs also improved the storage modulus of the nanocomposites at a higher temperature in the rubbery state as shown in Table 3.2. The results can be explained in terms of chemical interfacial interaction between the ANFs and the epoxy matrix. The interfacial interaction improved due to the epoxy functionalization of ANFs, and the mobility of the epoxy main chain can be restricted by the bonding between the ANFs and the epoxy matrix.[27,117,118] However, the untreated ANFs improved storage modulus less than EANFs which is attributed to the relatively weaker interfacial bonding between the untreated ANFs and the epoxy matrix.

The storage modulus of the composites can be predicted by theoretical models. Einstein suggested a simple equation to estimate the storage modulus using a volume fraction of the fillers in the composites.[119,120]

$$E_c = E_m(1 + V_f) \tag{3.4}$$

where E_c and E_m are the storage modulus of the composite and the matrix, respectively, and V_f is the volume fraction of the filler. The equation was modified by Guth as follows.[119,120]

$$E_c = E_m(1 + 2.5V_f + 14.1V_f{}^2) \tag{3.5}$$

Mooney suggested an exponential relation about the storage modulus of composites.[119,120]

$$E_c = E_m e^{\frac{2.5V_f}{1-SV_f}} \tag{3.6}$$

where S is the crowding factor that is defined as the ratio of the apparent volume of the filler to the true volume occupied by the filler. Here, S was taken to be 1 because it was reported in previous

studies for filler loading up to 30 wt %. The experimental storage modulus results of ANF and EANF reinforced epoxy in the glassy and rubbery state were compared with the theoretical predictions based on the models above and summarized in Table 3.2. It was observed that the models could predict the storage modulus of the EANF reinforced epoxy composites in the glassy state. However, the predictions using the models deviated from the experimental values for both ANF and EANF reinforced epoxy samples in the rubbery state.

The tan δ value is a ratio of the loss modulus to the storage modulus and is related to the amount of mobile polymer chains and the energy dissipation at the matrix and filler interface. The neat epoxy showed the highest tan δ peak value which decreased as the weight fraction of ANFs and EANFs increased. The lowered tan δ peak values indicate that the incorporation of ANFs and EANFs in the epoxy matrix limits the epoxy main chain movement and the energy dissipation process is slowed down by the ANFs and EANFs.[38,121] The tan δ peak values can be used to estimate the amount of constrained chains of epoxy resin based on the relationship between the energy loss fraction of the polymer nanocomposites (W) and tan δ value used by Zhang et al and Vijayan et al.[122,123]

$$W = \frac{\pi \tan \delta}{\pi \tan \delta + 1} \tag{3.7}$$

The energy loss fraction W can be expressed by the amount of constrained region by the following equation.

$$W = \frac{(1-C)W_0}{1-C_0} \tag{3.8}$$

where C and C_0 are the volume fraction of the constrained region of epoxy nanocomposites and neat epoxy resin, respectively, and W_0 is the energy loss fraction of the constrained region of neat epoxy resin. The energy loss fraction (W) of the ANF and EANF reinforced epoxy nanocomposites

can be calculated using the tan δ peak values according to the equation (3.8). The equation is rearranged as follows.

$$C = 1 - \frac{(1-C_0)W}{W_0} \qquad (3.9)$$

The value of C_0 is taken to be 0 for totally amorphous phase in epoxy matrix. Then, the fraction of the constrained region of ANF and EANF reinforced epoxy nanocomposites can be estimated from the equation (3.9) using calculated W values and summarized in Table 3.3. The values of C tend to increase with increasing ANFs and EANFs content and the values for the EANF reinforced epoxy resin are higher than those for the ANF reinforced epoxy resin up to 1 wt %. The results show that the enhanced interfacial interaction between ANFs and the matrix can effectively cause the configurational constraints of the epoxy chains which improve the fraction of constrained region and mechanical properties in the nanocomposites.[124]

The values of the glass transition temperature, T_g, were determined from the maxima of the tan δ peaks in Figure 3.11. The glass transition temperature versus the weight percent of ANFs and EANFs is summarized in Table 3.3. The T_g values of the 0.5 and 1.0 wt % ANF reinforced epoxy samples were slightly lower than that of the neat epoxy resin samples. However, the 1.5 wt % ANF reinforced epoxy showed an increased glass transition temperature. In contrast, it is shown that the T_g increased as more EANFs were incorporated into the nanocomposites. It is known that the glass transition behavior of a pure polymer or nanocomposites depends on the mobility of polymer chains in the matrix. The T_g can be affected by the chemical structure and flexibility of the polymer chains, and the nature and morphology of the nanofillers. The shifting of T_g to higher temperature corresponds to the decreased mobility of the polymer chains by the addition of nanofillers and the improved interfacial adhesion between the matrix and the nanofillers.[119,125] The incorporation of EANFs in the epoxy matrix may hinder the movement of polymer chains and

minimize the empty or free space in the matrix.[28,126] Moreover, the formation of covalent linkages between the ANFs and the epoxy matrix during the curing of resin restricts the mobility of the crosslinked epoxy structure which contributed to increase the T_g.[27,29,35,117] A similar trend was reported in another study where the addition of epoxy functionalized graphene oxide to an epoxy matrix increased the T_g as the amount of functionalized graphene oxide increased.[35] In another study, epoxy nanocomposites reinforced with silane treated carbon nanofibers showed a higher T_g than the nanocomposites reinforced with untreated carbon nanofibers.[27] These results thus further confirm the improved chemical interaction and interfacial adhesion between the EANFs and the epoxy matrix.
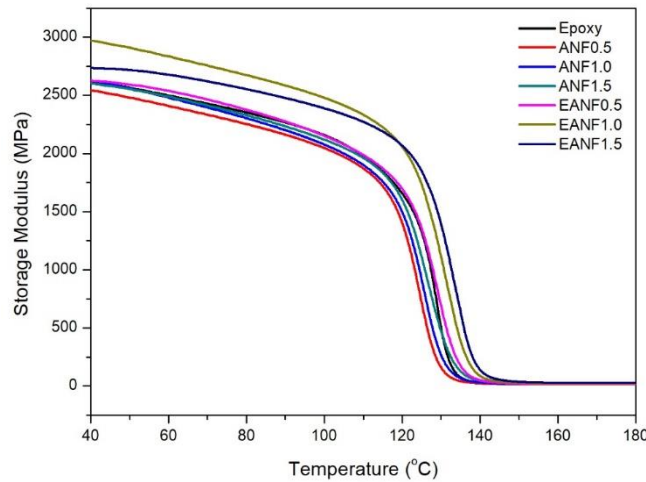
Figure 3.10. Storage modulus of ANF and EANF reinforced epoxy nanocomposites containing different weight fractions from 40 to 180 °C.
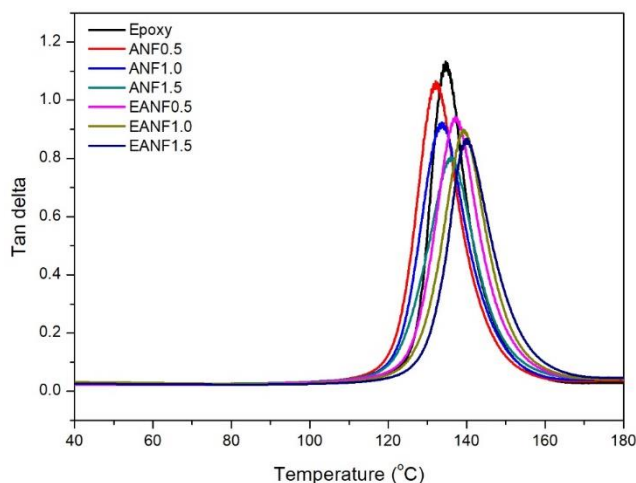
Figure 3.11. Tan δ of epoxy nanocomposites containing different weight fractions of ANFs and EANFs from 40 to 180 °C.

Table 3.2. Comparison of experimental and predicted storage modulus of ANF and EANF reinforced epoxy nanocomposites.

Fiber content (wt %)	ANF (Exp.)		EANF (Exp.)		Einstein		Guth		Mooney	
	E' at 40 °C (GPa)	E' at 160 °C (MPa)	E' at 40 °C (GPa)	E' at 160 °C (MPa)	E' at 40 °C (GPa)	E' at 160 °C (MPa)	E' at 40 °C (GPa)	E' at 160 °C (MPa)	E' at 40 °C (GPa)	E' at 160 °C (MPa)
0	2.62	15.72	2.62	15.72	2.62	15.72	2.62	15.72	2.62	15.72
0.5	2.54	15.90	2.63	19.96	2.63	15.80	2.65	15.92	2.65	15.92
1.0	2.63	18.98	2.97	24.27	2.65	15.88	2.69	16.14	2.69	16.12
1.5	2.60	23.46	2.74	29.01	2.66	15.96	2.73	16.36	2.72	16.33

Table 3.3. Summary of T_g, and constrained region for ANF and EANF reinforced epoxy nanocomposites.

Sample	T_g (°C)	Constrained region (C)
Epoxy resin	134.1	-
ANF 0.5 wt %	132.1	0.012
ANF 1.0 wt %	133.6	0.045

ANF 1.5 wt %	136.4	0.081
EANF 0.5 wt %	137.1	0.040
EANF 1.0 wt %	139.2	0.052
EANF 1.5 wt %	139.8	0.061

3.4 Chapter summary

In this chapter, EANFs were prepared through chemical treatment of the ANFs with a glycidyl ether silane coupling agent, and EANF reinforced epoxy nanocomposites were fabricated and tested to elucidate the impact of chemical bonding on the effectiveness of the polymer nanofiber reinforcement. The surface functionality of the ANFs were identified by FTIR and XPS before and after the ANFs were functionalized through silane treatment. The tensile properties, fracture properties and viscoelastic behavior of the EANF reinforced epoxy nanocomposites were studied and compared with neat epoxy resin and conventional ANF reinforced epoxy nanocomposites. The epoxy functional groups on the surface of the ANFs provided chemical linkages between the epoxy matrix and ANFs which was shown to enhance the overall mechanical properties of the nanocomposites. The experimental results showed that the Young's modulus and tensile strength of 1 wt % EANF reinforced nanocomposites increased by 16.8% and 14.0%, respectively. The 1 wt % EANF reinforced nanocomposites showed a 5.8% higher Young's modulus and a 4.3% higher tensile strength compared to the nanocomposites reinforced with the same weight fraction of untreated ANFs. Fracture toughness of the EANF reinforced epoxy composites also increased by 376% and 437% with the addition of 1.0 and 1.5 wt % EANFs, respectively. In dynamic mechanical analysis, the storage modulus increased by 13.4% for 1.0 wt % EANF reinforced nanocomposites compared to the neat epoxy resin at 40 °C, and the glass transition temperature increased as the amount of EANFs within the epoxy matrix increased. Thus,

through a simple modification of the ANFs, further enhancement of mechanical strength and viscoelastic properties were achieved for polymer nanocomposites.

Chapter 4

Synergetic Effect of Aramid Nanofiber-Graphene Oxide Hybrid Filler on the Properties of Rubber Compounds for Tire Tread Application

4.1 Chapter introduction

This chapter establishes the use of aramid nanofiber (ANF)-graphene oxide (GO) hybrid filler for the application of tire tread rubber compounds. The properties of rubber compounds used in tire tread largely contribute to the overall performance of tires in vehicles. Among the various ingredients used, reinforcing fillers are known for having the most significant effect on the static and dynamic properties of rubber compounds. As shown in our previous chapter, silane coupling agent modified ANFs improved the properties and performance of tire tread rubber compounds without deteriorating other properties. In addition to the use of one class of reinforcing fillers, the combination of two strong nanomaterials and the synergistic effect of the hybrid materials on the properties of polymer matrices have been investigated by researchers. In this work, two strong nanoscale materials, ANFs and GOs, are modified using a silane coupling agent and combined to form a novel hybrid filler. The functionalized ANF/GO (fANF/GO) hybrid filler is obtained by adding functionalized GOs (fGOs) into functionalized ANFs (fANFs). The fANF/GO reinforced rubber compounds are then fabricated and tested to investigate the effect of the novel hybrid filler on mechanical and dynamic mechanical properties. The prepared rubber compounds using hybrid fillers exhibit improved mechanical properties and abrasion resistance compared to rubber compounds only reinforced using fANF or fGO alone and reference compounds. Moreover, dynamic mechanical analysis reveals a 21.8% decrease in the rolling resistance of fANF/GO

reinforced rubber samples while preserving wet grip performance. Thus, this research demonstrates the potential of the ANFs and GOs-based functionalized hybrid fillers for the application of high-performance tire treads.

4.2 Preparation and characterization of fANF/GO hybrid filler

4.2.1 Preparation of fANF/GO hybrid filler

ANF/DMSO suspensions were prepared using the method developed by Yang et al.[4] A mixture consisting of Kevlar® (2 g, CS-800), potassium hydroxide (KOH, 3 g, Fisher Scientific), and dimethyl sulfoxide (DMSO, 1000 mL, Fisher Scientific) was stirred for 7 days at 25 °C until an ANF suspension is formed. In order to functionalize the ANFs' surfaces, 10 wt % of bis(triethoxysilylpropyl)tetrasulfide (TESPT, provided by Evonik) was added to the prepared suspension, which was then stirred at 80 °C for 24 h. Concurrently, GOs were synthesized using the modified Hummer's method using a preoxidized graphite precursor.[127] The prepared GOs (2 g) were dispersed in DMSO (500 mL), followed by the addition of 10 wt % of TESPT, and then stirring at 80 °C for 24 h. The functionalized GO/DMSO solution and the functionalized ANF/DMSO solution were combined and stirred at room temperature for 4 h to prepare functionalized ANF/GO hybrid filler (fANF/GO) (Figure 4.1).

An equivalent amount of deionized water to DMSO was added to the final mixture to isolate the fANF/GOs, which were then collected using a vacuum-assisted filtration process. The fANF/GOs were then washed with deionized water and acetone several times to neutralize the highly basic solution and remove any unreacted chemicals. The obtained fANF/GOs were dispersed in water using sonication (Fisher Scientific Sonic Dismembrator Model 500) and then slightly dried to form an fANF/GO paste with 90 wt % water content. Functionalized ANFs

(fANFs) and functionalized GOs (fGOs) were also prepared using the previously described procedures for comparison.
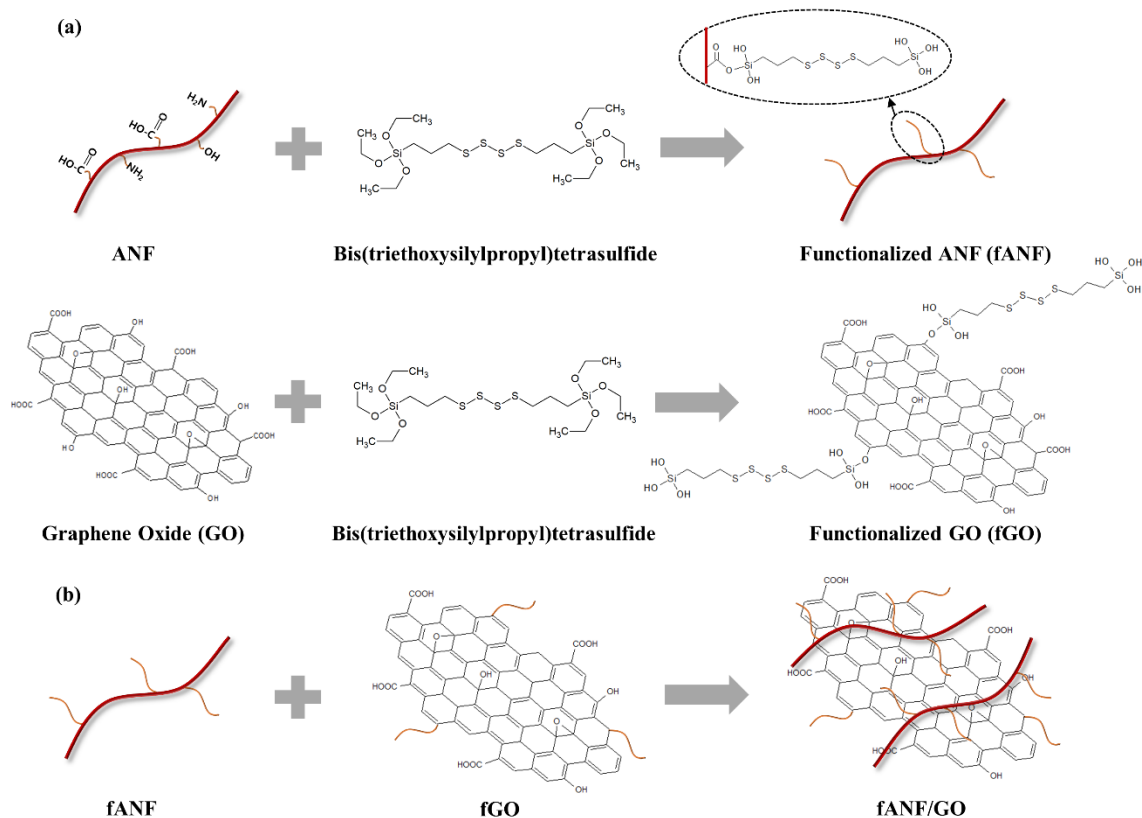
Figure 4.1. Illustration of the preparation of (a) fANF and fGO, and (b) fANF/GO hybrid filler.

4.2.2 Characterization of fANF/GO hybrid filler

The chemical compositions of the fANF, fGO, and fANF/GO before and after functionalization were characterized by attenuated total reflectance– Fourier transform infrared spectroscopy (ATR-FTIR), which was performed on a spectrometer (Nicolet iS60) equipped with a SMART iTR accessory. The FTIR spectra of fANFs, fGOs, and fANF/GOs before and after the functionalization and combination are shown in Figure 4.2. The characteristic peaks displayed by

ANFs after the dissolution of aramid fibers are consistent with those previously reported.[6,69,72,76] From the results in Figure 4.2a, the functionalization of the ANFs was confirmed based on the appearance of new characteristic peaks. Following functionalization, a peak at 2920 cm^{-1} corresponding to the methylene stretching vibration in the TESPT is observed in the fANFs' FTIR spectrum. The peaks at 1246, 1199, 1100, 1017, and 950 cm^{-1} are also attributed to the CH_2 wagging in $-CH_2-S-$, $Si-CH_2-R$, Si-O, Si-O-C, and Si-O stretching vibration, respectively, as a result of functionalization. Similar to fANFs, fGOs display a new methylene stretching vibration peak at 2920 cm^{-1} post-functionalization, as shown in Figure 4.2b. In addition to the new peak, the fGOs display CH_3 stretching, CH_2 wagging, Si-O-C, and Si-O stretching vibration peaks at 1391, 1298, 1017, and 950 cm^{-1}, respectively, after treatment. These new representative peaks confirm the introduction of a silane coupling agent on the surface of both ANFs and GOs. Once functionalized, both fANFs and fGOs were combined to obtain the fANF/GO hybrid fillers, which were subsequently characterized using FTIR. As seen in Figure 4.2c, the fANF/GOs FTIR spectra display the main characteristic peaks of both fANFs and fGOs. Thus, the chemical structural changes detected by FTIR confirm the functionalization of the ANFs and GOs in addition to their successful combination to form a new hybrid nanofiller.

71
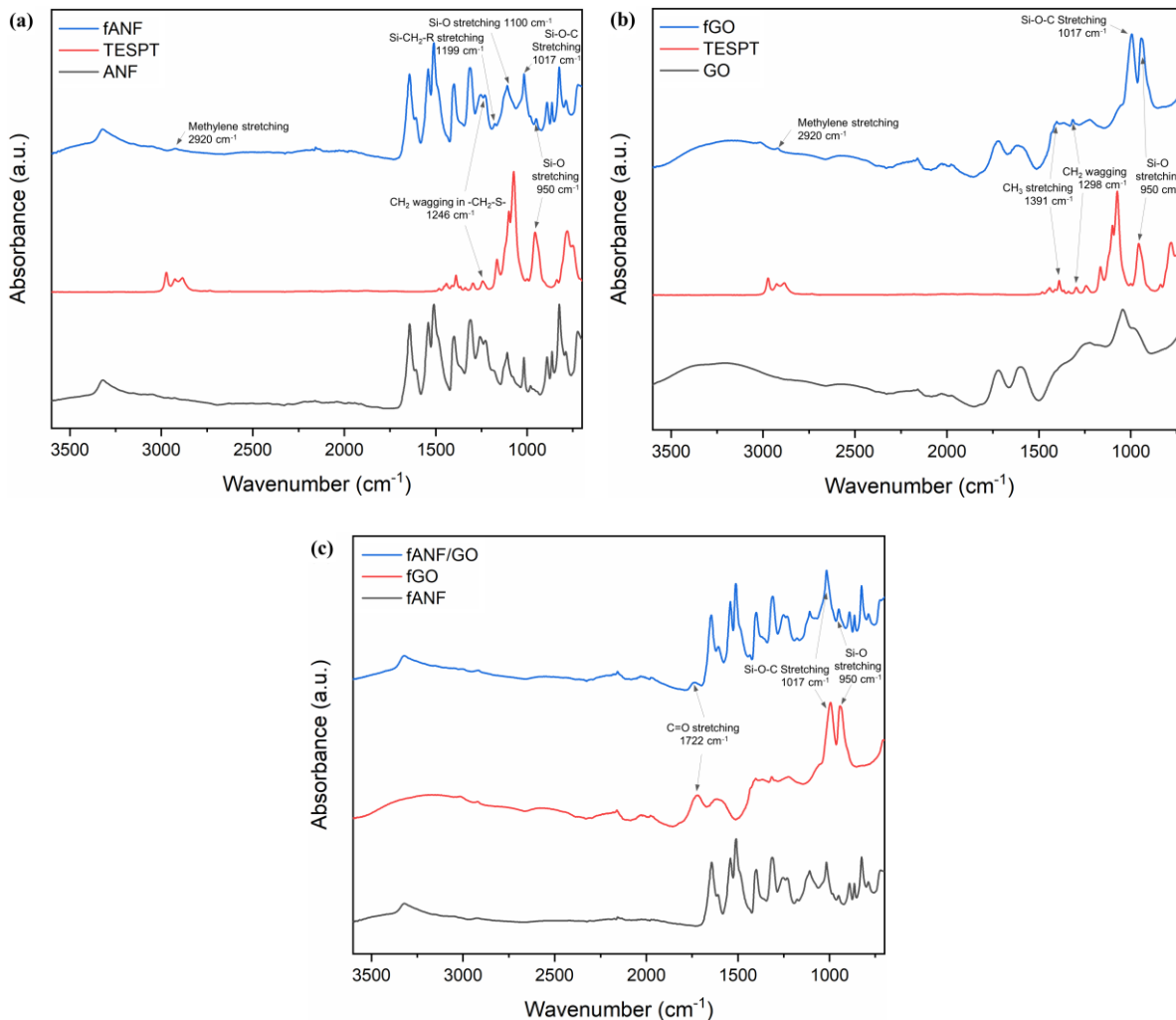
Figure 4.2. FTIR spectra of (a) fANFs, (b) fGOs, and (c) fANF/GOs.

The structure of the combined fillers was also characterized using X-ray diffraction (XRD) analysis and is shown in Figure 4.3a. The XRD patterns were monitored using CuKα radiation (λ = 0.154 nm) on an X-ray diffractometer (Rigaku Ultima IV). Due to the crystalline structure of Kevlar, the XRD patterns of both ANFs and fANFs display the characteristic peaks at 20.6° and 22.9°, corresponding to the 110 and 200 planes of Kevlar, respectively.[4,128] In contrast, GOs show a sharp characteristic peak at 12.8° with a d-spacing of 0.69 nm. However, the characteristic peak was observed to shift to 12.1° post-TESPT functionalization, corresponding to a d-spacing

of 0.74 nm. These results confirm the disruption of interlayer packing of GOs through functionalization.[50] Once fANFs and fGOs are combined, a small peak at 12.1° is observed, which is attributed to the characteristic peak of fGOs. Moreover, two peaks are also found at 20.6° and 22.9°, corresponding to the characteristic peaks of fANFs. The ultraviolet-visible spectroscopy (UV-vis) was also used to confirm the preparation of the fANF/GOs. UV-vis spectrophotometer (PerkinElmer Lambda 950) was used to obtain UV-vis spectra in the range between 250 and 800 nm. As seen in Figure 4.3b, fANFs, fGOs, and fANF/GOs all show a shoulder peak near 300 nm, which is attributed to the tetrasulfide in the TESPT.[129] Moreover, the ANF characteristic absorption peak at 335 nm is present in both the UV-vis spectra of fANFs and fANF/GOs.[4,68] These UV-vis spectra thus confirm the combination of fANFs and fGOs, and the functionalization of the hybrid fillers. Additionally, AFM scans using Park XE-70 shown in Figure 4.4 provide further information on the morphology and dimensions of fANFs, fGOs, and fANF/GOs. The diameters of fANFs are measured to range between 5 nm and 12 nm, which is consistent with previously reported studies,[69,130] while the thickness of fGOs is measured to be 1.6 nm, which is in good agreement with the results reported by Wu et al.[50] Furthermore, atomic force microscopy (AFM) scans of fANF/GOs indicate that fANFs are located on the surface and edge of fGOs, which confirms the interaction between them. Drawing from the FTIR, XRD, UV-vis, and AFM results, fANF/GOs can be considered as a hybrid filler that combines fANFs and fGOs through noncovalent interactions. The new hybrid filler can be useful for the reinforcement of the rubber matrix by establishing covalent bonding between the matrix and fillers, in addition to the noncovalent interfacial interactions between fANFs and fGOs.
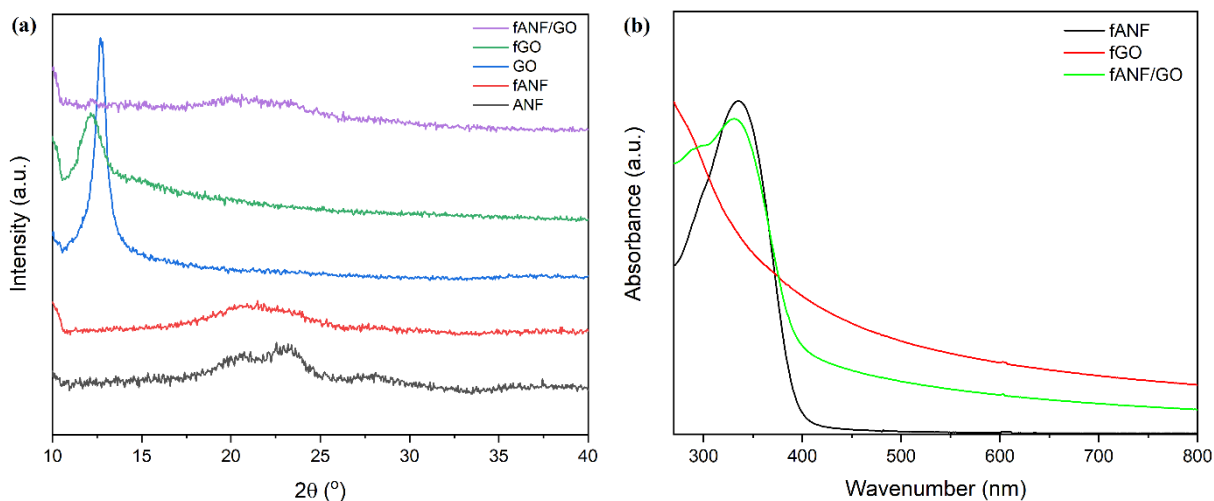
Figure 4.3. (a) XRD patterns of ANFs, fANFs, GOs, fGOs, and fANF/GOs and (b) UV-vis spectra of fANFs, fGOs, and fANF/GOs.
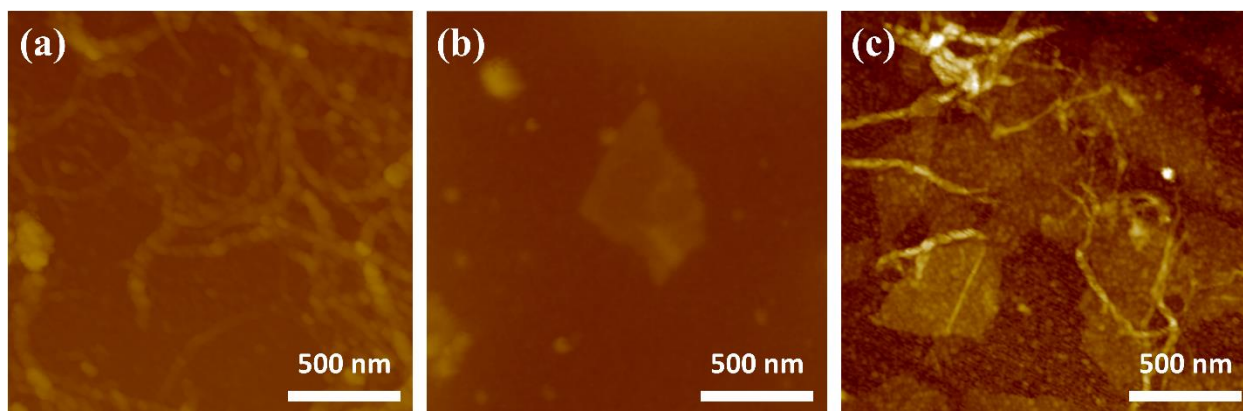
Figure 4.4. AFM scans of (a) fANFs, (b) fGOs, and (c) fANF/GOs.

4.3 Preparation and characterization of fANF/GO reinforced rubber compounds

4.3.1 Preparation of fANF/GO reinforced rubber compounds

A Brabender Plasti-corder internal mixer was used to prepare the fANF/GO reinforced rubber compounds according to the recipes presented in Table 4.1. The rubber compounding was conducted at fill factors of 70% and temperatures ranging between 145 and 150 °C. In the first

stage, SBR SOL-6270M (containing 37.5 parts of treated distillate aromatic extract oil, received from KKPC) and butadiene rubber KBR 01 (received from KKPC) were added to the mixer and blended for 1 min, before introducing carbon black (N339, provided by Birla Carbon), zinc oxide (received from Akrochem), stearic acid (received from Akrochem), and naphthenic oil (received from R.E. Carroll), followed by mixing for an additional 1 min. Then, fANF/GO was added to the rubber compound and mixed for an additional 5 min. The evaporation of water in the fANF/GO hybrid nanofiller was confirmed by the weight of the dumped mixture. In the second stage, sulfur and n-cyclohexyl-2-benzothiazole sulfonamide (CBS, received from Akrochem) were added to the original mixture and then mixed for 3 min prior to vulcanization using a hot press. The cure characteristics of rubber compounds were obtained using a Monsato MDR 2000 at 160 °C for 40 min.

Table 4.1. Recipes of reference, fANF, fGO, and fANF/GO reinforced rubber compounds (unit: phr, part per hundred parts of rubber).

Ingredients	Reference	0.3	0.7	1	2	3
SOL-6270M	96.25	96.25	96.25	96.25	96.25	96.25
KBR01	30	30	30	30	30	30
N339	50	49.7	49.3	49	48	47
fANF, fGO, or fANF/GO	-	0.3	0.7	1	2	3
Naphthenic oil	3.75	3.75	3.75	3.75	3.75	3.75
Zinc oxide	3	3	3	3	3	3
Stearic acid	1	1	1	1	1	1
Sulfur	1.5	1.5	1.5	1.5	1.5	1.5
CBS	2.2	2.2	2.2	2.2	2.2	2.2

4.3.2 Characterization and testing of fANF/GO reinforced rubber compounds

The crosslink density was measured and calculated through the swelling method using toluene according to the procedure described in chapter 2. Additionally, both tensile testing and dynamic mechanical analysis were performed on the reference and functionalized fillers reinforced compounds to investigate the effect of these fillers on their mechanical properties. Tensile testing was performed using an Instron universal load frame (Model 5982) at room temperature, where dumbbell-shaped specimens (ASTM D412 type C) were loaded at a 500 mm/min crosshead speed until failure. Viscoelastic properties were also determined in tensile mode using a dynamic mechanical analyzer (DMA TA Q800). Specimens with dimensions of 40.0 mm × 6.0 mm × 2.0 mm were mechanically loaded in air at 10 Hz, 0.5% strain, and a constant heating rate of 3 °C min^{-1} and temperatures ranging between -60 °C and 60 °C. The abrasion resistance was evaluated using a DIN abrasion tester (Aveno Technology) according to the DIN 53516 standard. Specimens with dimensions of 16 mm in diameter and 8 mm in thickness were prepared and abraded on a cylinder-type drum rotating at a speed of 40 rpm. The weight of the sample was measured before and after the abrasion, and equation (4.1) was used to calculate the abrasion loss.

$$A_A = \frac{\Delta m_t \times S_0}{d_t \times S} \tag{4.1}$$

where A_A is the loss from the abrasion (mm^3), Δm_t is the loss in mass (mg), d_t is the compound's density (g cm^{-3}), S is the abrasive grade (mg), and S_0 is the nominal abrasive grade (200 mg). The abraded surfaces of rubber compound samples were observed using a JEOL JSM-7800FLV field-emission scanning electron microscope (FE-SEM).

4.3.3 Mechanical properties

The mechanical properties of fANF, fGO, and fANF/GO reinforced rubber compounds were determined using tensile testing. Table 4.2 shows the average modulus at 100% and 300% elongation, tensile strength, and elongation at break of the rubber compounds, while their corresponding stress-strain curves are displayed in Figure 4.5. According to the tensile test results, fANF, fGO, and fANF/GO are found to be a viable alternative to carbon black due to their capability of improving the mechanical properties of rubber compounds. Despite all the prepared compounds having the same filler loading of 50 phr, the average tensile strength and elongation at break were found to be improved when incorporating fANF, fGO, and fANF/GO hybrid fillers. Specifically, fGO reinforced samples were found to exhibit a maximum tensile strength and elongation at break of 17.78 MPa and 648.9%, yielding 35.3% and 48.9% improvements compared to the reference compound, respectively. However, the 100% and 300% moduli of fGO reinforced rubber compounds were found to display a decreasing trend with increasing fGO content in compounds. In contrast, the moduli of rubber compounds reinforced with 0.3 to 3 phr of fANFs were found to be higher than those of the reference compound, yet their elongation at break was measured to be decreased compared to fGO reinforced samples. Given the contrast in mechanical performance, the overall tensile properties of fANF/GO hybrid filler reinforced rubber samples were found to be approximately a combined average of those of fANF and fGO reinforced rubber samples. When compared to reference compounds, the fANF/GO reinforced rubber compounds displayed improved tensile strength, 100% and 300% moduli, and elongation at break, therefore suggesting that a comprehensive reinforcement effect of fANF/GO in the rubber. According to the tensile testing results, these new hybrid fillers outperform carbon black when it comes to improving the mechanical properties of rubber compounds. These results can be explained by

77

examining the unique characteristics of both fANFs and fGOs. As investigated in our previous work, the large specific area and high aspect ratio of fANFs, along with their excellent strength and stiffness derived from their aramid molecular structure, can significantly contribute to reinforcing the rubber matrix.[130] Similarly, fGOs also have an extraordinarily high specific surface area and mechanical properties, which are beneficial for their performance as nano-reinforcement.[50,52,89] In addition to their physical characteristics, the strong interfacial interactions between these nanofillers and the rubber matrix through covalent linkage afforded by the silane coupling agent can also yield improvement in the overall mechanical properties, as proven by previous works.[50,130] The enhancement of the interaction between the fillers and rubber matrix can also be confirmed using crosslink density measurements in the rubber samples, which are detailed in Table 4.2. As the concentration of fANFs, fGOs, and fANF/GOs in the rubber compounds is increased, the calculated crosslink density is also observed to increase. The crosslink densities of fGO reinforced rubber samples were found to be higher than those of the reference samples, fANF and fANF/GO reinforced rubber samples, which is in agreement with the previously discussed trend in tensile strength. This enhancement of crosslink density can be attributed to the characteristics of the new fillers that can contribute to improving load and stress transfer within the rubber matrix through the chemical covalent bonding.
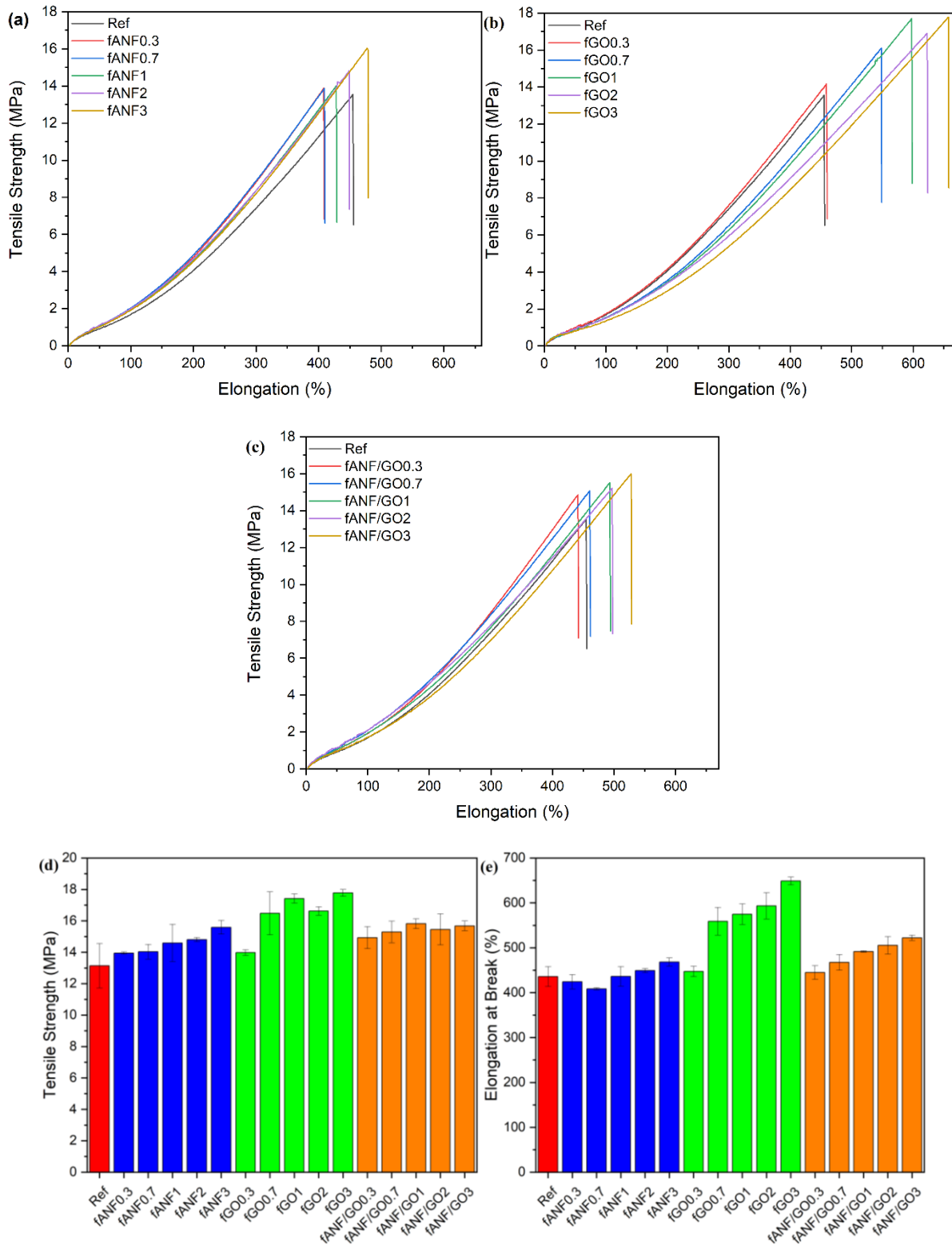
Figure 4.5. Stress-strain curves of (a) fANF0.3 to fANF3 samples, (b) fGO0.3 to fGO3 samples, and (c) fANF/GO0.3 to fANF/GO3 samples, and (d) tensile strength and (e) elongation at break of samples.

79

Table 4.2. Tensile test, and crosslink density measurement results of fANF, fGO, and fANF/GO reinforced rubber samples.

Parameters	100% Modulus (MPa)	300% Modulus (MPa)	Tensile Strength (MPa)	Elongation at Break (%)	Swelling Ratio, Q	Crosslink Density, ν_e (10^{-4} mol cm^{-3})
Reference	1.71 ± 0.01	7.61 ± 0.09	13.14 ± 1.42	435.9 ± 22.1	2.53	2.04
fANF0.3	1.91 ± 0.06	8.38 ± 0.42	13.95 ± 0.07	424.2 ± 16.1	2.47	2.15
fANF0.7	2.08 ± 0.06	9.02 ± 0.27	14.03 ± 0.47	408.5 ± 2.5	2.40	2.30
fANF1	1.96 ± 0.01	8.51 ± 0.10	14.59 ± 1.19	436.1 ± 21.7	2.34	2.44
fANF2	2.01 ± 0.05	8.37 ± 0.08	14.81 ± 0.13	449.1 ± 4.7	2.35	2.40
fANF3	1.93 ± 0.01	8.25 ± 0.02	15.59 ± 0.44	468.3 ± 9.1	2.25	2.64
fGO0.3	1.80 ± 0.05	7.82 ± 0.20	13.98 ± 0.18	447.3 ± 11.5	2.16	2.87
fGO0.7	1.53 ± 0.01	6.48 ± 0.07	16.48 ± 1.37	558.8 ± 30.9	2.22	2.72
fGO1	1.57 ± 0.05	6.63 ± 0.35	17.42 ± 0.29	574.8 ± 22.8	2.11	3.04
fGO2	1.57 ± 0.06	6.28 ± 0.32	16.63 ± 0.27	593.3 ± 29.4	2.15	2.93
fGO3	1.38 ± 0.03	5.51 ± 0.17	17.78 ± 0.22	648.9 ± 8.7	2.02	3.32
fANF/GO0.3	1.88 ± 0.04	8.39 ± 0.09	14.93 ± 0.70	444.9 ± 15.0	2.41	2.28
fANF/GO0.7	2.06 ± 0.01	8.29 ± 0.06	15.29 ± 0.69	467.4 ± 17.4	2.36	2.40
fANF/GO1	2.00 ± 0.05	7.92 ± 0.26	15.82 ± 0.31	491.6 ± 1.5	2.16	2.90
fANF/GO2	2.05 ± 0.05	7.68 ± 0.13	15.45 ± 0.99	505.4 ± 19.5	2.15	2.93
fANF/GO3	1.69 ± 0.03	6.93 ± 0.05	15.68 ± 0.32	522.0 ± 5.9	2.09	3.12

4.3.4 Abrasion resistance

In addition to the tensile properties, the abrasion resistance of fANF, fGO, and fANF/GO reinforced rubber compounds was studied using abrasion resistance testing. The collected measurements were converted to abrasion resistance indexes by determining the ratio of abrasion loss of the reference compound to that of the nano-reinforced specimens. Figure 4.6 shows the test

results of rubber compounds reinforced with 50 phr of total fillers, including 0.3 to 3 phr of new fillers. When examining test results, it can be seen that the fANF, fGO, and fANF/GO reinforced samples all showed improved abrasion resistance in comparison to that of the reference sample. Upon adding 1 phr of new fillers, the average abrasion resistance of the fANF, fGO, and fANF/GO reinforced samples displayed 11.0%, 14.2%, and 18.2% improvements, respectively. These test results suggest that the new functionalized fillers can enhance the abrasion resistance of rubber compounds, which is in agreement with the improved mechanical strength and toughness of these compounds previously concluded from tensile testing and crosslink density measurements. Moreover, the maximum abrasion resistance displayed by fANF/GO reinforced rubber compounds highlights the synergetic effect of the fANFs and fGOs for the reinforcement of the rubber matrix. This can be explained by the interaction between the fANFs and fGO, which reduces the stress concentrations in the rubber matrix by transferring it from the fANFs to the surface of fGOs.[68] Following abrasion resistance testing, the abraded surfaces of rubber compounds were examined using SEM imaging in order to further understand the effect of new fillers on rubber abrasion, and are shown in Figure 4.7. Post-abrasion, ridges were formed on the abraded rubber surfaces due to the detachment of abraded particles. While the abraded surface of the reference sample shows a rough texture, the abraded surfaces of fANF, fGO, and fANF/GO reinforced samples clearly display a considerable decrease in roughness. A large amount of debris and higher ridges were observed on the abraded surface of the reference compound, which corresponds to the high abrasion volume.[90,131] However, relatively lower ridges were formed on the surface of compounds reinforced with new fillers, showing low abrasion loss. Therefore, the observed characteristics of the abraded surfaces correlate well with the abrasion resistance test results.
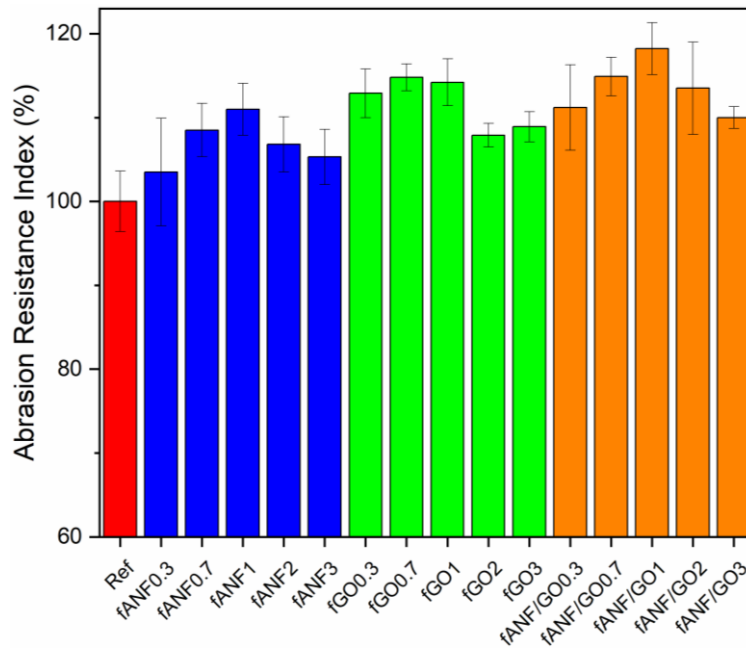
Figure 4.6. Abrasion resistance indexes of rubber compounds reinforced with fANFs, fGOs, and fANF/GOs.
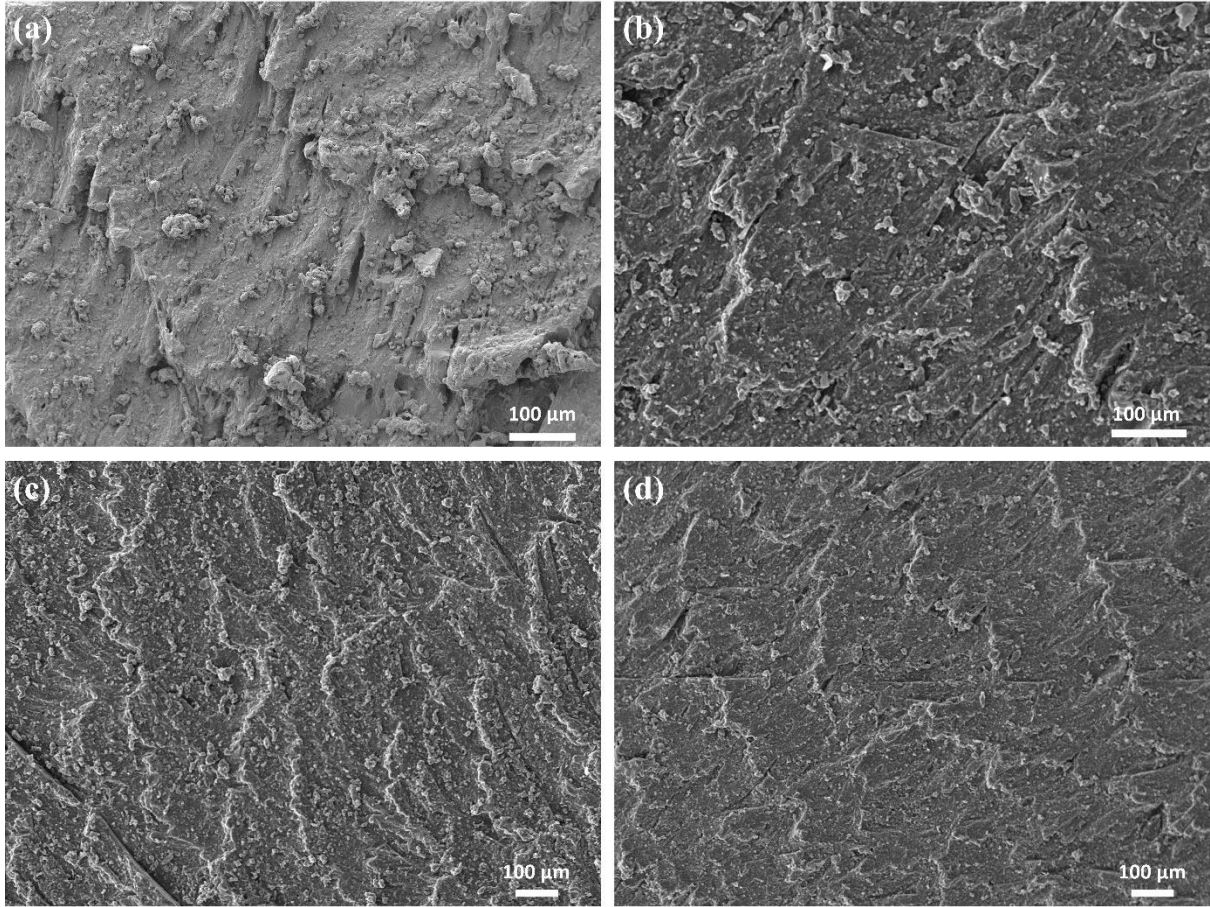
Figure 4.7. SEM images of abraded surfaces. (a) Reference compound sample, (b) fANF1 sample, (c) fGO1 sample, and (d) fANF/GO1 sample.

4.3.5 Dynamic mechanical analysis

In addition to tensile and abrasion resistance testing, the viscoelastic performance of the fANF/GO reinforced rubber compounds was examined by performing dynamic mechanical analysis. The viscoelastic properties of rubber compounds are important because they can be used to predict tire performance metrics such as wet traction and fuel efficiency.[107–109] Specifically, the values of tan δ at 0 °C and 60 °C are usually representative for the prediction of wet grip performance and fuel-saving efficiency: the higher tan δ value at 0 °C, the better wet grip performance, while the lower tan δ value at 60 °C, the lower rolling resistance which corresponds

to better fuel-saving efficiency. The resulting tan δ curves are presented in Figure 4.8, and the values of tan δ at 0 °C and 60 °C are shown in Table 4.3. The fANF reinforced samples displayed increased fuel-saving efficiency and comparable wet grip performance to reference compounds, which is in agreement with the trend shown in our previous work using the fANFs.[130] In contrast, the improvement in fuel efficiency was not significant for fGO reinforced rubber compounds, and wet grip performance remained comparable to reference compounds. However, the combination of fANFs and fGOs was clearly found to reduce rolling resistance through the synergetic effect. When rubber compounds were reinforced with fANF/GOs, the tire performance metric for the fuel-saving efficiency predicted by the ratio of tan δ values was found to improve by up to 21.8% compared to reference compounds, outperforming the fANF reinforced samples. These results can be explained by the covalent bonding between the rubber matrix and new fillers and the improved interfacial interaction between the fANFs and fGOs. The rolling resistance of the carbon black reinforced rubber is a result of the repetitive breakdown and reformation of the rubber-carbon black and carbon black-carbon black interactions, which dissipate energy during deformation.[110,111] The covalent bonding between the rubber matrix and the new fillers minimizes energy dissipation by preventing the breakdown and reformation of rubber-filler interaction.[130] In addition to the covalent bonding, the interfacial interaction between the fANFs and fGOs can also contribute to the reduced energy dissipation, which subsequently leads to improved fuel efficiency. Additionally, the glass transition temperature, T_g, obtained from the maximum peak value of tan δ is also found to be increased when fANFs and fANF/GOs were incorporated into the rubber compounds. It is known that the glass transition temperature of composite materials is related to the flexibility of polymer chains in the composites. Therefore, the T_g can be shifted to a higher temperature due to the restricted mobility of rubber molecules by the

incorporation of fANFs and fANF/GOs into the rubber matrix.[132] Such results further confirm the improved interfacial interaction and crosslink density between the rubber matrix and new fillers. Deduced from the DMA and abrasion resistance test results, the "magic triangle" of tire performance for the fANF, fGO, and fANF/GO reinforced rubber compounds can be seen in Figure 4.9. The wet skid resistance and fuel-saving efficiency were predicted by the ratio of the reference compound and fANF, fGO, and fANG/GO reinforced compounds' tan δ value at 0 °C and 60 °C, respectively. Therefore, both fANFs and fGOs can yield improved fuel-saving efficiency and abrasion resistance in rubber compounds while preserving wet skid resistance. These improvements can be further amplified when using fANFs/GO nanofillers, as their synergetic effect in tire rubber compounds can result in further improvements in abrasion resistance and fuel-saving efficiency without compromising the wet grip performance.

Table 4.3. DMA results of fANF, fGO, and fANF/GO reinforced rubber samples.

Parameters	tan δ at 0 ºC	tan δ at 60 ºC
Reference	0.386	0.123
fANF0.3	0.383	0.115
fANF0.7	0.398	0.111
fANF1	0.382	0.106
fANF2	0.391	0.109
fANF3	0.391	0.108
fGO0.3	0.391	0.120
fGO0.7	0.379	0.122
fGO1	0.402	0.119
fGO2	0.393	0.114
fGO3	0.391	0.120

fANF/GO0.3	0.405	0.106
fANF/GO0.7	0.391	0.106
fANF/GO1	0.400	0.101
fANF/GO2	0.395	0.108
fANF/GO3	0.382	0.109
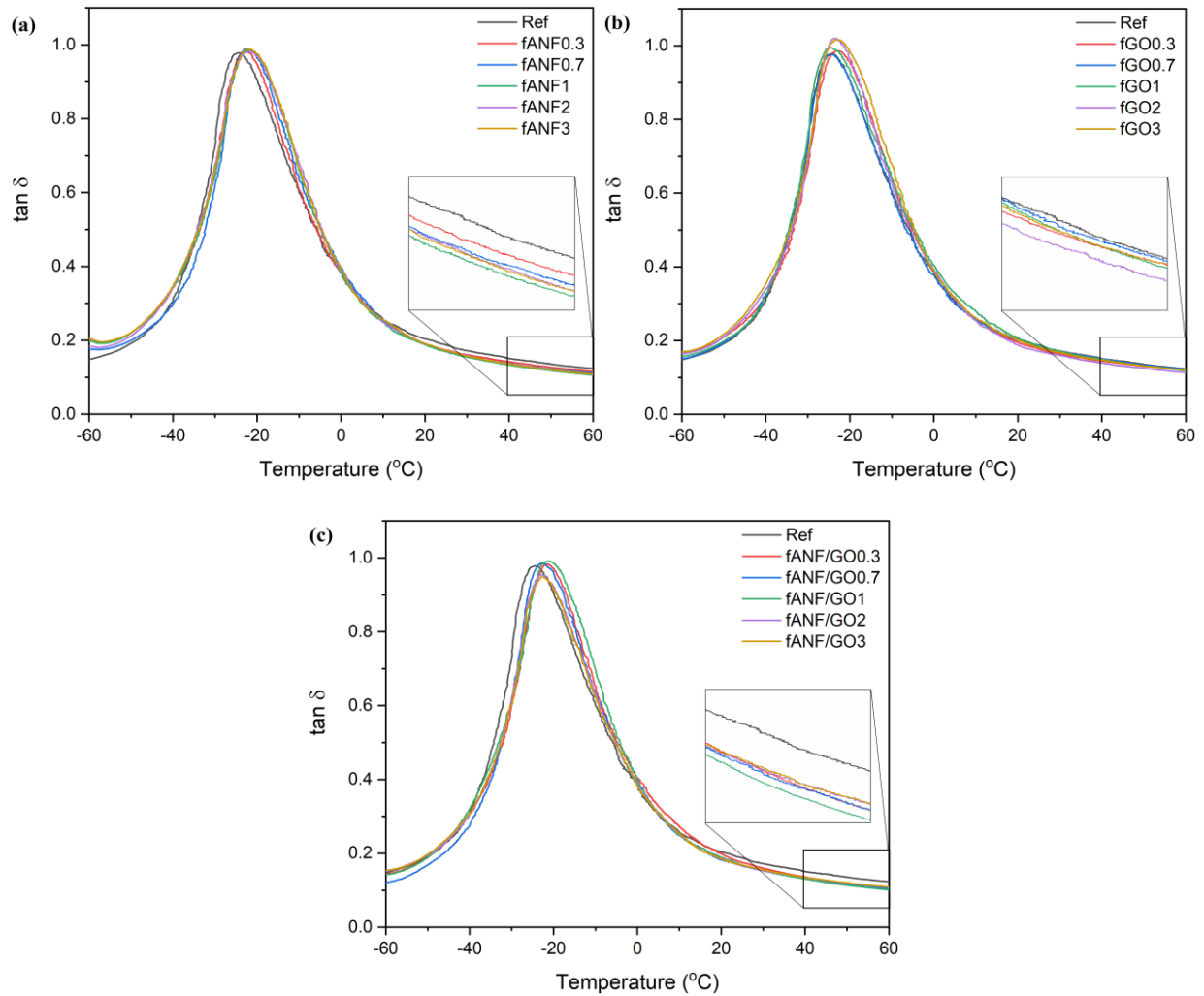
Figure 4.8. Tan δ curves of (a) fANF0.3 to fANF3 samples, (b) fGO0.3 to fGO3 samples, and (c) fANF/GO0.3 to fANF/GO3 samples.
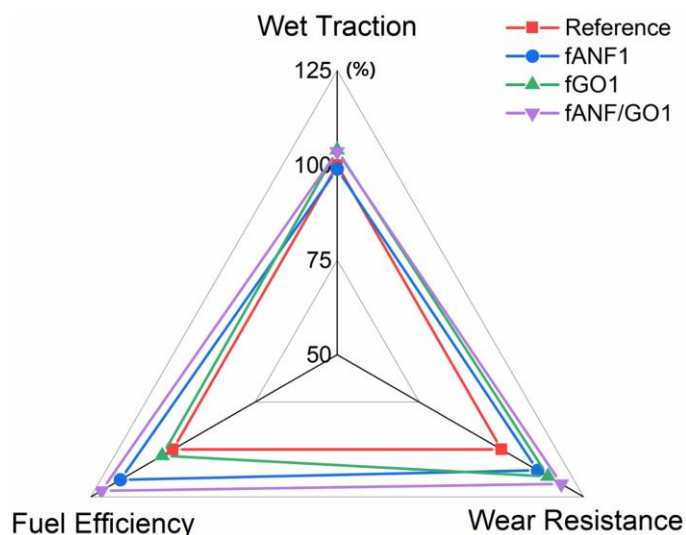
Figure 4.9. The "magic triangle" of tire performance indexes for fANF, fGO, and fANF/GO reinforced rubber compounds predicted by DMA and abrasion resistance results.

4.4 Chapter summary

In this chapter, ANFs and GOs were modified using TESPT and then combined to prepare fANF/GO hybrid filler for the reinforcement of tire tread rubber compounds. The results of characterization using FTIR, XRD, UV-vis, and AFM confirmed that the fANFs and fGOs are combined through noncovalent interactions. Rubber compounds reinforced with fANFs, fGOs, and fANF/GOs were prepared and tested to investigate and compare the effect of the new fillers on the properties related to the tire tread performances. Tensile testing results showed that fANF/GO reinforced rubber compounds exhibit improved average tensile strength and elongation at break relative to fANF reinforced samples, while also displaying higher moduli relative to fGO reinforced rubber compounds. The improvements of mechanical properties due to the new functionalized fillers were also supported by crosslink density measurement results. Moreover, the abrasion resistance of fANFs, fGOs, and fANF/GOs reinforced rubber compounds were found to be increased, with fANF/GO reinforced rubber samples displaying an 18.2% improvement in

abrasion resistance upon adding 1 part of the fANF/GO hybrid filler. In addition to mechanical properties, DMA testing results showed that the rolling resistance predicted by tan δ at 60 °C was improved in fANF, fGO, and fANF/GO reinforced rubber compounds while maintaining the wet skid resistance. Most notably, 1 part of fANF/GOs reinforced rubber specimens showed 21.8% improvement in rolling resistance. Therefore, this study demonstrates that the new fANF/GO hybrid filler can increase mechanical properties and overall tire performance without resulting in a performance trade-off.

Chapter 5

Cellulose Nanocrystal Functionalized Aramid Nanofiber Reinforced Rubber Compounds for Tire Tread Application

5.1 Chapter introduction

The focus of this chapter is the application of cellulose nanocrystal (CNC) functionalized aramid nanofibers (ANFs) for the reinforcement of rubber compounds for tire tread. Various filler materials have been used to reinforce rubber compounds for tire tread; however, it remains challenging to improve overall tire performance without resulting in trade-offs. As previously shown in chapter 4, functionalized hybrid fillers based on the ANFs exhibited synergetic effect on the mechanical properties, abrasion resistance, and fuel efficiency of rubber compounds without decreasing wet skid resistance. Nonetheless, interfacial interaction between the fillers remained strictly limited to noncovalent interaction, which hinders their performance. In this work, CNCs are modified using thionyl chloride, and then bonded to ANFs through chemical covalent interactions to form novel hybrid fillers. The hybrid fillers are functionalized using a silane coupling agent before incorporating them into rubber compounds, replacing from 0.3 to 3 parts of carbon black. The functionalized ANF/CNC (fAC) reinforced rubber compounds are tested and found to exhibit enhanced mechanical properties and crosslink density compared to reference samples. Moreover, the abrasion resistance and fuel-saving efficiency of fAC reinforced compounds are found to improve by 15.0% and 23.8%, respectively, without compromising wet skid resistance performance. Therefore, this study demonstrates the effect of CNC functionalized

89

ANF fillers on the mechanical properties and overall performance requirements of rubber compounds for tire tread applications.

5.2 Preparation and characterization of fAC hybrid filler

5.2.1 Preparation of fAC hybrid filler

The method proposed by Yang et al. was used to prepare 0.2 wt % ANF/DMSO solution.[4] Aramid fibers (KM2+, CS-800) and potassium hydroxide (KOH, Fisher Scientific) were dissolved into dimethyl sulfoxide (DMSO, Fisher Scientific) and stirred for 7 days at 23 °C. CNCs (received from CelluForce) were chlorinated using thionyl chloride before being reacted with ANF/DMSO solution. CNCs (10 g) were added to 200 mL of N,N-dimethylformamide (DMF, Fisher Scientific), and the suspension was then stirred and heated at 80 °C for 12 h. Thionyl chloride (35 mL, $SOCl_2$) was slowly added to the CNC/DMF suspension and constantly stirred for 12 h at 80 °C. Subsequently, the chlorinated CNC (CNC-Cl)/DMF suspension was added to the ANF/DMSO solution, followed by stirring and heating overnight at 80 °C to prepare ANF/CNC-Cl hybrid fillers. The amount of the added CNC-Cl/DMF suspension to the ANF/DMSO solution was controlled to prepare an ANF/CNC-Cl hybrid filler with three different weight ratios of 2 to 1, 1 to 1, and 1 to 2. To functionalize the ANF/CNC-Cl in the resulting suspension, bis(triethoxysilylpropyl)tetrasulfide (TESPT, MilliporeSigma) was added to the suspension and subsequently stirred overnight at 80 °C (Figure 5.1). The prepared fAC hybrid fillers were labeled fA2C1, fA1C1, and fA1C2, respectively, according to the ratio of ANF and CNC-Cl. Additionally, a CNC/DMSO suspension was also prepared and mixed with ANF/DMSO solution, followed by TESPT functionalization to prepare ANF/CNC hybrid filler (AC, 1 to 1 weight ratio) without covalent bonding between the two nanofillers.

Deionized water was added to the fAC/DMSO solution to precipitate the fACs, followed by the use of vacuum-assisted filtration to collect the nanofibers. The fACs were then washed thoroughly with deionized water and acetone (MilliporeSigma). Horn sonication (Fisher Scientific Model 500) was used to disperse the obtained fACs in deionized water, followed by a drying step to yield fAC paste (90 wt % water content in the paste). TESPT-functionalized ANFs, CNCs, and ANF/CNCs paste (labeled ANFs, CNCs, and ACs, respectively, in the following sections) were also fabricated for the purpose of comparison.
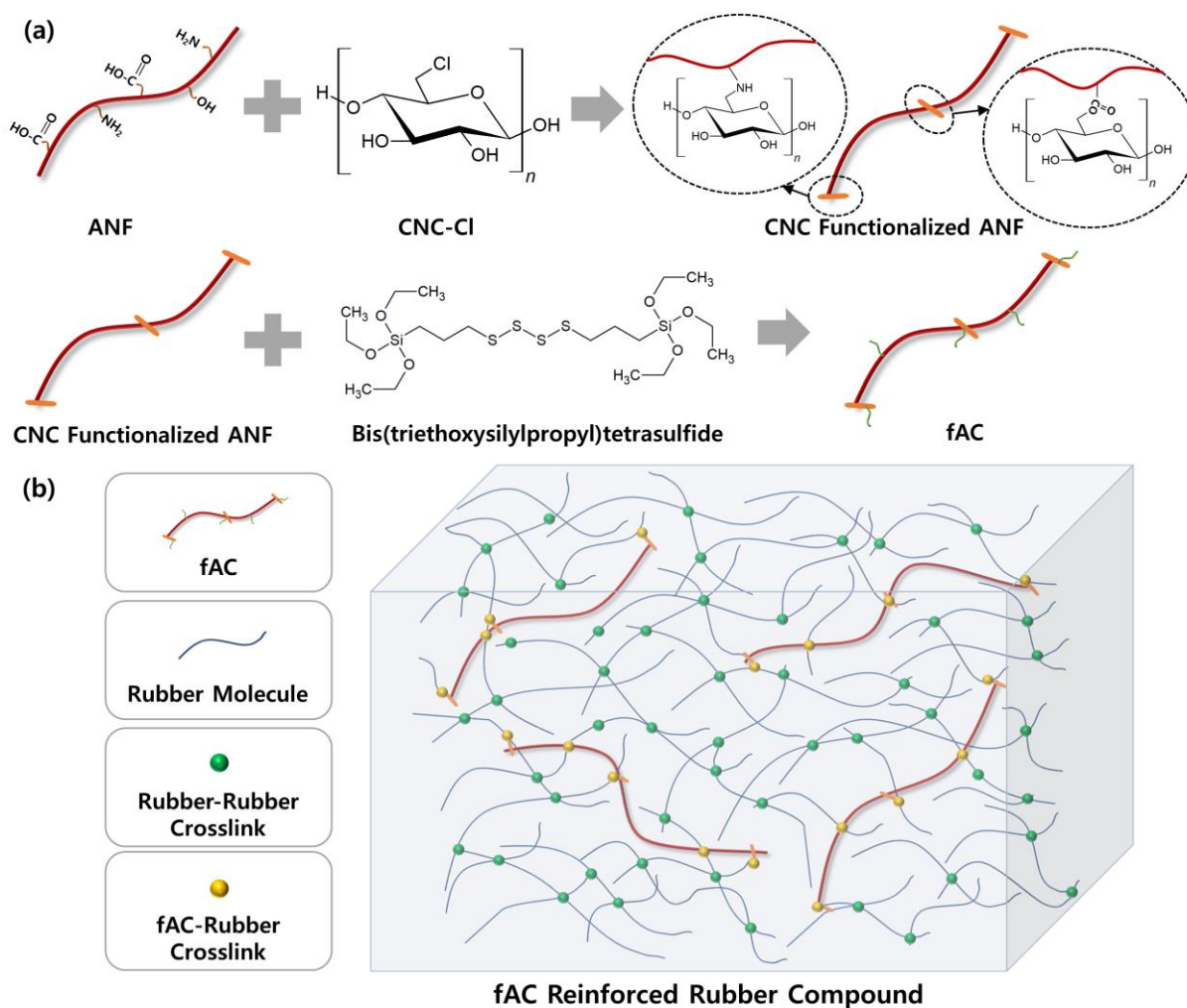
Figure 5.1. (a) The preparation of fAC hybrid filler, and (b) fAC reinforced rubber compound.

5.2.2 Characterization of fAC hybrid filler

The novel hybrid fillers were characterized to investigate their role in reinforcing rubber compounds. Firstly, attenuated total reflectance–Fourier transform infrared spectroscopy (ATR-FTIR) was used to examine the chemical structure changes after the TESPT functionalization and for a combination of ANFs and CNCs with or without covalent linkages. Figure 5.2 displays the FTIR spectra of ANFs, CNCs, ACs, and fA1C1s before and after functionalization. According to the spectra shown in Figure 5.2a, the surface modification of ANFs and CNCs using TESPT was confirmed by the appearance of additional characteristic peaks at 1200, 1100, 1018, and 950 cm^{-1}, assigned to Si-CH$_2$-R, Si-O, Si-O-C, and Si-O stretching, respectively. Additionally, a peak appearing at 2921 cm^{-1} can be assigned to the C-H stretching vibration of methylene in the chemical structure of TESPT. Thus, the chemical structure changes reveal the TESPT-functionalization on the surface of ANFs and CNCs. Elsewhere, ANFs and CNCs were combined after functionalization to prepare ACs, while chlorinated CNCs were reacted with ANFs and were then functionalized using TESPT to fabricate fA1C1s. The AC hybrid fillers formed without covalent bonding between ANFs and CNCs exhibit all the individual characteristic peaks of both ANFs and CNCs. In addition to the characteristic peaks of both ANFs and CNCs, the FTIR spectra of fA1C1s showed new characteristic peaks at 1720 and 3460 cm^{-1}, which correspond to ester C=O stretching vibration and a secondary amine. These new peaks from the hybrid fillers confirm the covalent linkages between ANFs and CNCs. Therefore, the chemical structure changes investigated using FTIR confirm the functionalization of nanofillers and the preparation of novel hybrid fillers with chemical covalent bonding.
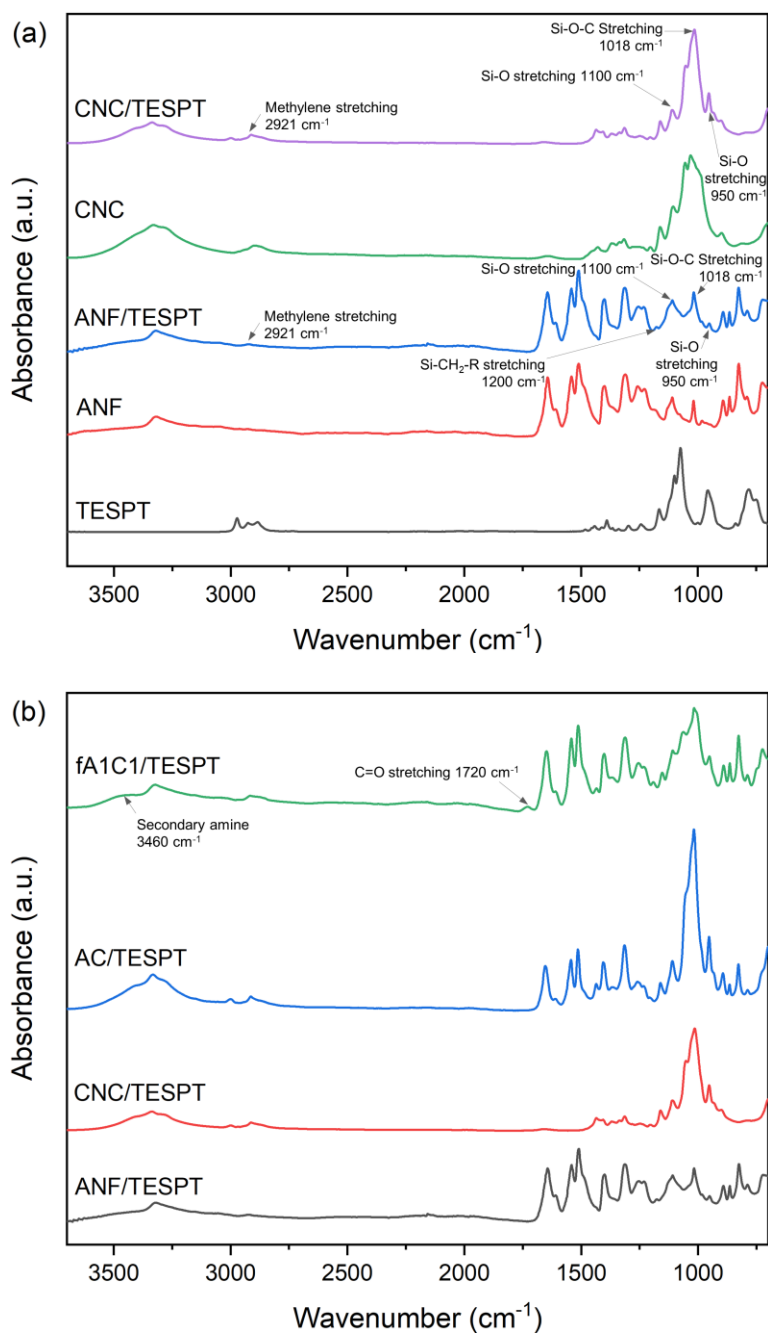
Figure 5.2. FTIR spectra of (a) TESPT, ANF, ANF/TESPT, CNC, and CNC/TESPT, and (b) ANF/TESPT, CNC/TESPT, AC/TESPT, and fA1C1/TESPT.

X-ray diffraction (XRD) analysis was also conducted to characterize the crystalline structure of the new hybrid fillers. XRD patterns were obtained using an X-ray diffractometer (Rigaku Ultima IV) in a 2θ range of 5 to 40°. The obtained XRD patterns of ANFs, CNCs, ACs,

and fA1C1s are shown in Figure 5.3. The diffraction peaks of ANFs were shown at 20.7° and 22.8°, corresponding to the [110] and [200] planes of Kevlar.[4,128] The XRD patterns of new hybrid fillers, including ACs and fA1C1s, also showed characteristic peaks at the same position as ANF due to the incorporation of ANFs in the fillers. CNCs displayed diffraction peaks at 14.6°, 16.6°, 22.8°, and 34.6°, which are attributed to the crystalline cellulose structure.[133,134] After combining ANFs and CNCs, the ACs showed the characteristic peaks of CNCs; however, the peaks were not present when the ANFs and CNCs were combined through covalent bonding. These results suggest that the covalent linkages between the ANFs and CNCs attenuated the crystalline structure of cellulose, leading to the disappearance of the peaks.[135] In addition to the XRD results, atomic force microscopy (AFM) images were collected using Park XE-70. The AFM images presented in Figure 5.4 show further information on the structure and morphology of ACs and fA1C1s. The ANFs have diameters in the range of 4 to 11 nm, while the diameters of CNCs range between 3 to 8 nm, which is similar to the data shown in previous studies. The AFM image of fA1C1s in Figure 5.4d shows that all the CNCs are located on the middle or edge of the ANFs; however, the CNCs and ANFs are observed separately and individually in the case of ACs shown in Figure 5.4c. Therefore, the AFM scans of fA1C1s indicate the establishment of chemical interaction between ANFs and CNCs. According to the FTIR, XRD, and AFM results, fACs are prepared by combining ANFs and CNCs through chemical covalent bonding. Moreover, the new hybrid materials can be a promising filler for reinforcing rubber compounds by establishing both interfacial chemical interaction through functionalization using silane coupling agent and improved mechanical interaction between the matrix and fillers due to the chemically attached CNCs on ANFs.
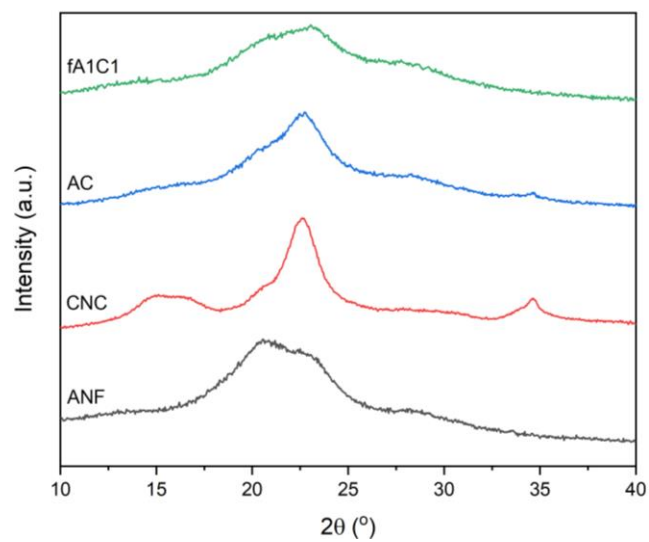
Figure 5.3. XRD plots of ANFs, CNCs, ACs, and fA1C1s.
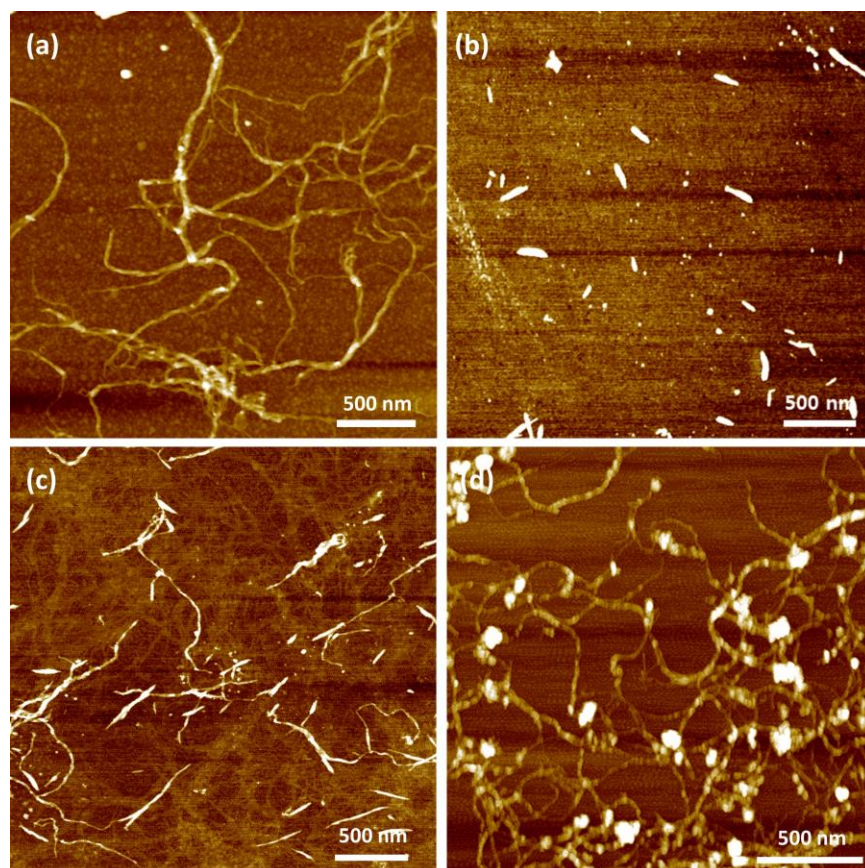
Figure 5.4. AFM images of (a) ANFs, (b) CNCs, (c) ACs and (d) fA1C1s.

5.3 Preparation and characterization of fAC reinforced rubber compounds

5.3.1 Preparation of fAC reinforced rubber compounds

An internal mixer (Plasti-corder, Brabender) was used to prepare the rubber compounds following the recipes displayed in Table 5.1. The internal temperature was controlled to range between 140 and 150 °C, and the compounding was performed with fill factors of 70%. In the first stage, SOL-6270M and KBR 01 (supplied by KKPC) were mixed for 60 sec, followed by adding and mixing of carbon black (N339 grade), zinc oxide, stearic, and processing oil (obtained from Akrochem) for 60 sec. fAC paste was also added into the mixer and mixed for 300 sec. The weight of the dumped compounds was obtained to confirm the evaporation of water in the fAC paste. In the next stage, sulfur and n-cyclohexyl-2-benzothiazole sulfonamide (CBS) were introduced to the compounds from the first stage and mixed for another 180 sec. Finally, rubber compounds were vulcanized using a hot press to prepare specimens for tests. Uncured rubber compounds were tested using MDR 2000 (MonTech) at 160 °C for 40 min to determine the vulcanization conditions.

Table 5.1. Compound recipes of reference, ANF, CNC, AC, fA2C1, fA1C1, and fA1C2 reinforced samples (Unit: phr. Total oil content: 30 phr, including pre-mixed oil in SOL-6270M).

Items		Reference	0.3	0.7	1	2	3
Rubber	SOL-6270M	96.25	96.25	96.25	96.25	96.25	96.25
	KBR01	30	30	30	30	30	30
Filler	N339	50	49.7	49.3	49	48	47
	ANF, CNC, AC or fAC	-	0.3	0.7	1	2	3
Additive	Processing oil	3.75	3.75	3.75	3.75	3.75	3.75
	Zinc oxide	3	3	3	3	3	3
	Stearic acid	1	1	1	1	1	1

Curative	Sulfur	1.5	1.5	1.5	1.5	1.5	1.5
Accelerator	CBS	2.2	2.2	2.2	2.2	2.2	2.2

5.3.2 Characterization and testing of fAC reinforced rubber compounds

A toluene swelling technique shown in chapter 2 was used to calculate the crosslink density of rubber. Tensile tests were conducted to investigate the role of fillers on the mechanical properties of rubber compounds. Specimens (ASTM D412) were prepared and tested on a Model 5982 Instron universal testing machine at room temperature and a 50 cm/min crosshead speed. Viscoelastic properties were also obtained using a dynamic mechanical analyzer (TA DMA Q800) at 10 Hz, 0.5% strain, and a temperature range from -60 °C to 60 °C. To evaluate the abrasion resistance of rubber samples, a DIN abrasion tester (Aveno Tech) was used. Specimens were prepared according to DIN 53516, and the rotating speed of the drum was set at 40 rpm. The abrasion loss data of each sample was obtained following the procedure described in chapter 2.

5.3.3 Mechanical properties

The mechanical properties of rubber compounds were investigated using tensile tests. The average 100% and 300% modulus, tensile strength, and elongation at break of samples are presented in Table 5.2, while the stress versus strain curves of ANF, CNC, AC, fA2C1, fA1C1, and fA1C2 reinforced rubber compounds are presented in Figure 5.5. The test results revealed that the overall mechanical properties, including modulus, tensile strength, and elongation at break, improved when replacing carbon black with the same amount of novel nanofillers. According to the test results, it was shown that ANFs could contribute to improving 100% and 300% modulus and tensile strength of rubber compounds, while the effect of CNCs on those properties plateaued

as the amount of CNCs was further increased. When using a combination of ANFs and CNCs that lacks covalent bonding between them, the increment in tensile properties was determined to be inferior to those of ANF reinforced samples. However, once the CNC functionalized ANFs were incorporated into the rubber compounds, all the tensile properties were observed to improve with increased concentration of hybrid fillers. Moreover, fA2C1, fA1C1, and fA1C2 reinforced rubber compounds all displayed improved mechanical properties compared to the reference, ANF, CNC, and AC reinforced rubber compounds. Most notably, 3 phr of fA1C2 reinforced compounds were found to exhibit a maximum 300% modulus and tensile strength of 2.34 MPa and 16.58 MPa, yielding 41.0% and 33.5% enhancements compared to the reference samples, respectively. Drawing from the results, these novel fAC fillers outperform carbon black when it comes to reinforcing rubber compounds under tensile loading conditions. These results can be attributed to the individual characteristics of both ANFs and CNCs, along with the improved interaction between the hybrid fillers and rubber molecules. As previously shown in our work, the outstanding mechanical strength of ANFs, in addition to their high aspect ratio and large specific area, can effectively contribute to enhancing the mechanical properties of rubber composites.[130] Additionally, CNCs possess a high aspect ratio and large surface area, which are beneficial for a nanofiller performance. In addition to their unique characteristics, CNCs are attached at the end or middle of ANFs, which can improve the mechanical interlocking when blended into the rubber matrix. Moreover, the functionalization of the novel nanofillers using a silane coupling agent enhances interfacial interactions between the hybrid nanofillers and the rubber matrix, yielding improvement in the overall mechanical properties. Furthermore, crosslink density measurement results also confirm the enhanced interactions between the CNC functionalized ANFs and rubber chains. The swelling ratio and calculated crosslink density are presented in Table 5.2, where it can

be seen that as the amount of ANF, CNC, AC, fA2C1, fA1C1, and fA1C2 in the samples is increased, the swelling ratio is decreased, while crosslink density is increased accordingly. It can therefore be concluded that the crosslink densities of CNC functionalized ANF reinforced samples were higher than those of the reference, ANF, CNC, and AC reinforced compounds, which is in agreement with the tensile test results trend. These results demonstrate that the CNC functionalization on the ANFs can improve stress and load transfer between the rubber matrix and hybrid filler materials through a combination of mechanical interlocking and covalent bonding between them.
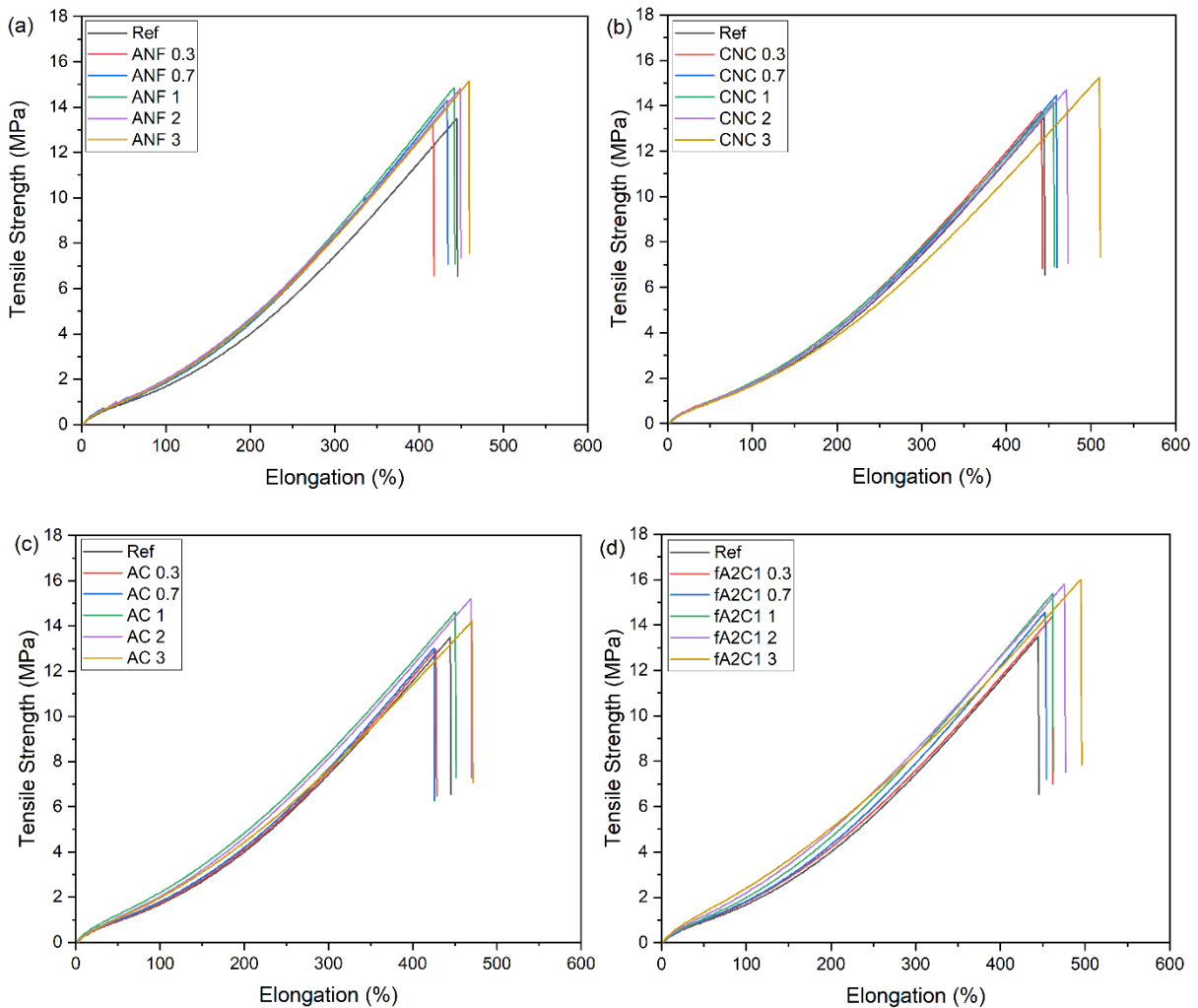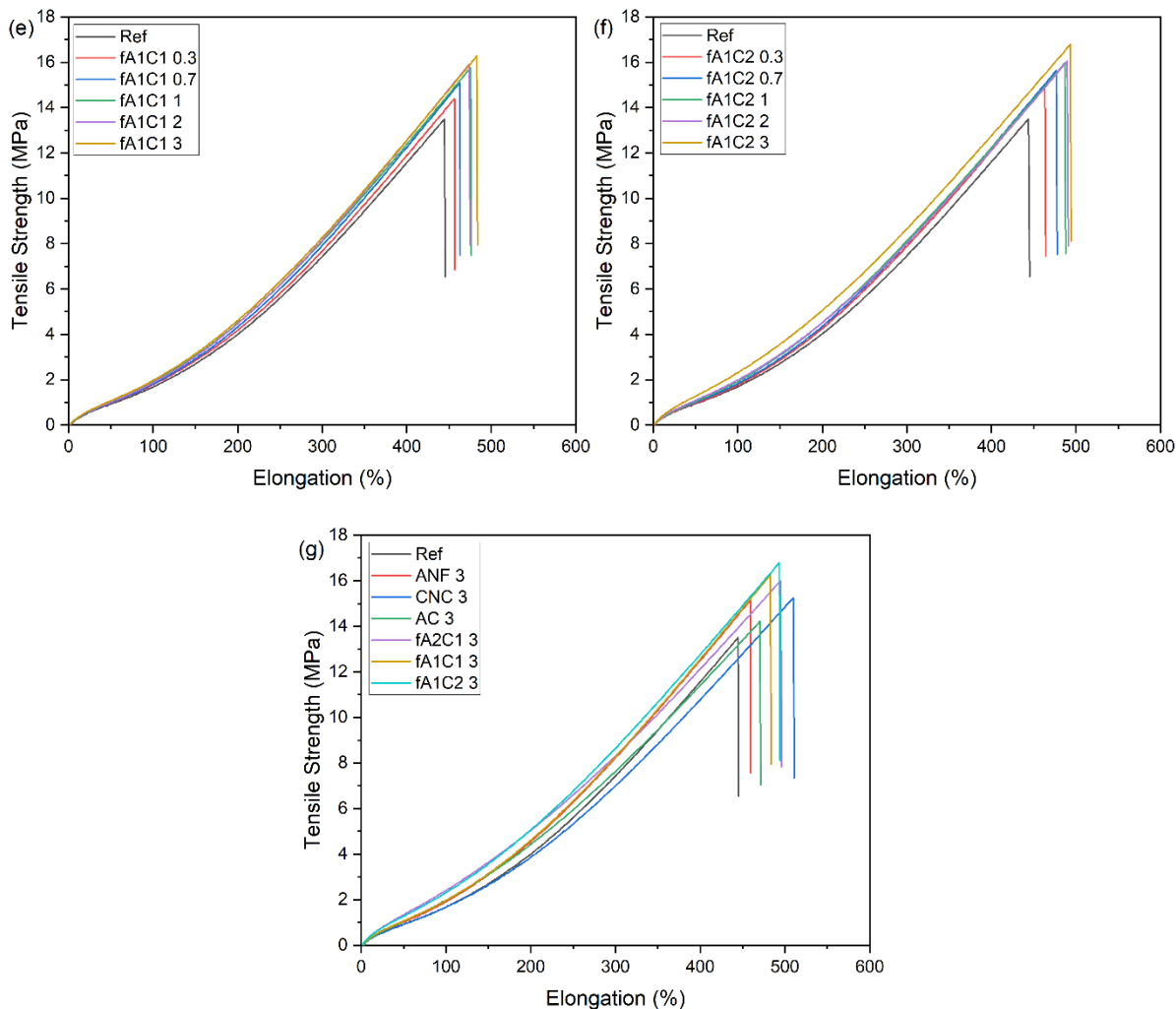
Figure 5.5. Stress versus strain curves of (a) ANF 0.3 to ANF 3 samples, (b) CNC 0.3 to CNC 3 samples, (c) AC 0.3 to AC 3 samples, (d) fA2C1 0.3 to fA2C1 3 samples, (e) fA1C1 0.3 to fA1C1 3 samples, (f) fA1C2 0.3 to fA1C2 3 samples, and (g) 3 parts of nanofillers reinforced samples.

Table 5.2. Tensile test, and crosslink density measurement results of ANF, CNC, AC, fA2C1, fA1C1, and fA1C2 reinforced rubber samples.

Parameters	100% Modulus (MPa)	300% Modulus (MPa)	Tensile Strength (MPa)	Elongation at Break (%)	Swelling Ratio, Q	Crosslink Density, ν_e (10^{-4} mol cm^{-3})
Reference	1.66 ± 0.04	7.33 ± 0.20	12.42 ± 1.20	424.2 ± 22.1	2.53	2.04
ANF 0.3	1.92 ± 0.04	8.41 ± 0.09	13.61 ± 0.28	412.4 ± 4.3	2.47	2.15
ANF 0.7	1.95 ± 0.10	8.46 ± 0.45	14.13 ± 0.24	426.7 ± 14.9	2.40	2.30

ANF 1	1.95 ± 0.03	8.49 ± 0.11	14.88 ± 0.90	442.6 ± 15.2	2.34	2.44
ANF 2	2.04 ± 0.03	8.37 ± 0.09	14.76 ± 0.06	450.1 ± 6.7	2.35	2.40
ANF 3	1.95 ± 0.03	8.37 ± 0.24	15.65 ± 0.38	464.8 ± 12.6	2.25	2.64
CNC 0.3	1.83 ± 0.04	7.89 ± 0.13	13.95 ± 0.20	443.1 ± 2.0	2.44	2.21
CNC 0.7	1.78 ± 0.04	7.89 ± 0.27	14.11 ± 0.35	444.2 ± 14.9	2.48	2.15
CNC 1	1.80 ± 0.03	7.91 ± 0.16	14.31 ± 0.16	451.3 ± 4.3	2.38	2.35
CNC 2	1.73 ± 0.03	7.42 ± 0.12	14.27 ± 0.92	463.8 ± 20.9	2.35	2.42
CNC 3	1.63 ± 0.04	6.79 ± 0.21	14.70 ± 0.55	504.9 ± 5.0	2.39	2.33
AC 0.3	1.75 ± 0.05	7.60 ± 0.24	13.00 ± 0.09	427.3 ± 5.6	2.48	2.15
AC 0.7	1.83 ± 0.09	7.85 ± 0.38	12.81 ± 0.90	417.1 ± 8.5	2.44	2.21
AC 1	2.02 ± 0.18	8.10 ± 0.24	14.25 ± 0.37	446.1 ± 4.3	2.36	2.40
AC 2	2.01 ± 0.01	8.11 ± 0.01	14.58 ± 0.62	455.3 ± 13.9	2.35	2.42
AC 3	2.01 ± 0.05	7.76 ± 0.21	14.16 ± 0.81	464.4 ± 21.8	2.35	2.42
fA2C1 0.3	1.80 ± 0.06	7.65 ± 0.14	13.95 ± 0.58	448.9 ± 13.5	2.47	2.17
fA2C1 0.7	1.80 ± 0.04	7.76 ± 0.15	14.39 ± 0.87	455.6 ± 22.4	2.40	2.30
fA2C1 1	1.95 ± 0.08	8.01 ± 0.33	15.00 ± 0.41	464.5 ± 9.9	2.34	2.44
fA2C1 2	2.17 ± 0.05	8.33 ± 0.19	15.67 ± 0.68	477.7 ± 23.0	2.30	2.52
fA2C1 3	2.29 ± 0.14	8.19 ± 0.12	15.59 ± 0.76	487.3 ± 13.5	2.26	2.61
fA1C1 0.3	1.79 ± 0.01	7.78 ± 0.09	14.65 ± 0.63	460.1 ± 10.5	2.38	2.35
fA1C1 0.7	1.83 ± 0.06	8.01 ± 0.18	15.16 ± 0.76	463.2 ± 11.2	2.34	2.44
fA1C1 1	1.91 ± 0.06	8.10 ± 0.14	15.70 ± 0.57	473.8 ± 9.0	2.31	2.49
fA1C1 2	2.01 ± 0.11	8.11 ± 0.08	15.83 ± 0.52	483.3 ± 17.5	2.23	2.69
fA1C1 3	2.12 ± 0.16	8.39 ± 0.40	16.30 ± 0.04	486.4 ± 14.3	2.21	2.74
fA1C2 0.3	1.79 ± 0.06	7.76 ± 0.25	14.81 ± 0.83	467.2 ± 9.6	2.33	2.44
fA1C2 0.7	1.81 ± 0.04	7.88 ± 0.14	15.65 ± 0.75	482.5 ± 24.0	2.32	2.47
fA1C2 1	1.91 ± 0.02	8.05 ± 0.12	15.89 ± 0.08	487.6 ± 0.8	2.20	2.79
fA1C2 2	1.98 ± 0.04	8.07 ± 0.09	15.95 ± 0.11	489.6 ± 2.8	2.17	2.87

fA1C2 3	2.34 ± 0.01	8.72 ± 0.06	16.58 ± 0.22	485.8 ± 7.6	2.24	2.66

5.3.4 Abrasion resistance

In order to evaluate the abrasion resistance of rubber compounds reinforced with novel hybrid fillers, abrasion resistance tests were performed to examine the samples. The abrasion loss data of samples of various data sets were collected and used to calculate abrasion resistance indexes by dividing the abrasion loss values of the reference sample with those of the novel filler-reinforced ones. The resulting abrasion resistance indexes are presented in Figure 5.6. According to the test results, ANF reinforced rubber compounds showed improved abrasion resistance in agreement with our previous chapters, while the abrasion resistance of CNC or AC reinforced rubber samples was comparable to or less than that of the reference compounds. This is likely due to the relatively lower aspect ratio of CNCs compared to ANFs, along with their lower interfacial interaction with the rubber matrix relative to carbon black. However, it can be seen that the fA2C1, fA1C1, and fA1C2 reinforced rubber compounds exhibited increased abrasion resistance of 11.0%, 12.1%, and 15.2%, respectively, by replacing 2 parts of carbon black with fAC fillers. The improved abrasion resistance of hybrid filler reinforced rubber compounds is in accordance with the mechanical testing results shown in the previous section as it correlates to the improved tensile strength and toughness of the compounds. Additionally, these test results highlight the synergetic effect of ANFs and CNCs when they are covalently linked to each other and crosslinked in the rubber matrix. The CNCs adhered at the end of ANFs could improve the interaction between the ANFs and rubber chains through increased mechanical interlocking in addition to chemical interaction through the employed TESPT-functionalization, which contributes to the increased abrasion resistance.

102
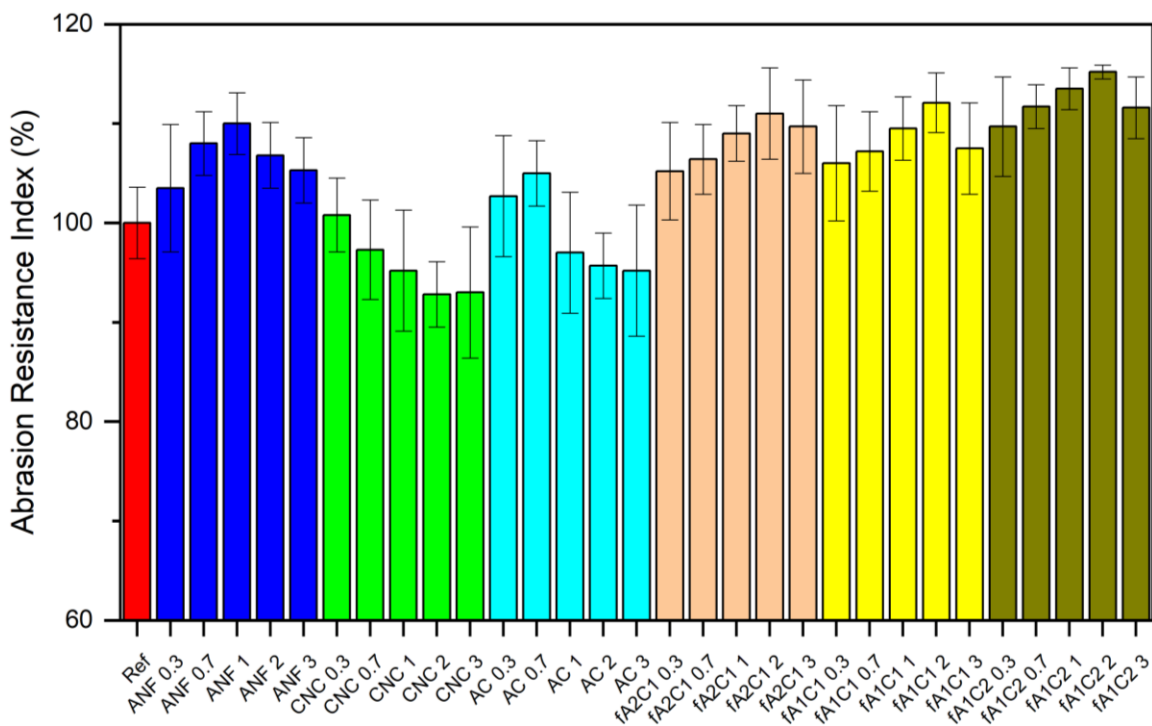
Figure 5.6. Abrasion resistance indexes of ANFs, CNCs, ACs, fA2C1s, fA1C1s, and fA1C2s reinforced samples at various weight fractions which is represented by the number following the reinforcement type in phr.

5.3.5 Dynamic mechanical analysis

The dynamic mechanical properties of rubber compounds reinforced with novel hybrid fillers were measured to predict tire performance metrics. Among the data from the dynamic mechanical analysis, tan δ value at 0 °C can be used to predict wet grip performance of tires, while tan δ value at 60 °C is representative for the prediction of fuel efficiency. A higher value of tan δ at 0 °C indicates improved traction on wet roads, while a lower value of tan δ at 60 °C presents improved fuel efficiency, which is attributed to reduced rolling resistance.[107–109] DMA test results are displayed in Table 5.3, and the tan δ curves are shown in Figure 5.7. As shown from our previous chapters, fuel efficiency was found to be improved and wet grip performance was largely maintained when ANFs were used to reinforce rubber compounds in this work.[73,130] As

103

seen in Figure 5.7b and 5.7c, both CNCs and ACs displayed a limited effect on reducing the rolling resistance of rubber compounds when compared to ANFs, as they follow the same trend obtained during mechanical tests, whereas their corresponding wet grip performance was comparable to reference samples. In contrast, fAC reinforced rubber compounds showed improved fuel efficiency. As compared to reference samples, the fuel efficiencies of fA2C1, fA1C1, and fA1C2 reinforced samples predicted by the ratio of tan δ value were determined to enhance by 19.0, 21.4, and 23.8%, respectively, when replacing 2 parts of carbon black with fAC fillers. These results can be attributed to the improved interfacial interaction between the rubber chains and novel hybrid fillers through chemical covalent linkages and mechanical interaction. The major source for the rolling resistance is energy dissipation during the deformation of tires resulting from the repetitive breakdown and reformation of filler-filler and rubber-filler interaction.[110,111] The chemical bonding between fACs and the rubber molecules can contribute to reducing energy loss at the interphase through increasing rubber-filler interaction.[130] Additionally, the improved mechanical interaction achieved by the CNC functionalization on ANFs can also minimize energy dissipation, which results in improved fuel efficiency. Drawing from the abrasion resistance results and viscoelastic properties, the effect of fACs on the tire performance metrics can be seen in Figure 5.8. Performance metrics such as fuel efficiency and wet skid resistance performance used in the "magic triangle" were calculated using tan δ data at 60 °C, and 0 °C of reference and novel hybrid filler reinforced samples, respectively. As seen from Figure 5.8, rubber compounds reinforced with fA1C2s exhibited further improvements in fuel efficiency and abrasion resistance compared to ANF reinforced rubber compounds and reference compounds without deteriorating the wet grip performance.
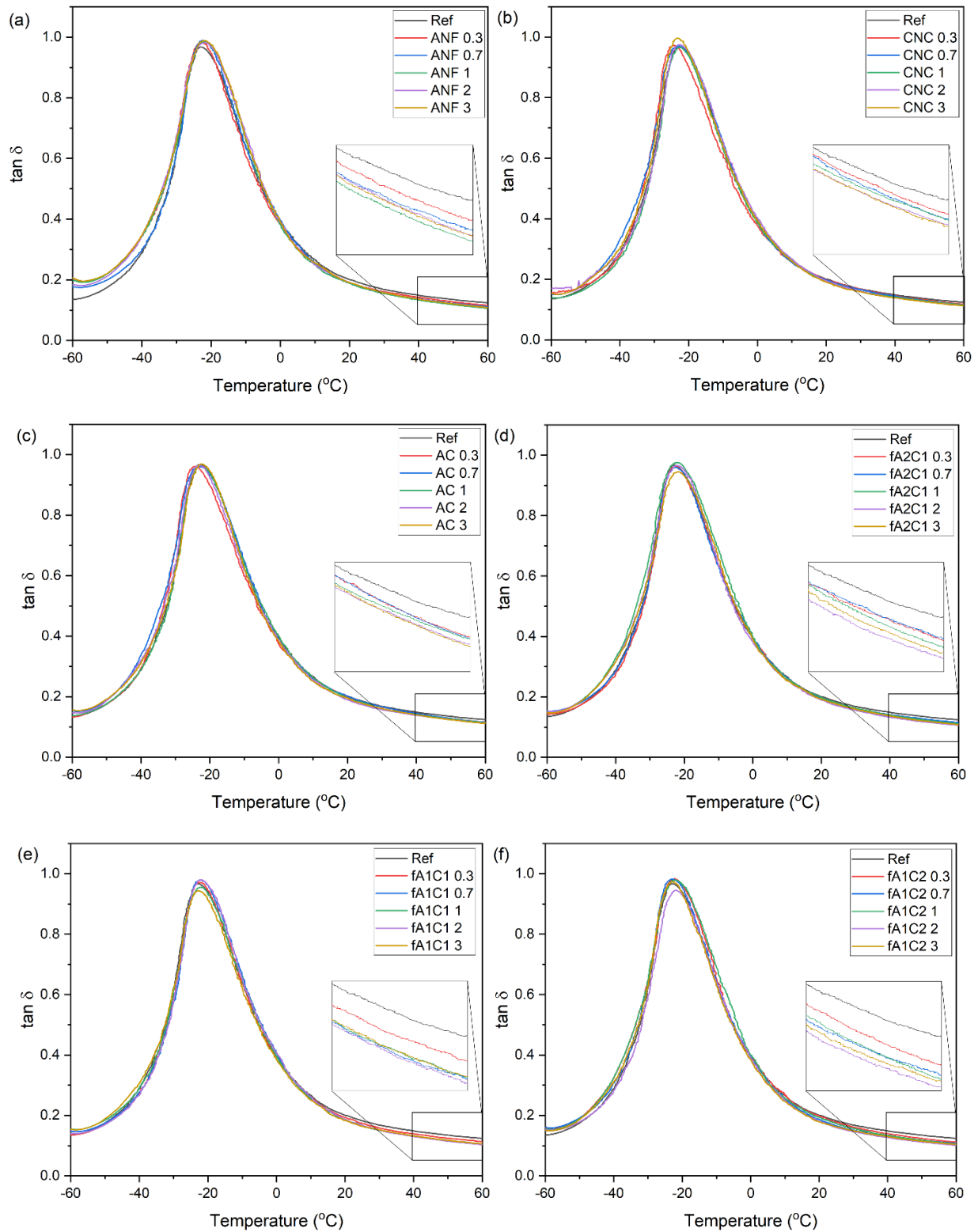
Figure 5.7. Tan δ versus temperature curves of (a) ANF 0.3 to ANF 3 samples, (b) CNC 0.3 to CNC 3 samples, (c) AC 0.3 to AC 3 samples, (d) fA2C1 0.3 to fA2C1 3 samples, (e) fA1C1 0.3 to fA1C1 3 samples, and (f) fA1C2 0.3 to fA1C2 3 samples.

Table 5.3. DMA results of rubber samples reinforced with ANF, CNC, AC, fA2C1, fA1C1, and fA1C2.

Items	tan δ at 0 ºC	tan δ at 60 ºC	Items	tan δ at 0 ºC	tan δ at 60 ºC
Reference	0.393	0.125	Reference	0.393	0.125
ANF 0.3	0.383	0.115	fA2C1 0.3	0.394	0.114
ANF 0.7	0.398	0.111	fA2C1 0.7	0.395	0.115
ANF 1	0.382	0.106	fA2C1 1	0.399	0.111
ANF 2	0.391	0.109	fA2C1 2	0.383	0.105
ANF 3	0.391	0.108	fA2C1 3	0.390	0.108
CNC 0.3	0.378	0.118	fA1C1 0.3	0.396	0.113
CNC 0.7	0.388	0.116	fA1C1 0.7	0.391	0.111
CNC 1	0.385	0.115	fA1C1 1	0.396	0.106
CNC 2	0.402	0.113	fA1C1 2	0.407	0.103
CNC 3	0.392	0.112	fA1C1 3	0.386	0.107
AC 0.3	0.374	0.115	fA1C2 0.3	0.395	0.111
AC 0.7	0.385	0.115	fA1C2 0.7	0.392	0.107
AC 1	0.399	0.115	fA1C2 1	0.399	0.105
AC 2	0.388	0.112	fA1C2 2	0.389	0.101
AC 3	0.384	0.112	fA1C2 3	0.385	0.104
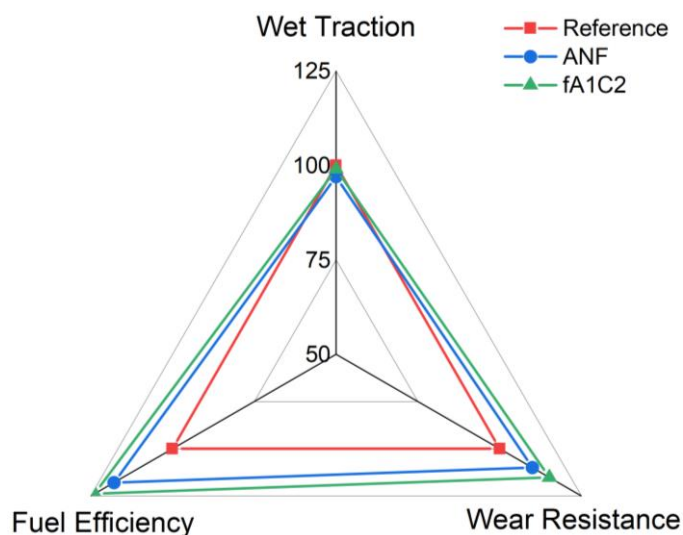
Figure 5.8. The "magic triangle" of performance metrics for reference, ANF, and fA1C2 samples.

5.4 Chapter summary

This chapter has investigated the effect of CNC functionalized ANFs on the properties and performance of rubber compounds for tire tread. CNCs were attached to the surface of ANFs through covalent bonding, and the hybrid fillers were functionalized using TESPT before mixing them as nanofillers in rubber compounds. Characterization techniques, including FTIR, XRD, and AFM, revealed the combination of ANFs and CNCs and tests were performed to investigate the role of novel hybrid fillers on the tire tread performance in addition to mechanical and viscoelastic properties. Rubber samples reinforced with fACs were found to exhibit enhanced tensile strength, 100% and 300% modulus, and elongation at break when compared to the reference, ANF, and CNC reinforced samples. Moreover, fA2C1, fA1C1, and fA1C2 reinforced rubber compounds experienced 11.0%, 12.1%, and 15.2% improvement in abrasion resistance, respectively, when they replaced only 2 parts of carbon black. Finally, DMA results showed that the rolling resistance of rubber compounds was decreased by 23.8% when 2 parts of fA1C2 were incorporated into them,

while the wet grip performance was maintained. Overall, the mechanical properties and tire performance were maximized when a 1 to 2 weight ratio of ANFs and CNCs were combined and used to prepare rubber compounds. Thus, this work demonstrates that the novel fAC hybrid fillers can improve mechanical properties and the overall performance of tire tread rubber compounds.

Chapter 6

High Strength and Toughness Epoxy Nanocomposites Reinforced by Cellulose Nanocrystal Functionalized Aramid Nanofibers

6.1 Chapter introduction

The work described in this chapter further exploits cellulose nanocrystal (CNC) reinforced aramid nanofiber (ANF) reinforced epoxy nanocomposites with high strength and toughness. The mechanical properties of polymer nanocomposites have been improved by incorporating various types of nanofillers. The hybridization of nanofillers through the covalent linkages between nanofillers with different dimensions and morphology can further increase the properties of nanocomposites. In this work, ANFs are functionalized using chlorinated CNCs and modified with a glycidyl ether silane coupling agent to improve the chemical and mechanical interaction in an epoxy matrix. Integration of the CNC functionalized ANFs (fACs) in the epoxy matrix simultaneously improves Young's modulus, tensile strength, fracture toughness, and dynamic mechanical properties. The test results show that 1.5 wt % fAC reinforced epoxy nanocomposites improve Young's modulus and tensile strength by 15.1% and 10.1%, respectively, and fracture toughness also improves by 2.5 times compared to the neat epoxy resin. Moreover, storage modulus and glass transition temperature are observed to increase when fACs are incorporated. Thus, this study demonstrates that the enhanced chemical and mechanical interaction by the CNC functionalization on the ANFs can further improve the static and dynamic mechanical properties of polymer nanocomposites.

6.2 Preparation and characterization of fAC hybrid filler

6.2.1 Preparation of fAC hybrid filler

ANF/dimethyl sulfoxide (DMSO) solution (500 mL of 0.2 wt %) was prepared using the Yang's modified method.[136] KM2+ Kevlar fibers (1 g, CS-800), potassium hydroxide (KOH, 1.5 g, Fisher Scientific), and deionized (DI) water (20 ml) were added to DMSO (500 ml, Fisher Scientific), and the solution was stirred for 4 h at 23 °C. CNCs (1 g, CelluForce) were dispersed in N,N-dimethylformamide (DMF, 20 mL, Fisher Scientific), and the suspension was heated at 80 °C for 12 h to activate the CNCs. Thionyl chloride (3.5 mL, $SOCl_2$, MilliporeSigma) was added dropwise into the suspension, and the suspension was stirred and heated at 80 °C for 24 h to form a chlorinated CNC (CNC-Cl) solution. Then, the CNC-Cl solution and ANF/DMSO solution were mixed and heated overnight at 80 °C overnight, followed by adding and mixing 10 wt % of 3-glycidoxypropyltrimethoxysilane (GPTMS, MilliporeSigma) at 80 °C for 24 h to prepare functionalized ANF/CNCs (fACs) with covalent bonding between the nanomaterials (Figure 6.1a). In addition to the preparation of fACs, CNCs were added to ANF/DMSO solution, followed by GPTMS functionalization to fabricate ANF/CNCs without covalent bonding (ACs) for the purpose of comparison with fACs.

DI water was used to precipitate the fACs from the solution, and a vacuum-assisted filtration set was used to wash the nanofibers thoroughly with DI water and acetone (MilliporeSigma). After the filtration, the fACs were dispersed in acetone using horn sonication (Fisher, Model 500) before drying them to yield fAC paste with 50 wt % acetone content. GPTMS modified ANFs, CNCs, and ACs were also prepared to fabricate epoxy nanocomposites.
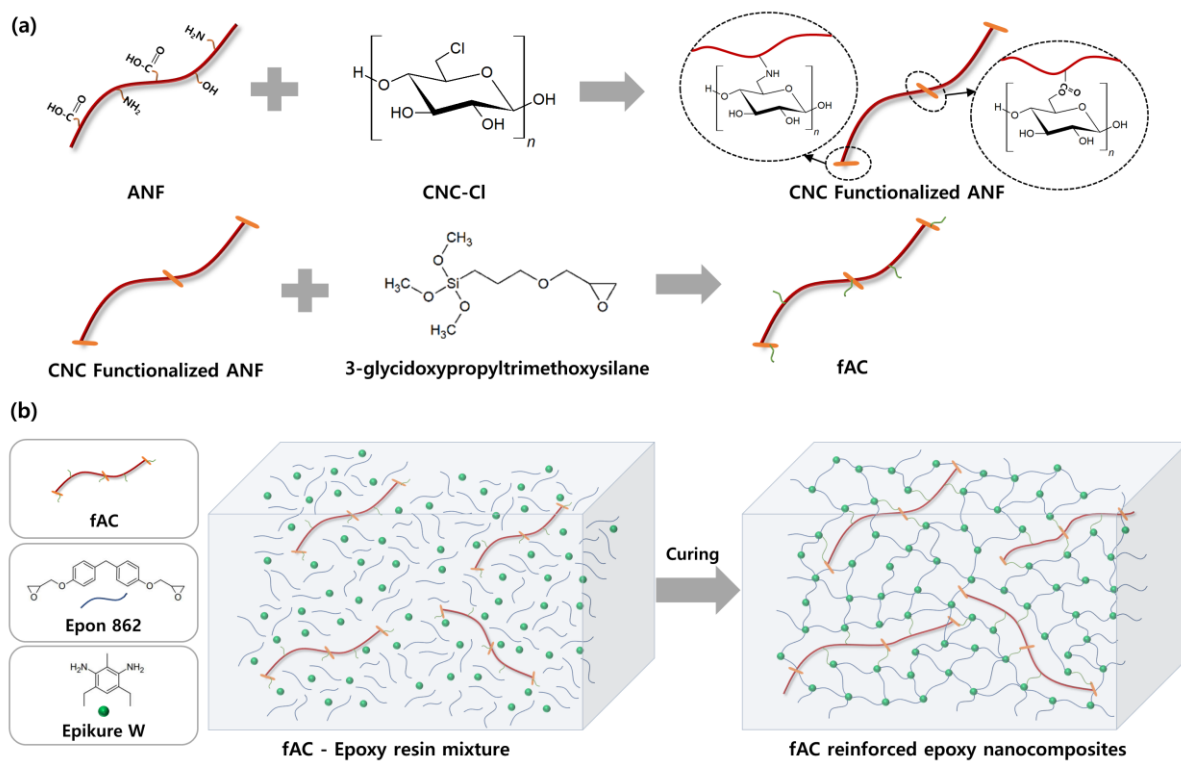
Figure 6.1. Schematic illustration of the reactions for (a) the preparation of fACs, and (b) the fAC reinforced epoxy nanocomposites.

6.2.2 Characterization of fAC hybrid filler

The effect of CNC functionalized ANFs were investigated using several characterization techniques. Attenuated total reflection-Fourier transform infrared spectroscopy (ATR-FTIR, Nicolet iS50 spectrometer) was performed to characterize the chemical structure alterations before and after the GPTMS treatment and CNC functionalization on the ANFs. The FTIR spectra of ANFs, CNCs, ACs, and fACs are displayed in Figure 6.2. After the surface modification using GPTMS, new peaks are shown in the spectra of ANFs and CNCs in Figure 6.2a. The peaks at 2923, 1100, 1008, and 988 cm^{-1} correspond to the C-H stretching vibration of methylene, Si-O, Si-O-C, and Si-O stretching vibration from the silane coupling agent, respectively. Thus, the alterations of FTIR spectra before and after the treatment show that ANFs and CNCs were functionalized using

GPTMS. The chemical structure changes after functionalizing ANFs using CNCs and combining ANFs and CNCs are shown in Figure 6.2b. Both AC and fAC displayed all the characteristic peaks of both ANFs and CNCs, however, fAC showed two new characteristic peaks in the FTIR spectra. The peaks at 1720 and 3460 cm^{-1} are attributed to ester C=O stretching and a secondary amine, respectively, and they can be shown from the reaction between the functionalities of ANFs and CNC-Cl. The results confirm that ANFs and CNCs are linked through covalent bonding. Therefore, the FTIR spectra of ANFs, CNCs, ACs, and fACs demonstrate the modification of nanofillers and the successful preparation of fACs with chemical covalent linkages.
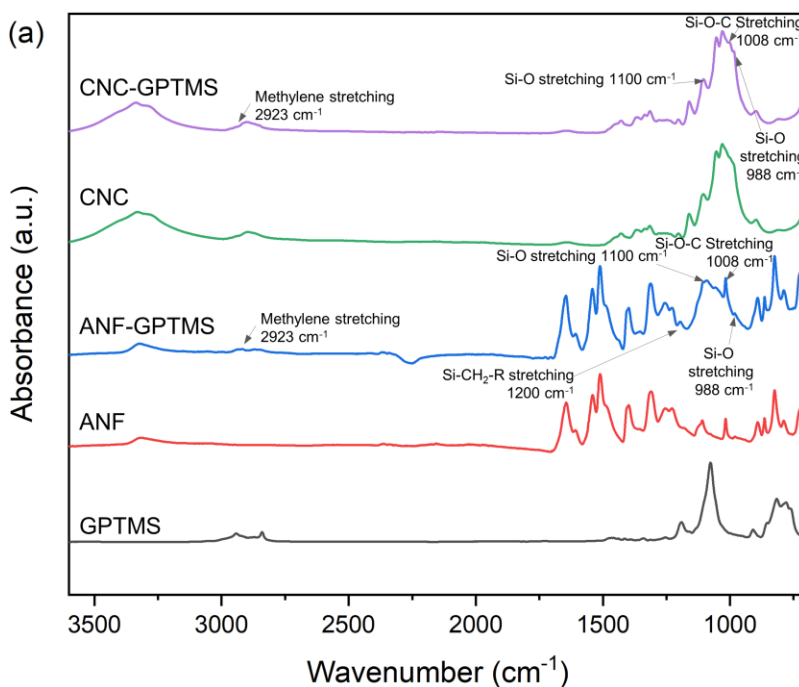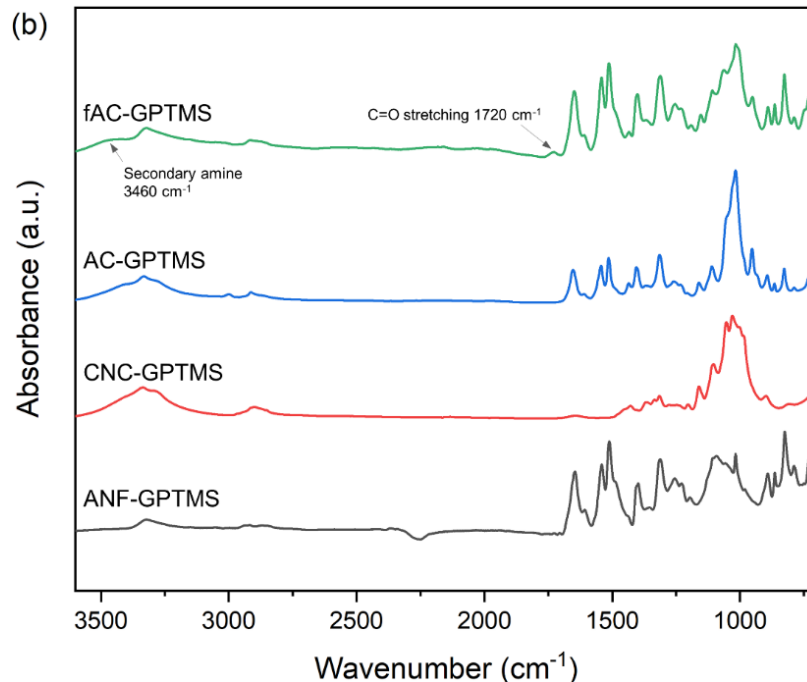
Figure 6.2. FTIR spectra of (a) GPTMS, ANF, ANF-GPTMS, CNC, and CNC-GPTMS, and (b) ANF-GPTMS, CNC-GPTMS, AC-GPTMS, and fAC-GPTMS.

To investigate the crystalline structure of fACs, X-ray diffraction (XRD) patterns were obtained using a Rigaku Ultima IV X-ray diffractometer. Figure 6.3 displays the XRD patterns of ANFs, CNCs, ACs, and fACs. As shown from the previous research, ANFs showed their diffraction peaks at 20.6° and 22.9°, which are attributed to the (110) and (200) planes of aramid fibers.[4,128] The characteristic peaks of ANFs were also shown from the XRD patterns of ACs and fACs because ANFs were used to prepare both. The XRD patterns of CNCs showed peaks of the crystalline cellulose structure at 14.6°, 16.7°, 22.8°, and 34.7°.[133,134] While these diffraction peaks of CNCs appeared in the XRD pattern of ACs after the combination of ANFs and CNCs, they were not shown in the XRD pattern of fACs, which were prepared through the chemical covalent linkages. The disappearance of the peaks could be due to the attenuated crystalline structure of CNCs following the reaction between ANFs and CNCs.[135] Additionally,

atomic force microscopy (AFM, Park XE-70) was used to examine the changes in the morphology and dimensions of ACs and fACs. Figure 6.4 displays the AFM images of ANFs, CNCs, ACs, and fACs. The diameters of ANFs and CNCs are measured to be in the range of 4 to 12 nm and 3 to 8 nm, respectively, which is in accordance with the results from previous research.[69,137] In the image of ACs, CNCs are observed to be separated from ANFs. However, in the image of fACs, CNCs are shown on the edge or middle of ANFs, and the shape of CNCs is likely changed due to the chemical reaction between the ANFs and CNCs. Therefore, the AFM images show the absence of chemical interaction between ANFs and CNCs in ACs, and the establishment of covalent linkages in fACs. Drawing from the characterization results in this section, the preparation of fACs with covalent bonding between ANFs and CNCs is confirmed. The new hybrid materials based on ANFs and CNCs are expected to contribute to improved mechanical interlocking interaction between the polymer and nanofillers due to the extensive branching and network structures of the nanofillers, in addition to the enhanced chemical interaction due to the modification using a silane coupling agent.
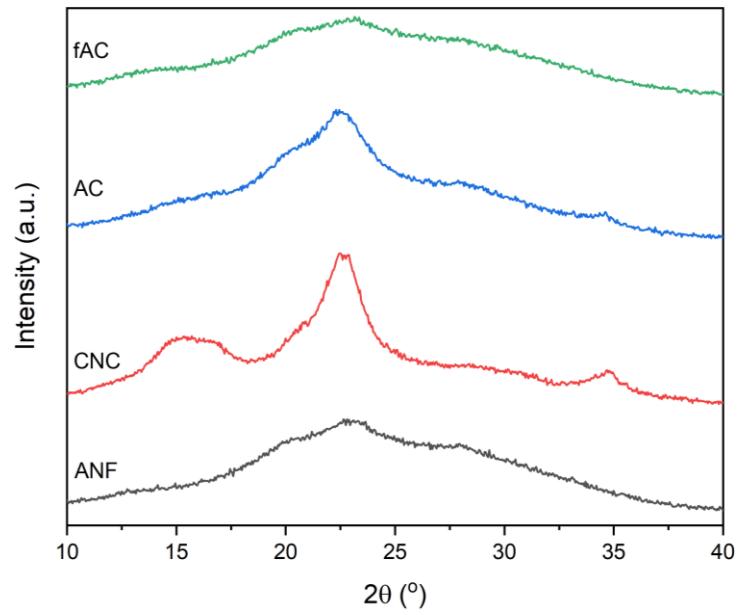
Figure 6.3. XRD patterns of ANF, CNCs, ACs, and fACs.
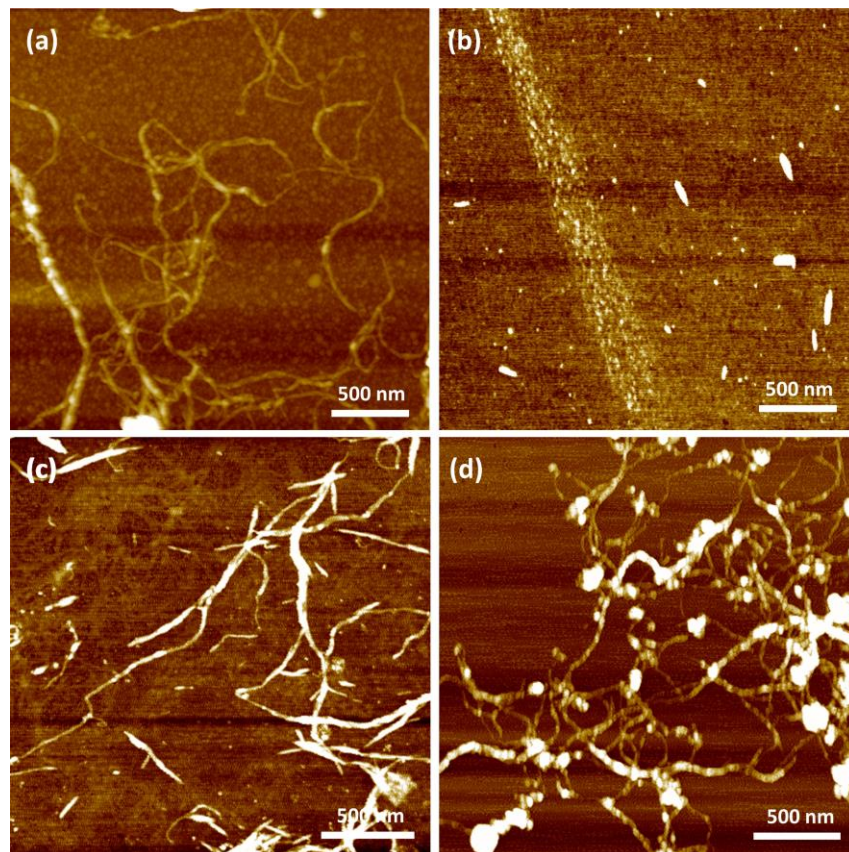
Figure 6.4. AFM images of (a) ANFs, (b) CNCs, (c) ACs, and (d) fACs.

6.3 Fabrication and characterization of fAC reinforced epoxy nanocomposites

6.3.1 Fabrication of fAC reinforced epoxy nanocomposites

The fAC reinforced epoxy nanocomposites were prepared by adding 0.2 wt % to 1.5 wt % of fACs to the epoxy resin based on Epon 862 (diglycidyl ether of bisphenol-F epoxy, Hexion) and Epikure W (diethyltoluenediamine, Hexion). The fAC paste was dispersed into the Epon 862 using horn sonication and centrifugal mixing (FlackTek Speed mixer) for 20 min. After the dispersion, the mixture was dried under vacuum at 70 ℃ for 24 h to remove acetone from the fAC paste. Then, Epikure W (26.4 part per hundred resin) was added to the fAC mixture and mixed for 20 min, followed by degassing at 70 ℃ under vacuum prior to being cast into silicone molds. The mixture was subsequently cured in a convection oven with a 30 min temperature ramp from 25 °C to 121 °C followed by a 240 min isothermal hold at 121 °C. (Figure 6.1b). ANF, CNC, and AC reinforced epoxy nanocomposites were also fabricated using the same process described above.

6.3.2 Tensile properties

Tensile tests were performed using an Instron universal testing machine (model 5982) according to ASTM D638 to examine the effect of CNC functionalization on the ANFs for the mechanical properties of epoxy composites. Type V specimens were prepared and tested at a crosshead speed of 1 mm/min. The concentration of nanofillers in the samples was limited to 1.5 wt % due to the formation of micro voids in samples with a higher concentration of nanofillers even after the degassing procedure. The surface modification using GPTMS increased the viscosity of the epoxy resin mixture significantly during the mixing process.[116] The average Young's modulus and tensile strength of ANF, CNC, AC, and fAC reinforced epoxy nanocomposites are

displayed in Figure 6.5, and Figure 6.6 shows representative stress-strain curves of epoxy samples reinforced with 1.5 wt % nanofillers. As shown from our previous studies, ANFs and CNCs were found to be beneficial for reinforcing epoxy nanocomposites due to their high aspect ratio and surface area. The Young's modulus and tensile strength of ANF reinforced epoxy samples improved up to 7.5% and 9.1%, and those of CNC reinforced epoxy resin improved by 8.1% and 6.9%, respectively, compared to the neat epoxy samples. When ACs were incorporated into the epoxy matrix, tensile properties were in the middle of ANF and CNC reinforced epoxy nanocomposites. This means that there is no synergetic effect of ACs when they are simply combined without covalent linkages. However, fAC reinforced samples outperformed other samples in tensile properties. The Young's modulus of fAC reinforced samples was observed to increase up to 3.29 ± 0.06 GPa with 1.5 wt % fACs, showing a 15.7% improvement relative to the reference sample. The samples reinforced with 1.5 wt % fAC also displayed the highest tensile strength, 87.2 ± 1.5 MPa, which is 10.1% higher than that of the neat epoxy samples. Moreover, the lowest tensile strength of fAC reinforced samples at 0.2 wt % was even higher than the highest tensile strength of all the ANF, CNC, and AC reinforced epoxy samples. The average Young's modulus of 1.5 wt % fAC reinforced epoxy samples was found to be 7.6%, 6.0%, and 5.5% higher than that of the 1.5 wt % ANF, CNC, and AC reinforced nanocomposites, respectively. These results show the effect of CNC functionalization on the ANFs for the tensile properties of epoxy nanocomposites in addition to the individual characteristics from both ANFs and CNCs. The ANFs maintain the excellent mechanical properties of Kevlar after the dissolution, and their high aspect ratio and large specific area are beneficial for the reinforcement of the epoxy matrix. CNCs also have a high aspect ratio and large surface area with excellent mechanical properties. In addition to the characteristics of the nanomaterials, CNCs functionalized at the middle or end of ANFs can

117

improve the mechanical interlocking of nanofillers in the epoxy matrix through branched network structures. Moreover, the surface modification of fACs using GPTMS improves the chemical interaction between the epoxy matrix and fACs.[69] Therefore, the enhanced chemical and mechanical interaction improved the stress transfer between the epoxy matrix and nanofillers, yielding improvement in the overall mechanical properties of epoxy nanocomposites.[29,35,117]
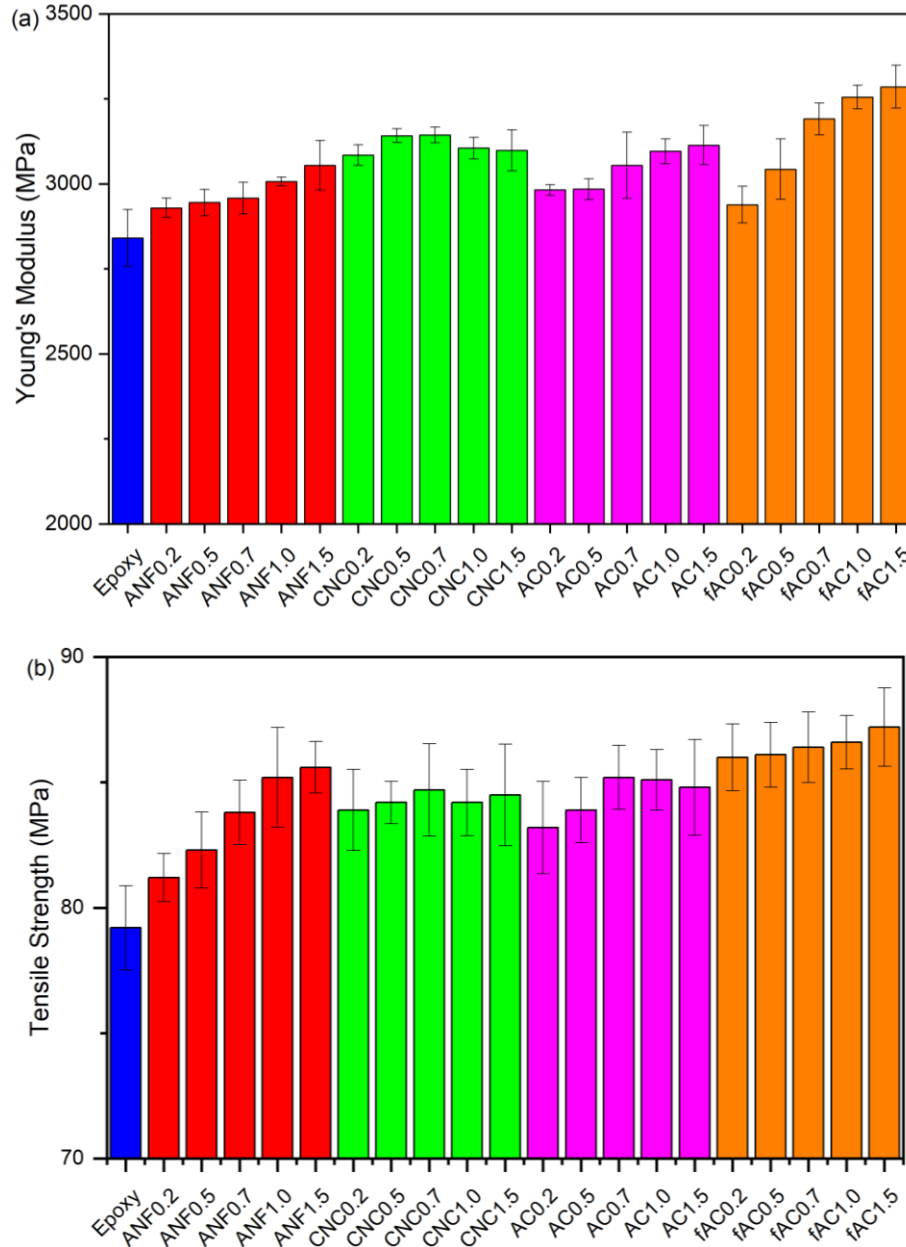
Figure 6.5. (a) Young's modulus and (b) tensile strength of ANF, CNC, AC, and fAC reinforced epoxy nanocomposites.
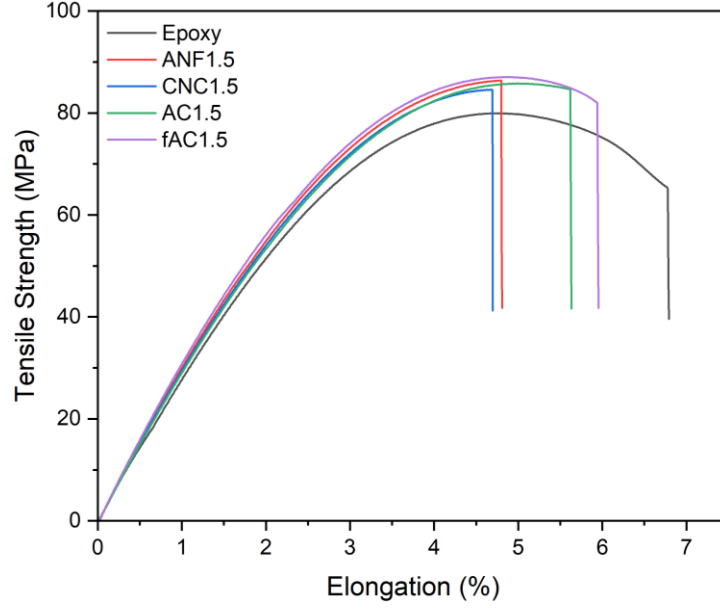
Figure 6.6. Stress-strain curves of epoxy nanocomposites reinforced with 1.5 wt % nanofillers.

6.3.3 Fracture properties

Three-point bend specimens were prepared and tested to conduct fracture toughness tests following ASTM D5045-99. After testing, the critical stress intensity factor (K_{Ic}) and fracture toughness (G_{Ic}) were obtained using the following equations.

$$K_{Ic} = \frac{P_{max}}{BW^{\frac{1}{2}}} f(x) \tag{6.1}$$

$$f(x) = 6x^{1/2} \frac{[1.99 - x(1-x)(2.15 - 3.93x + 2.7x^2)]}{(1+2x)(1-x)^{3/2}}, x = a/W \tag{6.2}$$

$$G_{Ic} = \frac{K_{Ic}^2}{E}(1 - v^2) \tag{6.3}$$

where, P_{max} is the maximum load, B is the specimen thickness, W is the specimen width, a is the crack length, E is the Young's modulus of samples, and v is the Poisson's ratio (assumed to be 0.353). The calculated K_{Ic} and G_{Ic} of ANF, CNC, AC, and fAC reinforced epoxy samples are displayed in Figure 6.7. From the test results, both K_{Ic} and G_{Ic} of epoxy nanocomposites improved

as the weight fraction of the nanofillers in the samples increased. The improvement of K_{Ic} and G_{Ic} of CNC reinforced samples compared to the neat epoxy resin was slightly better than that of ANF reinforced samples, and both K_{Ic} and G_{Ic} of AC reinforced samples were in the middle of ANF and CNC reinforced samples. These results indicate that ANFs and CNCs can enhance the fracture properties, but the non-covalent interaction between the ANFs and CNCs is not significant for the further reinforcement of composites. However, the fracture properties of fAC reinforced epoxy samples were higher than those of all the other samples. The test results show that the 1.5 wt % fAC reinforced samples can improve K_{Ic} by 104.4% and G_{Ic} by 249.6% compared to the reference samples. Both K_{Ic} and G_{Ic} of epoxy composites reinforced with 1.5 wt % fACs were 11.5% and 17.5% higher than those of 1.5 wt % CNC reinforced epoxy composites, respectively. The improved fracture properties can be attributed to the characteristics of CNC functionalized ANFs and the chemical covalent interaction between the epoxy matrix and fACs.[69] The sliding of large network structured fACs in the epoxy matrix can contribute to the energy dissipation at the interphase region and impede crack propagation in the nanocomposites. The fACs with a high aspect ratio and CNC functionalization on the surface, which provides mechanical interlocking in the matrix, can also contribute to crack bridging during crack propagation. Moreover, chemical covalent interaction between the epoxy matrix and fACs through surface modification using a silane coupling agent can enhance crack bridging in epoxy nanocomposites. Drawing from the test results, CNC functionalization on the ANFs is found to be beneficial for enhancing both the tensile strength and fracture resistance simultaneously.
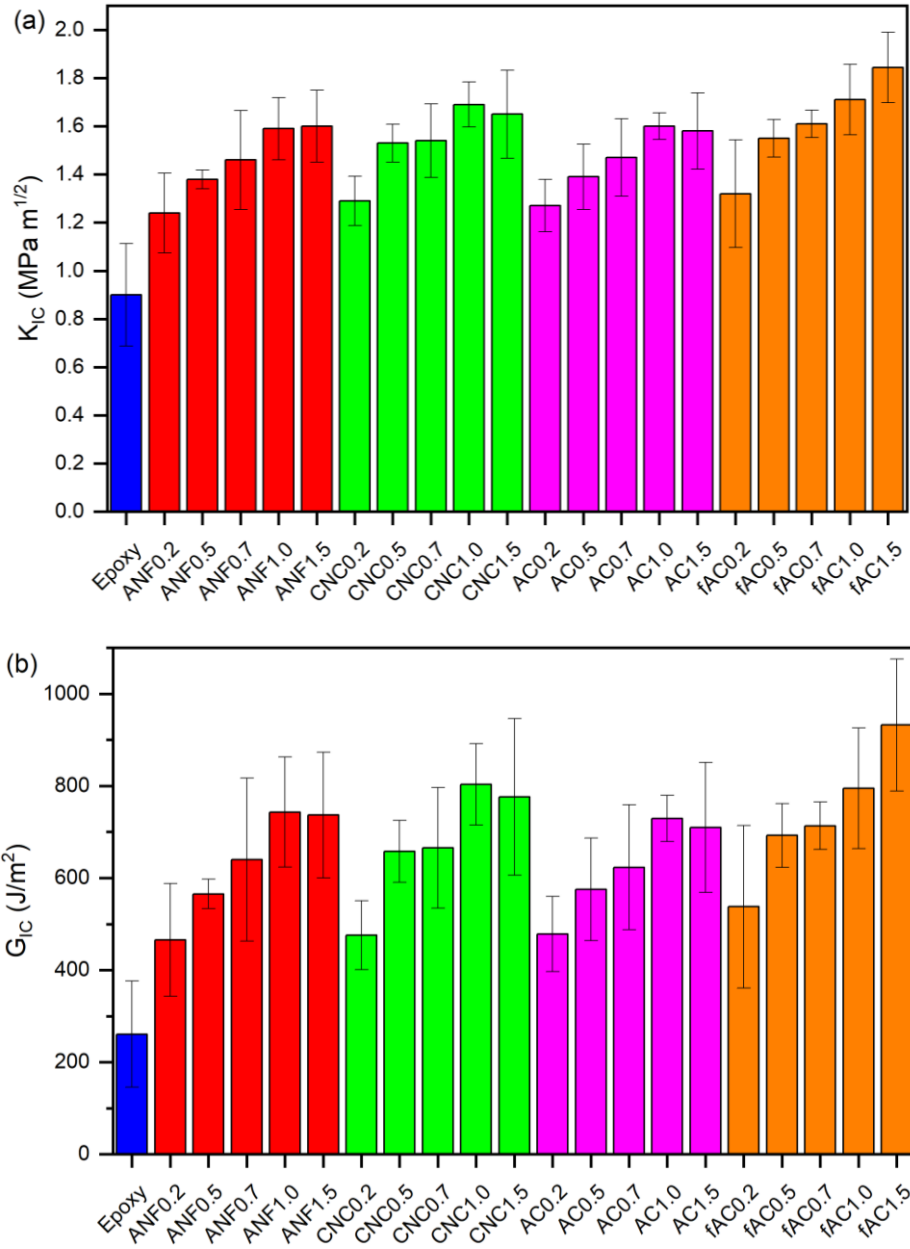
Figure 6.7. (a) Critical stress intensity factor, K_{Ic}, and (b) fracture toughness, G_{Ic}, of ANF, CNC, AC, and fAC reinforced epoxy nanocomposites.

6.3.4 Dynamic mechanical analysis

Dynamic mechanical analyzer (TA DMA 800) was used to investigate the dynamic mechanical properties of the epoxy nanocomposites over a broad temperature range. Specimens were tested at 1 Hz with a constant heating rate of 3 °C/min in a temperature range of 25 to 200 °C. Representative storage modulus and tan δ curves versus temperature are displayed in Figure 6.8, and storage modulus at 40 °C and 160 °C, and glass transition temperature (T_g) of epoxy nanocomposites are summarized in Table 6.1. The value of T_g was obtained from the maximum tan δ peak value of each sample. As the temperature increased during the test, the storage modulus decreased for all the samples and showed a relaxation above 128 °C, corresponding to the glass transition of polymeric materials. The ANF, CNC, AC, and fAC reinforced epoxy nanocomposites exhibited improved storage modulus at 40 °C and 160 °C. The storage modulus below and above T_g increased as the nanofiller weight fraction increased, although a slight decrease was observed for some samples which is likely due to nonuniform dispersion. The 1.0 wt % fAC reinforced epoxy nanocomposites exhibited a maximum of 25.1% and 68.0% increase in storage modulus at 40 °C and 160 °C, respectively, compared to the reference sample. The results show that fAC can improve the storage modulus of epoxy samples both in a glassy state and rubbery state. This could be due to the enhanced chemical and mechanical interaction between the epoxy matrix and fACs through the CNC functionalization on the ANFs and surface modification using GPTMS. The chain mobility of the epoxy matrix can be restricted by the incorporation of fACs and covalent linkages between them.[27,117,118] Moreover, the high thermal stability and T_g of aramid polymer chains can contribute to the dynamic mechanical properties over the broad temperature range, as shown from the results. However, the contribution of ACs for improving the storage

modulus was less than that of fACs due to the relatively weak interfacial interaction between the polymer chains and ACs.

The glass transition behavior of epoxy nanocomposites was observed using the T_g values obtained from the maxima of the tan δ peaks. As displayed in Table 6.1, the T_g value of ANF and fAC reinforced epoxy nanocomposites shifted to a higher temperature compared to the neat samples, while the improvement of T_g value was not significant for the AC reinforced nanocomposites. The T_g of nanocomposites shifted 6.7 °C higher when 1.0 wt % of fACs was incorporated into the epoxy resin. The T_g is known to represent the chain mobility of the polymer matrix in polymer nanocomposites and shifts to a higher temperature when the chain mobility is hindered. The factors affecting the glass transition behavior include the morphology of nanosized fillers, chemical structure and flexibility of the polymer matrix.[119,125] The fACs with attached CNCs on the middle or edge of ANFs can restrict the movement of the epoxy matrix by mechanical interlocking between them. Additionally, covalent bonding formed between the fACs and epoxy chains can hinder the mobility of the crosslinked epoxy network, resulting in an increase of T_g. The restriction of mobility of a polymer matrix by modified nanofillers has also been reported by previous research.[27,35] In addition to the shifted T_g value, tan δ peak value also indicates the mobility of polymer chains and interfacial energy dissipation of polymer nanocomposites. The tan δ peak value decreased when nanofillers were incorporated into the epoxy nanocomposites, and the fAC reinforced samples exhibited the lowest tan δ peak value. The results can be explained by the limitation of polymer chain movement and reduced energy dissipation by the incorporated fACs.[38,121] Therefore, the dynamic mechanical analysis of epoxy composites confirms the improved chemical and mechanical interaction between the epoxy matrix and CNC functionalized ANFs.
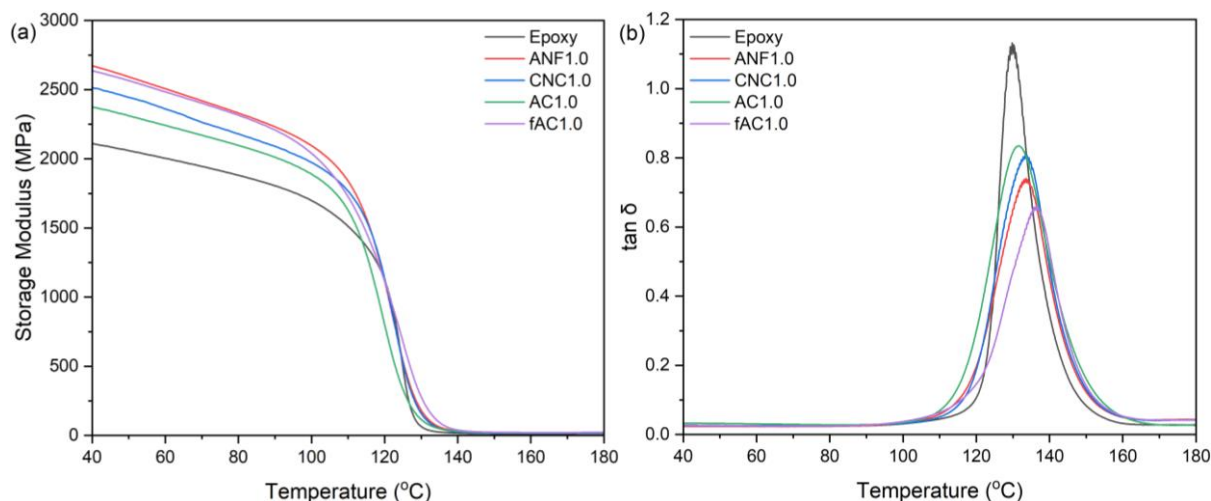
Figure 6.8. (a) Storage modulus and (b) tan δ graph of epoxy nanocomposite reinforced with 1.0 wt % nanofillers from 40 to 180 °C.

Table 6.1. Summary of storage modulus and T_g of ANF, CNC, AC, fAC reinforced epoxy nanocomposites.

Sample	E' at 40 °C (GPa)	E' at 160 °C (MPa)	T_g (°C)
Epoxy resin	2.11	12.8	129.8
ANF0.5	2.52	18.7	130.4
ANF1.0	2.67	21.1	133.6
ANF1.5	2.54	21.4	131.1
CNC0.5	2.28	14.2	129.4
CNC1.0	2.51	16.5	133.3
CNC1.5	2.57	14.9	129.4
AC0.5	2.40	16.4	130.4
AC1.0	2.45	19.0	129.3
AC1.5	2.43	19.3	128.6
fAC0.5	2.57	16.0	131.2
fAC1.0	2.64	21.5	136.5
fAC1.5	2.60	23.0	134.0

6.4 Chapter summary

In this chapter, fACs were prepared by a reaction between ANFs and chlorinated CNCs, following modification using a silane coupling agent with epoxy group. Then, the fACs were used to prepare epoxy nanocomposites, and the resulting nanocomposites were tested to investigate the effect of CNC functionalization on the ANFs. The characterization techniques, including FTIR, XRD, and AFM, revealed that CNCs were functionalized on the surface of the ANFs through covalent bonding. From the static and dynamic mechanical test results, it was shown that the fACs could improve the overall mechanical properties of epoxy nanocomposites, and the improvement was greater than that of epoxy samples reinforced with ANF, CNC, or AC filler without covalent bonding between them. The tensile test results showed that Young's modulus and tensile strength of 1.5 wt % fAC reinforced epoxy nanocomposites were improved by 15.1% and 10.1%, respectively, compared to the neat epoxy resin. The improvements were 7.6% and 1.9% higher than those of ANF reinforced epoxy samples with the same amount of nanofillers. Fracture toughness was also improved by up to 249.6% when 1.5 wt % of fACs were used. Moreover, the storage modulus of fAC reinforced samples at 40 °C and 160 °C was improved by 25.1% and 68.0%, respectively, compared to the neat epoxy samples, and T_g also shifted to a higher temperature. Therefore, improved chemical and mechanical interaction through CNC functionalization on the ANFs exhibited further enhancement in tensile properties, fracture toughness, and dynamic mechanical properties of polymer nanocomposites.

Chapter 7
Conclusion

This work investigated the effect of functionalized ANFs on the properties and performance of rubber nanocomposites for tire tread and epoxy nanocomposites. Compared to traditional composites, polymer nanocomposites can provide superior mechanical strength, toughness, thermal properties, and dynamic mechanical properties with a relatively low weight fraction of nano-sized fillers. Because of these advantages, the applications of polymer nanocomposites are continuously growing. The properties and performance of polymer nanocomposites depend on the type of nanofillers. Among various types of nanofillers, ANFs were chosen to reinforce rubber and epoxy matrices due to their high aspect ratio, large surface area, and excellent mechanical properties, in addition to the rich functionalities that can be used for surface modification. Researchers have used the ANFs to reinforce polar polymer matrices because of the polar chemical nature of the ANFs. However, the surface functionalization of ANFs using silane coupling agents can improve the interfacial interaction between polymer matrices and ANFs and widen the range of applications to non-polar polymer matrices, such as diene rubbers. In this work, functionalized ANFs using a silane coupling agent with polysulfide were used to reinforce rubber compounds for tire tread. Test results showed that tensile properties and tire performances, including abrasion resistance and fuel efficiency, improved due to the enhanced dispersion in the rubber matrix and interfacial interaction between the matrix and ANFs through covalent bonding. The enhanced fuel efficiency of ANF reinforced rubber compounds can be attributed to the reduced

energy dissipation during the deformation of rubber samples due to the covalent linkages between rubber molecules and ANFs. The advantages of functionalized ANFs were also shown from the study regarding the epoxy nanocomposites reinforced with EANFs. EANF reinforced epoxy nanocomposites exhibited improved tensile strength, elastic modulus, fracture toughness, and dynamic mechanical properties compared to the untreated ANF reinforced epoxy nanocomposites. These results correspond to the enhanced load and stress transfer from the epoxy matrix to ANFs through improved chemical interfacial interactions between them. In addition to the silane coupling agent treatment, ANFs were hybridized with other strong nanomaterials such as GOs and CNCs. A synergetic effect of ANF/GO hybrid fillers was observed from the study regarding ANF/GO reinforced rubber compounds. The mechanical properties and tire performances, including abrasion resistance and fuel efficiency, improved without any trade-offs when ANF/GO hybrid fillers were used to reinforce rubber compounds compared to the reference rubber compounds. The improvements were greater than those of ANF or GO alone reinforced rubber compounds due to the additional stress transfer between the ANFs and GOs in addition to the chemical interfacial interaction between the rubber matrix and hybrid fillers. Moreover, CNC functionalized ANFs were prepared by the reaction between chlorinated CNCs and ANFs, and were used to reinforce both rubber compounds for tire tread and epoxy resin. ANF/CNC hybrid fillers without covalent linkages were also prepared for comparison. Test results showed that mechanical properties, abrasion resistance, and fuel efficiency improved when CNC functionalized ANFs were used to reinforce rubber compounds. Additionally, epoxy nanocomposites reinforced with CNC functionalized ANFs also exhibited enhanced tensile strength, Young's modulus, fracture toughness, and dynamic mechanical properties through improved chemical and mechanical interaction due to the attached CNCs on the middle or edge of

127

ANFs. Thus, the silane coupling agent treatment and hybridization of ANFs result in improved properties and performance of tire tread rubber compounds and epoxy nanocomposites through the enhanced chemical and mechanical interactions between their matrices and nanofillers.

7.1 Contributions

This dissertation investigated the mechanical properties and performances of novel nanofiller reinforced polymer nanocomposites and developed several novel functionalization methods of ANFs for various polymer matrices. This work has provided solutions to improve the interfacial interaction between polymer matrices and nanofillers in nanocomposites.

The main contributions of this work center around the development of novel silane coupling agent functionalization and hybridization of ANFs for the reinforcement of rubber compounds. Furthermore, the methods used throughout this dissertation overcome current barriers restricting the use of ANF due to their polar chemical nature and allow for the reinforcement of non-polar diene rubber matrices. These methods have contributed significantly to simultaneously enhancing important tire performance metrics, such as wet grip performance, fuel efficiency, and wear resistance, without decreasing any of them. Increasing the loading of conventional fillers such as carbon black used for tire tread rubber compounds can typically improve one aspect of the performance, but usually deteriorates fuel efficiency due to the increased energy dissipation between the fillers and rubber matrix. However, functionalized ANFs can improve all performance metrics simultaneously because of the reduced energy dissipation through the covalent linkages between the matrix and ANFs, and the unique characteristics of ANFs such as large surface area, high aspect ratio, and outstanding mechanical strength. Moreover, hybridization of ANFs using GOs or CNCs contributed to enhanced chemical and mechanical interactions in the rubber

compounds reinforced with the hybrid fillers. Therefore, the rubber nanocomposites reinforced with functionalized ANFs are expected to contribute to the overall performance of tires, including fuel efficiency and abrasion resistance which can help save cost and reduce impact on the environment.

Another contribution of this work is the development of epoxy nanocomposites reinforced with EANFs and CNC functionalized ANFs. The newly developed functionalization methods have led to significant contributions to improving tensile properties, fracture properties, and dynamic mechanical properties of epoxy nanocomposites. By studying the chemical interfacial interactions between the epoxy matrix and novel nanofillers based on ANFs, highly crosslinked epoxy nanocomposite networks are formed through a simple curing process. The introduced epoxy functionalized silane coupling agent and CNCs on ANFs establishes a strong network in the nanocomposites, as reflected through the enhanced tensile and fracture properties. The functionalized ANF reinforced epoxy nanocomposites are demonstrated to exhibit improved tensile and fracture properties at the same time, which are mutually exclusive properties of nanocomposites. The results show the potential of functionalized ANFs as novel reinforcement fillers for polymer nanocomposites. Thus, the functionalized ANF reinforced thermosetting polymers are expected to have a great impact in the field of structural polymeric materials with improved static and dynamic mechanical properties even in high temperatures.

7.2 Recommendations for future work

This dissertation performed extensive research on improving the properties and performance of thermosetting polymers and rubber compounds using functionalized ANFs. The results demonstrated that various chemicals and nanomaterials could be introduced to the surface

of ANFs through the rich functionalities on the ANFs, and the properties and performance of polymer nanocomposites can be enhanced when the functionalized ANFs are incorporated as reinforcing fillers. Although several methods and techniques for the functionalization of ANFs were provided in this dissertation, additional studies can be conducted as future work to expand the potential of the presented work.

In this work, the effect of functionalized ANFs on tire performance was investigated using carbon black-filled rubber compounds. Various types of recipes can be tested, such as silica-filled rubber compounds, to broaden the applications further. The effect of ANFs can be studied by varying the amount and type of main fillers in rubber compounds. In addition, natural rubber can be used as a matrix instead of styrene-butadiene rubber and butadiene rubber to apply the usage of functionalized ANFs from passenger car tires to commercial vehicle tires. The different chemical structures and nature of polymer matrices and fillers can affect the interaction with functionalized ANFs. Therefore, investigating the effect of different compound recipes will be an interesting topic.

In addition, one of the last aspects of this dissertation was the development of CNC functionalized ANFs for the reinforcement of polymer nanocomposites. While the CNCs were used to provide additional mechanical interaction in the nanocomposites, their morphological changes were not fully understood. When CNCs were functionalized on the surface of ANFs, the CNCs appeared to change their shape quite significantly. A further study that addresses the changes can clarify their integration on the surface of ANFs and maximize the performance of functionalized ANFs in the polymer nanocomposites.

Finally, additive manufacturing methods can be applied to prepare functionalized ANF reinforced thermosetting polymers and rubber compounds. The 3D printing technique is very promising in the fabrication of composite materials because the technique enables a customized

design according to customers' needs. The conventional methods to prepare samples or products require a pre-designed mold which is not flexible for changing the shape or functionality of products. However, curing processes have inhibited the application of additive manufacturing methods in the field of rubber nanocomposites. Therefore, further study in the development of rubber 3D printing techniques should focus on utilizing the customized design and novel curing processes for rubber nanocomposites.

References

[1]   J. Cheon, M. Lee, M. Kim, Study on the stab resistance mechanism and performance of the carbon, glass and aramid fiber reinforced polymer and hybrid composites, Compos. Struct. 234 (2020) 111690. https://doi.org/10.1016/j.compstruct.2019.111690.

[2]   B. Zhang, L. Jia, M. Tian, N. Ning, L. Zhang, W. Wang, Surface and interface modification of aramid fiber and its reinforcement for polymer composites: A review, Eur. Polym. J. 147 (2021) 110352. https://doi.org/10.1016/j.eurpolymj.2021.110352.

[3]   P. Priyanka, A. Dixit, H.S. Mali, High strength Kevlar fiber reinforced advanced textile composites, Iran. Polym. J. (English Ed. 28 (2019) 621–638. https://doi.org/10.1007/s13726-019-00721-7.

[4]   M. Yang, K. Cao, L. Sui, Y. Qi, J. Zhu, A. Waas, E.M. Arruda, J. Kieffer, M.D. Thouless, N.A. Kotov, Dispersions of aramid nanofibers: A new nanoscale building block, ACS Nano. 5 (2011) 6945–6954. https://doi.org/10.1021/nn2014003.

[5]   B.A. Patterson, M.H. Malakooti, J. Lin, A. Okorom, H.A. Sodano, Aramid nanofibers for multiscale fiber reinforcement of polymer composites, Compos. Sci. Technol. 161 (2018) 92–99. https://doi.org/10.1016/j.compscitech.2018.04.005.

[6]   J. Nasser, J. Lin, H. Sodano, High strength fiber reinforced composites with surface fibrilized aramid fibers, J. Appl. Phys. 124 (2018). https://doi.org/10.1063/1.5026987.

[7]   J. Lin, S.H. Bang, M.H. Malakooti, H.A. Sodano, Isolation of Aramid Nanofibers for High Strength and Toughness Polymer Nanocomposites, ACS Appl. Mater. Interfaces. 9 (2017) 11167–11175. https://doi.org/10.1021/acsami.7b01488.

[8]   J. Jordan, K.I. Jacob, R. Tannenbaum, M.A. Sharaf, I. Jasiuk, Experimental trends in polymer nanocomposites - A review, Mater. Sci. Eng. A. 393 (2005) 1–11. https://doi.org/10.1016/j.msea.2004.09.044.

[9]   B.P. Sahoo, D.K. Tripathy, Properties and applications of polymer nanocomposites: Clay and carbon based polymer nanocomposites, 2017. https://doi.org/10.1007/978-3-662-53517-2.

[10]   I.A. Kinloch, J. Suhr, J. Lou, R.J. Young, P.M. Ajayan, Composites with carbon nanotubes and graphene: An outlook, 553 (2018) 547–553. https://doi.org/10.1126/science.aat7439.

[11]   Y. Zhou, F. Pervin, L. Lewis, S. Jeelani, Experimental study on the thermal and mechanical properties of multi-walled carbon nanotube-reinforced epoxy, Mater. Sci. Eng. A. 452–453 (2007) 657–664. https://doi.org/10.1016/j.msea.2006.11.066.

[12]   A. Montazeri, N. Montazeri, Viscoelastic and mechanical properties of multi walled carbon nanotube/epoxy composites with different nanotube content, Mater. Des. 32 (2011) 2301–2307. https://doi.org/10.1016/j.matdes.2010.11.003.

[13]   Y. Feng, C. He, Y. Wen, X. Zhou, X. Xie, Y. Ye, Y.W. Mai, Multi-functional interface tailoring for enhancing thermal conductivity, flame retardancy and dynamic mechanical property of epoxy/Al2O3 composites, Compos. Sci. Technol. 160 (2018) 42–49. https://doi.org/10.1016/j.compscitech.2018.03.009.

[14]   H.P.S. Abdul Khalil, M. Jawaid, P. Firoozian, E.S. Zainudin, M.T. Paridah, Dynamic Mechanical Properties of Activated Carbon-Filled Epoxy Nanocomposites, Int. J. Polym. Anal. Charact. 18 (2013) 247–256. https://doi.org/10.1080/1023666X.2013.766553.

[15]   J. Zhu, J.D. Kim, H. Peng, J.L. Margrave, V.N. Khabashesku, E. V. Barrera, Improving the dispersion and integration of single-walled carbon nanotubes in epoxy composites through functionalization, Nano Lett. 3 (2003) 1107–1113. https://doi.org/10.1021/nl0342489.

[16]   C. Acebo, X. Fernández-Francos, M. Messori, X. Ramis, À. Serra, Novel epoxy-silica hybrid coatings by using ethoxysilyl-modified hyperbranched poly(ethyleneimine) with improved scratch resistance, Polymer (Guildf). 55 (2014) 5028–5035. https://doi.org/10.1016/j.polymer.2014.08.021.

[17]   H. Abdollahi, A. Ershad-Langroudi, A. Salimi, A. Rahimi, Anticorrosive coatings prepared using epoxy-silica hybrid nanocomposite materials, Ind. Eng. Chem. Res. 53 (2014) 10858–10869. https://doi.org/10.1021/ie501289g.

[18]   X. Shi, T.A. Nguyen, Z. Suo, Y. Liu, R. Avci, Effect of nanoparticles on the anticorrosion and mechanical properties of epoxy coating, Surf. Coatings Technol. 204 (2009) 237–245. https://doi.org/10.1016/j.surfcoat.2009.06.048.

[19]   K.T. Hsiao, J. Alms, S.G. Advani, Use of epoxy/multiwalled carbon nanotubes as adhesives to join graphite fibre reinforced polymer composites, Nanotechnology. 14 (2003) 791–793. https://doi.org/10.1088/0957-4484/14/7/316.

[20]   X. Zhang, Q. He, H. Gu, H.A. Colorado, S. Wei, Z. Guo, Flame-retardant electrical conductive nanopolymers based on bisphenol F epoxy resin reinforced with nano polyanilines, ACS Appl. Mater. Interfaces. 5 (2013) 898–910. https://doi.org/10.1021/am302563w.

[21] E. Tuncer, I. Sauers, D.R. James, A.R. Ellis, M.P. Paranthaman, T. Aytu, S. Sathyamurthy, K. L More, J. Li, A. Goyal, Electrical properties of epoxy resin based nano-composites, Nanotechnology. 18 (2007). https://doi.org/10.1088/0957-4484/18/2/025703.

[22] A. Toldy, B. Szolnoki, G. Marosi, Flame retardancy of fibre-reinforced epoxy resin composites for aerospace applications, Polym. Degrad. Stab. 96 (2011) 371–376. https://doi.org/10.1016/j.polymdegradstab.2010.03.021.

[23] H. Gu, J. Guo, Q. He, S. Tadakamalla, X. Zhang, X. Yan, Y. Huang, H.A. Colorado, S. Wei, Z. Guo, Flame-retardant epoxy resin nanocomposites reinforced with polyaniline-stabilized silica nanoparticles, Ind. Eng. Chem. Res. 52 (2013) 7718–7728. https://doi.org/10.1021/ie400275n.

[24] H. Gu, C. Ma, J. Gu, J. Guo, X. Yan, J. Huang, Q. Zhang, Z. Guo, An overview of multifunctional epoxy nanocomposites, J. Mater. Chem. C. 4 (2016) 5890–5906. https://doi.org/10.1039/c6tc01210h.

[25] K. Wang, L. Wang, J. Wu, L. Chen, C. He, Preparation of highly exfoliated epoxy/clay nanocomposites by "slurry compounding": Process and mechanisms, Langmuir. 21 (2005) 3613–3618. https://doi.org/10.1021/la047709u.

[26] J. Park, S.C. Jana, Mechanism of exfoliation of nanoclay particles in epoxy-clay nanocomposites, Annu. Tech. Conf. - ANTEC, Conf. Proc. 2 (2003) 1438–1442. https://doi.org/10.1021/ma021509c.

[27] J. Zhu, S. Wei, J. Ryu, M. Budhathoki, G. Liang, Z. Guo, In situ stabilized carbon nanofiber (CNF) reinforced epoxy nanocomposites, J. Mater. Chem. 20 (2010) 4937–4948. https://doi.org/10.1039/c0jm00063a.

[28] Y.K. Choi, K.I. Sugimoto, S.M. Song, Y. Gotoh, Y. Ohkoshi, M. Endo, Mechanical and physical properties of epoxy composites reinforced by vapor grown carbon nanofibers, Carbon N. Y. 43 (2005) 2199–2208. https://doi.org/10.1016/j.carbon.2005.03.036.

[29] P.C. Ma, J.K. Kim, B.Z. Tang, Effects of silane functionalization on the properties of carbon nanotube/epoxy nanocomposites, Compos. Sci. Technol. 67 (2007) 2965–2972. https://doi.org/10.1016/j.compscitech.2007.05.006.

[30] Z. Wang, X. Yang, Q. Wang, H.T. Hahn, S.G. Lee, K.H. Lee, Z. Guo, Epoxy resin nanocomposites reinforced with ionized liquid stabilized carbon nanotubes, Int. J. Smart Nano Mater. 2 (2011) 176–193. https://doi.org/10.1080/19475411.2011.594104.

[31] K.S. Khare, F. Khabaz, R. Khare, Effect of carbon nanotube functionalization on mechanical and thermal properties of cross-linked epoxy-carbon nanotube nanocomposites: Role of strengthening the interfacial interactions, ACS Appl. Mater. Interfaces. 6 (2014) 6098–6110. https://doi.org/10.1021/am405317x.

[32] F.H. Gojny, M.H.G. Wichmann, B. Fiedler, K. Schulte, Influence of different carbon nanotubes on the mechanical properties of epoxy matrix composites - A comparative study, Compos. Sci. Technol. 65 (2005) 2300–2313. https://doi.org/10.1016/j.compscitech.2005.04.021.

[33] I. Zaman, T.T. Phan, H.C. Kuan, Q. Meng, L.T. Bao La, L. Luong, O. Youssf, J. Ma, Epoxy/graphene platelets nanocomposites with two levels of interface strength, Polymer (Guildf). 52 (2011) 1603–1611. https://doi.org/10.1016/j.polymer.2011.02.003.

[34] L.C.O. Silva, G.G. Silva, P.M. Ajayan, B.G. Soares, Long-term behavior of epoxy/graphene-based composites determined by dynamic mechanical analysis, J. Mater. Sci. 50 (2015) 6407–6419. https://doi.org/10.1007/s10853-015-9193-8.

[35] Y.J. Wan, L.X. Gong, L.C. Tang, L. Bin Wu, J.X. Jiang, Mechanical properties of epoxy composites filled with silane-functionalized graphene oxide, Compos. Part A Appl. Sci. Manuf. 64 (2014) 79–89. https://doi.org/10.1016/j.compositesa.2014.04.023.

[36] L.C. Tang, Y.J. Wan, D. Yan, Y.B. Pei, L. Zhao, Y.B. Li, L. Bin Wu, J.X. Jiang, G.Q. Lai, The effect of graphene dispersion on the mechanical properties of graphene/epoxy composites, Carbon N. Y. 60 (2013) 16–27. https://doi.org/10.1016/j.carbon.2013.03.050.

[37] S. Rim, M. Park, S. Il Hong, J. Kim, S. Kang, C.R. Choe, Preparation and characterization of epoxy composites filled with functionalized nanosilica particles obtained via sol–gel process, Polymer (Guildf). 42 (2002) 879–887. https://doi.org/10.1016/s0032-3861(00)00392-x.

[38] N. Saba, A. Safwan, M.L. Sanyang, F. Mohammad, M. Pervaiz, M. Jawaid, O.Y. Alothman, M. Sain, Thermal and dynamic mechanical properties of cellulose nanofibers reinforced epoxy composites, Int. J. Biol. Macromol. 102 (2017) 822–828. https://doi.org/10.1016/j.ijbiomac.2017.04.074.

[39] R. Bond, G.F. Morton, L.H. Krol, A tailor-made polymer for tyre applications, Polymer (Guildf). 25 (1984) 132–140. https://doi.org/10.1016/0032-3861(84)90278-7.

[40] Official Journal of the European Union L342 46-58, 2009.

[41] S. Wagner, T. Hüffer, P. Klöckner, M. Wehrhahn, T. Hofmann, T. Reemtsma, Tire wear particles in the aquatic environment - A review on generation, analysis, occurrence, fate and effects, Water Res. 139 (2018) 83–100. https://doi.org/10.1016/j.watres.2018.03.051.

[42] P. Manoharan, K. Naskar, Exploring a highly dispersible silica-elastomer composite for tire applications, J. Appl. Polym. Sci. 133 (2016). https://doi.org/10.1002/app.43531.

[43] P. Thaptong, P. Sae-Oui, C. Sirisinha, Influences of styrene butadiene rubber and silica types on performance of passenger car radial tire tread, Rubber Chem. Technol. 90 (2017) 699–713. https://doi.org/10.5254/rct.17.83724.

[44] M.L. Studebaker, The Chemistry of Carbon Black and Reinforcement, Rubber Chem. Technol. 30 (1957) 1400–1483. https://doi.org/10.5254/1.3542764.

[45] S. Mihara, R.N. Datta, J.W.M. Noordermeer, Flocculation in silica reinforced rubber compounds, Rubber Chem. Technol. 82 (2009) 524–540. https://doi.org/10.5254/1.3548262.

[46] K.E. Polmanteer, C.W. Lentz, Reinforcement Studies - Effect of Silica Structure on Properties and Crosslink Density., Rubber Chem. Technol. 48 (1975) 795–809. https://doi.org/10.5254/1.3539687.

[47] S. Praveen, P.K. Chattopadhyay, P. Albert, V.G. Dalvi, B.C. Chakraborty, S. Chattopadhyay, Synergistic effect of carbon black and nanoclay fillers in styrene butadiene rubber matrix: Development of dual structure, Compos. Part A Appl. Sci. Manuf. 40 (2009) 309–316. https://doi.org/10.1016/j.compositesa.2008.12.008.

[48] J. Carretero-González, H. Retsos, R. Verdejo, S. Toki, B.S. Hsiao, E.P. Giannelis, M.A. López-Manchado, Effect of nanoclay on natural rubber microstructure, Macromolecules. 41 (2008) 6763–6772. https://doi.org/10.1021/ma800893x.

[49] Z. Tang, X. Wu, B. Guo, L. Zhang, D. Jia, Preparation of butadiene-styrene-vinyl pyridine rubber-graphene oxide hybrids through co-coagulation process and in situ interface tailoring, J. Mater. Chem. 22 (2012) 7492–7501. https://doi.org/10.1039/c2jm00084a.

[50] J. Wu, G. Huang, H. Li, S. Wu, Y. Liu, J. Zheng, Enhanced mechanical and gas barrier properties of rubber nanocomposites with surface functionalized graphene oxide at low content, Polymer (Guildf). 54 (2013) 1930–1937. https://doi.org/10.1016/j.polymer.2013.01.049.

[51] W. Xing, H. Li, G. Huang, L.H. Cai, J. Wu, Graphene oxide induced crosslinking and reinforcement of elastomers, Compos. Sci. Technol. 144 (2017) 223–229. https://doi.org/10.1016/j.compscitech.2017.03.006.

[52] Z. Yang, J. Liu, R. Liao, G. Yang, X. Wu, Z. Tang, B. Guo, L. Zhang, Y. Ma, Q. Nie, F. Wang, Rational design of covalent interfaces for graphene/elastomer nanocomposites, Compos. Sci. Technol. 132 (2016) 68–75. https://doi.org/10.1016/j.compscitech.2016.06.015.

[53] A. Das, K.W. Stöckelhuber, R. Jurk, M. Saphiannikova, J. Fritzsche, H. Lorenz, M. Klüppel, G. Heinrich, Modified and unmodified multiwalled carbon nanotubes in high performance solution-styrene–butadiene and butadiene rubber blends, Polymer (Guildf). 49 (2008) 5276–5283. https://doi.org/10.1016/j.polymer.2008.09.031.

[54] H.H. Le, M.N. Sriharish, S. Henning, J. Klehm, M. Menzel, W. Frank, S. Wießner, A. Das, K.W. Stöckelhuber, G. Heinrich, H.J. Radusch, Dispersion and distribution of carbon nanotubes in ternary rubber blends, Compos. Sci. Technol. 90 (2014) 180–186. https://doi.org/10.1016/j.compscitech.2013.11.008.

[55] Y. Lu, J. Liu, G. Hou, J. Ma, W. Wang, F. Wei, L. Zhang, From nano to giant? Designing carbon nanotubes for rubber reinforcement and their applications for high performance tires, Compos. Sci. Technol. 137 (2016) 94–101. https://doi.org/10.1016/j.compscitech.2016.10.020.

[56] V.G. Geethamma, R. Joseph, S. Thomas, Short coir fiber-reinforced natural rubber composites: Effects of fiber length, orientation, and alkali treatment, J. Appl. Polym. Sci. 55 (1995) 583–594. https://doi.org/10.1002/app.1995.070550405.

[57] R.N. Datta, Reduced hysteresis in truck tread compounds by using aramid short fibers, Rubber Chem. Technol. 79 (2006) 26–38. https://doi.org/Doi 10.5254/1.3547927.

[58] N. Vleugels, W.K. Dierkes, A. Blume, L.A.E.M. Reuvekamp, J.W.M. Noordermeer, Main Governing Factors Influencing Mechanical Properties of Short-Cut Aramid Fiber–Reinforced Elastomers, Rubber Chem. Technol. 92 (2019) 445–466. https://doi.org/10.5254/rct.19.82593.

[59] Q. He, Y. Zhou, W. Qu, Y. Zhang, L. Song, Z. Li, Wear property improvement by short carbon fiber as enhancer for rubber compound, Polym. Test. (2019) 0–1. https://doi.org/10.1016/j.polymertesting.2019.04.026.

[60] M.R. Kashani, Aramid-Short-Fiber Reinforced Rubber as a Tire Tread Composite, J. Appl. Polym. Sci. 113 (2009) 1355–1363.

[61] J.T. Byers, Fillers for balancing passenger tire tread properties, Rubber Chem. Technol. 75 (2002) 527–547. https://doi.org/10.5254/1.3547681.

[62] W. Kaewsakul, K. Sahakaro, W.K. Dierkes, J.W.M. Noordermeer, Optimization of mixing conditions for silica-reinforced natural rubber tire tread compounds, Rubber Chem. Technol. 85 (2012) 277–294. https://doi.org/10.5254/rct.12.88935.

[63] M. Nillawong, P. Sae-oui, K. Suchiva, C. Sirisinha, Properties of Sbr Filled With Carbon Black and Aramid Pulp Hybrid Filler: Comparison Between Predispersed Aramid Pulp and Conventional Aramid Pulp, Rubber Chem. Technol. 89 (2016) 640–652. https://doi.org/10.5254/rct.16.83803.

[64] M. Yang, K. Cao, B. Yeom, M.D. Thouless, A. Waas, E.M. Arruda, N.A. Kotov, Aramid nanofiber-reinforced transparent nanocomposites, J. Compos. Mater. 49 (2015) 1873–1879. https://doi.org/10.1177/0021998315579230.

[65] Y. Guan, W. Li, Y. Zhang, Z. Shi, J. Tan, F. Wang, Y. Wang, Aramid nanofibers and poly (vinyl alcohol) nanocomposites for ideal combination of strength and toughness via hydrogen bonding interactions, Compos. Sci. Technol. 144 (2017) 193–201. https://doi.org/10.1016/j.compscitech.2017.03.010.

[66] L. Xu, X. Zhao, C. Xu, N.A. Kotov, Water-Rich Biomimetic Composites with Abiotic Self-Organizing Nanofiber Network, Adv. Mater. 30 (2018) 1–6. https://doi.org/10.1109/CEC.2008.4630985.

[67] Q. Kuang, D. Zhang, J.C. Yu, Y.W. Chang, M. Yue, Y. Hou, M. Yang, Toward Record-High Stiffness in Polyurethane Nanocomposites Using Aramid Nanofibers, J. Phys. Chem. C. 119 (2015) 27467–27477. https://doi.org/10.1021/acs.jpcc.5b08856.

[68] J. Fan, Z. Shi, L. Zhang, J. Wang, J. Yin, Aramid nanofiber-functionalized graphene nanosheets for polymer reinforcement, Nanoscale. (2012). https://doi.org/10.1039/c2nr31907a.

[69] J. Jung, H.A. Sodano, High strength epoxy nanocomposites reinforced by epoxy functionalized aramid nanofibers, Polymer (Guildf). 195 (2020) 122438. https://doi.org/10.1016/j.polymer.2020.122438.

[70] K.P. Surya, S. Bhattacharya, R. Mukhopadhyay, K. Naskar, A.K. Bhowmick, Natural Rubber Nanocomposites Based on New Fibrous Nanofillers With Improved Barrier Properties for Use in Tire Innerliner Applications, Rubber Chem. Technol. (2020) 000–000. https://doi.org/10.5254/rct.20.80424.

[71] Y. Chen, Q. Yin, X. Zhang, W. Zhang, H. Jia, Q. Ji, F. Yang, X. Rui, Rational design of multifunctional properties for styrene-butadiene rubber reinforced by modified Kevlar nanofibers, Compos. Part B Eng. 166 (2019) 196–203. https://doi.org/10.1016/j.compositesb.2018.11.132.

[72] J. Jung, H.A. Sodano, Aramid Nanofiber Reinforced Rubber Compounds for the Application of Tire Tread with High Abrasion Resistance and Fuel Saving Efficiency, ACS Appl. Polym. Mater. 2 (2020) 4874–4884. https://doi.org/10.1021/acsapm.0c00797.

[73] J. Jung, H.A. Sodano, Synergetic effect of aramid nanofiber-graphene oxide hybrid filler on the properties of rubber compounds for tire tread application, J. Appl. Polym. Sci. (2021) 51856. https://doi.org/10.1002/app.51856.

[74] H. Gu, S. Tadakamalla, X. Zhang, Y. Huang, Y. Jiang, H.A. Colorado, Z. Luo, S. Wei, Z. Guo, Epoxy resin nanosuspensions and reinforced nanocomposites from polyaniline stabilized multi-walled carbon nanotubes, J. Mater. Chem. C. 1 (2013) 729–743. https://doi.org/10.1039/c2tc00379a.

[75] Q. He, T. Yuan, X. Zhang, Z. Luo, N. Haldolaarachchige, L. Sun, D.P. Young, S. Wei, Z. Guo, Magnetically Soft and hard polypropylene/cobalt nanocomposites: Role of maleic

anhydride grafted polypropylene, Macromolecules. 46 (2013) 2357–2368. https://doi.org/10.1021/ma4001397.

[76]   B.A. Patterson, M.H. Malakooti, J. Lin, A. Okorom, H.A. Sodano, Aramid nanofibers for multiscale fiber reinforcement of polymer composites, Compos. Sci. Technol. 161 (2018) 92–99. https://doi.org/10.1016/j.compscitech.2018.04.005.

[77]   J. Nasser, K. Steinke, L. Zhang, H. Sodano, Enhanced interfacial strength of hierarchical fiberglass composites through an aramid nanofiber interphase, Compos. Sci. Technol. 192 (2020) 108109. https://doi.org/10.1016/j.compscitech.2020.108109.

[78]   M. Iijima, H. Kamiya, Non-aqueous colloidal processing route for fabrication of highly dispersed aramid nanofibers attached with Ag nanoparticles and their stability in epoxy matrixes, Colloids Surfaces A Physicochem. Eng. Asp. 482 (2015) 195–202. https://doi.org/10.1016/j.colsurfa.2015.05.007.

[79]   H.J. Oh, H.Y. Kim, S.S. Kim, Effect of the core/shell-structured meta-aramid/epoxy nanofiber on the mechanical and thermal properties in epoxy adhesive composites by electrospinning, J. Adhes. 90 (2014) 787–801. https://doi.org/10.1080/00218464.2013.843458.

[80]   S.Y. On, M.S. Kim, S.S. Kim, Effects of post-treatment of meta-aramid nanofiber mats on the adhesion strength of epoxy adhesive joints, Compos. Struct. 159 (2017) 636–645. https://doi.org/10.1016/j.compstruct.2016.10.016.

[81]   X. Xue, K. Jiang, Q. Yin, X. Zhang, W. Zhang, H. Jia, Q. Ji, Tailoring the structure of Kevlar nanofiber and its effects on the mechanical property and thermal stability of carboxylated acrylonitrile butadiene rubber, J. Appl. Polym. Sci. 136 (2019) 1–10. https://doi.org/10.1002/app.47698.

[82]   J. Fan, Z. Shi, L. Zhang, J. Wang, J. Yin, Aramid nanofiber-functionalized graphene nanosheets for polymer reinforcement, Nanoscale. 4 (2012) 7046–7055. https://doi.org/10.1039/c2nr31907a.

[83]   E. Wang, Y. Dong, M.Z. Islam, L. Yu, F. Liu, S. Chen, X. Qi, Y. Zhu, Y. Fu, Z. Xu, N. Hu, Effect of graphene oxide-carbon nanotube hybrid filler on the mechanical property and thermal response speed of shape memory epoxy composites, Compos. Sci. Technol. 169 (2019) 209–216. https://doi.org/10.1016/j.compscitech.2018.11.022.

[84]   S.H. Song, Synergistic Effect of Clay Platelets and Carbon Nanotubes in Styrene–Butadiene Rubber Nanocomposites, Macromol. Chem. Phys. 217 (2016) 2617–2625. https://doi.org/10.1002/macp.201600344.

[85]   B. Pradhan, S.K. Srivastava, Synergistic effect of three-dimensional multi-walled carbon nanotube-graphene nanofiller in enhancing the mechanical and thermal properties of high-

performance silicone rubber, Polym. Int. 63 (2014) 1219–1228. https://doi.org/10.1002/pi.4627.

[86]   C.Y. Lee, J.H. Bae, T.Y. Kim, S.H. Chang, S.Y. Kim, Using silane-functionalized graphene oxides for enhancing the interfacial bonding strength of carbon/epoxy composites, Compos. Part A Appl. Sci. Manuf. 75 (2015) 11–17. https://doi.org/10.1016/j.compositesa.2015.04.013.

[87]   Y.K. Kim, D.H. Min, Preparation of scrolled graphene oxides with multi-walled carbon nanotube templates, Carbon N. Y. 48 (2010) 4283–4288. https://doi.org/10.1016/j.carbon.2010.07.039.

[88]   X. Li, W. Nie, Y. Xu, Y. Zhou, P. Chen, C. Zhang, Functionalized GO/polysulfide rubber composites with excellent comprehensive properties based interfacial optimum design, Compos. Part B Eng. 198 (2020) 108234. https://doi.org/10.1016/j.compositesb.2020.108234.

[89]   X. Liu, W. Kuang, B. Guo, Preparation of rubber/graphene oxide composites with in-situ interfacial design, Polymer (Guildf). 56 (2015) 553–562. https://doi.org/10.1016/j.polymer.2014.11.048.

[90]   Y. Mao, S. Wen, Y. Chen, F. Zhang, P. Panine, T.W. Chan, L. Zhang, Y. Liang, L. Liu, High performance graphene oxide based rubber composites, Sci. Rep. 3 (2013) 1–7. https://doi.org/10.1038/srep02508.

[91]   P. Phanthong, P. Reubroycharoen, X. Hao, G. Xu, A. Abudula, G. Guan, Nanocellulose: Extraction and application, Carbon Resour. Convers. 1 (2018) 32–43. https://doi.org/10.1016/j.crcon.2018.05.004.

[92]   L. Bacakova, J. Pajorova, M. Bacakova, A. Skogberg, P. Kallio, K. Kolarova, V. Svorcik, Versatile application of nanocellulose: From industry to skin tissue engineering and wound healing, Nanomaterials. 9 (2019). https://doi.org/10.3390/nano9020164.

[93]   S. Singh, G.L. Dhakar, B.P. Kapgate, P.K. Maji, C. Verma, M. Chhajed, K. Rajkumar, C. Das, Synthesis and chemical modification of crystalline nanocellulose to reinforce natural rubber composites, Polym. Adv. Technol. 31 (2020) 3059–3069. https://doi.org/10.1002/pat.5030.

[94]   K. Roy, A. Pongwisuthiruchte, S. Chandra Debnath, P. Potiyaraj, Application of cellulose as green filler for the development of sustainable rubber technology, Curr. Res. Green Sustain. Chem. 4 (2021) 100140. https://doi.org/10.1016/j.crgsc.2021.100140.

[95]   Y. Park, M. You, J. Shin, S. Ha, D. Kim, M.H. Heo, J. Nah, Y.A. Kim, J.H. Seol, Thermal conductivity enhancement in electrospun poly(vinyl alcohol) and poly(vinyl alcohol)/cellulose nanocrystal composite nanofibers, Sci. Rep. 9 (2019) 1–10. https://doi.org/10.1038/s41598-019-39825-8.

[96]   X. Ni, W. Cheng, S. Huan, D. Wang, G. Han, Electrospun cellulose nanocrystals/poly(methyl methacrylate) composite nanofibers: Morphology, thermal and mechanical properties, Carbohydr. Polym. 206 (2019) 29–37. https://doi.org/10.1016/j.carbpol.2018.10.103.

[97]   W. Luo, L. Cheng, C. Yuan, Z. Wu, G. Yuan, M. Hou, J.Y. Chen, C. Luo, W. Li, Preparation, characterization and evaluation of cellulose nanocrystal/poly(lactic acid) in situ nanocomposite scaffolds for tissue engineering, Int. J. Biol. Macromol. 134 (2019) 469–479. https://doi.org/10.1016/j.ijbiomac.2019.05.052.

[98]   V. Kupka, Q. Zhou, F. Ansari, H. Tang, M. Šlouf, L. Vojtová, L.A. Berglund, J. Jančář, Well-dispersed polyurethane/cellulose nanocrystal nanocomposites synthesized by a solvent-free procedure in bulk, Polym. Compos. 40 (2019) E456–E465. https://doi.org/10.1002/pc.24748.

[99]   A. Li, Z. Xu, N. Sun, Z. Si, Y. Xu, X. Guo, Cellulose-reinforced catechol-modified polyacrylic acid-Zn2+ coacervate as strong composite adhesive, J. Appl. Polym. Sci. 136 (2019) 3–9. https://doi.org/10.1002/app.47126.

[100]   J.-S. Kang, A.J. Myles, K.D. Harris, Thermally-Degradable Thermoset Adhesive Based on a Cellulose Nanocrystals/Epoxy Nanocomposite, ACS Appl. Polym. Mater. (2020). https://doi.org/10.1021/acsapm.0c00698.

[101]   L. Lin, N. Ecke, S. Kamerling, C. Sun, H. Wang, X. Song, K. Wang, S. Zhao, J. Zhang, A.K. Schlarb, Study on the impact of graphene and cellulose nanocrystal on the friction and wear properties of SBR/NR composites under dry sliding conditions, Wear. 414–415 (2018) 43–49. https://doi.org/10.1016/j.wear.2018.07.027.

[102]   Z. Guo, D. Guo, F. Liu, H. Wang, J. Song, Aramid nanofiber reinforced nitrile rubber assisted by cellulose nanocrystals, J. Appl. Polym. Sci. (2021). https://doi.org/10.1002/app.50546.

[103]   J. Nasser, J. Lin, K. Steinke, H.A. Sodano, Enhanced interfacial strength of aramid fiber reinforced composites through adsorbed aramid nanofiber coatings, Compos. Sci. Technol. 174 (2019) 125–133. https://doi.org/10.1016/j.compscitech.2019.02.025.

[104]   P.J. Flory, J. Rehner, Statistical mechanics of cross-linked polymer networks II. Swelling, J. Chem. Phys. 11 (1943) 521–526. https://doi.org/10.1063/1.1723792.

[105]   Y.H. Zhan, G.Q. Liu, H.S. Xia, N. Yan, Natural rubber/carbon black/carbon nanotubes composites prepared through ultrasonic assisted latex mixing process, Plast. Rubber Compos. 40 (2011) 32–39. https://doi.org/10.1179/174328911X12940139029284.

[106]   Y. Nakaramontri, C. Nakason, C. Kummerlöwe, N. Vennemann, Enhancement of Electrical Conductivity and Filler Dispersion of Carbon Nanotube Filled Natural Rubber

Composites By Latex Mixing and in Situ Silanization, Rubber Chem. Technol. 89 (2016) 272–291. https://doi.org/10.5254/rct.15.84848.

[107] E. Cichomski, W.K. Dierkes, T. V. Tolpekina, S. Schultz, J.W.M. Noordermeer, Influence of physical and chemical polymer-filler bonds on tire wet-traction performance indicators for passenger car tire tread materials, KGK Kautschuk Gummi Kunststoffe. 67 (2014) 50–57.

[108] R.R. Rahalkar, Dependence of wet skid resistance upon the entanglement density and chain mobility according to the rouse theory of viscoelasticity, Rubber Chem. Technol. 62 (1989) 246–271. https://doi.org/10.5254/1.3536243.

[109] G. Heinrich, Hysteresis friction of sliding rubbers on rough and fractal surfaces, Rubber Chem. Technol. 70 (1997) 1–13. https://doi.org/10.5254/1.3538415.

[110] J.B. Donnet, Black and white fillers and tire compound, Rubber Chem. Technol. 71 (1998) 323–341. https://doi.org/10.5254/1.3538488.

[111] J. Han, X. Zhang, W. Guo, C. Wu, Effect of modified carbon black on the filler-elastomer interaction and dynamic mechanical properties of SBR vulcanizates, J. Appl. Polym. Sci. 100 (2006) 3707–3712. https://doi.org/10.1002/app.23233.

[112] B. Seo, J. Kang, S. Jang, Y. Kang, W. Kim, Characteristics of styrene-butadiene rubber/silica/nanoprene compounds for application in tire tread, J. Nanosci. Nanotechnol. 13 (2013) 2179–2188. https://doi.org/http://dx.doi.org/10.1166/jnn.2013.7088.

[113] N. Natchimuthu, AFM studies on silica dispersion in EPDM rubber, Rubber Chem. Technol. 83 (2010) 123–132. https://doi.org/10.5254/1.3548270.

[114] K. Cao, C.P. Siepermann, M. Yang, A.M. Waas, N.A. Kotov, M.D. Thouless, E.M. Arruda, Reactive aramid nanostructures as high-performance polymeric building blocks for advanced composites, Adv. Funct. Mater. 23 (2013) 2072–2080. https://doi.org/10.1002/adfm.201202466.

[115] J. Lin, S.H. Bang, M.H. Malakooti, H.A. Sodano, Isolation of Aramid Nanofibers for High Strength and Toughness Polymer Nanocomposites, ACS Appl. Mater. Interfaces. 9 (2017) 11167–11175. https://doi.org/10.1021/acsami.7b01488.

[116] J. Zhu, H. Peng, F. Rodriguez-Macias, J.L. Margrave, V.N. Khabashesku, A.M. Imam, K. Lozano, E. V. Barrera, Reinforcing epoxy polymer composites through covalent integration of functionalized nanotubes, Adv. Funct. Mater. 14 (2004) 643–648. https://doi.org/10.1002/adfm.200305162.

[117] P.C. Ma, N.A. Siddiqui, G. Marom, J.K. Kim, Dispersion and functionalization of carbon nanotubes for polymer-based nanocomposites: A review, Compos. Part A Appl. Sci. Manuf. 41 (2010) 1345–1367. https://doi.org/10.1016/j.compositesa.2010.07.003.

[118] P.C. Ma, S.Y. Mo, B.Z. Tang, J.K. Kim, Dispersion, interfacial interaction and re-agglomeration of functionalized carbon nanotubes in epoxy composites, Carbon N. Y. 48 (2010) 1824–1834. https://doi.org/10.1016/j.carbon.2010.01.028.

[119] N. Rasana, K. Jayanarayanan, B.D.S. Deeraj, K. Joseph, The thermal degradation and dynamic mechanical properties modeling of MWCNT/glass fiber multiscale filler reinforced polypropylene composites, Compos. Sci. Technol. 169 (2019) 249–259. https://doi.org/10.1016/j.compscitech.2018.11.027.

[120] K. Jayanarayanan, N. Rasana, R.K. Mishra, Dynamic Mechanical Thermal Analysis of Polymer Nanocomposites, Elsevier Inc., 2017. https://doi.org/10.1016/B978-0-323-46139-9.00006-2.

[121] G. Chen, M. Wei, J. Chen, J. Huang, A. Dufresne, P.R. Chang, Simultaneous reinforcing and toughening: New nanocomposites of waterborne polyurethane filled with low loading level of starch nanocrystals, Polymer (Guildf). 49 (2008) 1860–1870. https://doi.org/10.1016/j.polymer.2008.02.020.

[122] X. Zhang, L.S. Loo, Study of glass transition and reinforcement mechanism in polymer/layered silicate nanocomposites, Macromolecules. 42 (2009) 5196–5207. https://doi.org/10.1021/ma9004154.

[123] P.P. Vijayan, D. Puglia, J.M. Kenny, S. Thomas, Effect of organically modified nanoclay on the miscibility, rheology, morphology and properties of epoxy/carboxyl-terminated (butadiene-co- acrylonitrile) blend, Soft Matter. 9 (2013) 2899–2911. https://doi.org/10.1039/c2sm27386a.

[124] Y.Q. Rao, J.M. Pochan, Mechanics of polymer-clay nanocomposites, Macromolecules. 40 (2007) 290–296. https://doi.org/10.1021/ma061445w.

[125] J.M.G. Cowie, Polymers: Chemistry and Physics of Modern Materials, 2nd Ed., Blackie Academic & Professional, 1991.

[126] S.B. Jagtap, V.S. Rao, S. Barman, D. Ratna, Nanocomposites based on epoxy resin and organoclay functionalized with a reactive modifier having structural similarity with the curing agent, Polymer (Guildf). 63 (2015) 41–51. https://doi.org/10.1016/j.polymer.2015.02.038.

[127] S. Stankovich, D.A. Dikin, R.D. Piner, K.A. Kohlhaas, A. Kleinhammes, Y. Jia, Y. Wu, S.B.T. Nguyen, R.S. Ruoff, Synthesis of graphene-based nanosheets via chemical reduction of exfoliated graphite oxide, Carbon N. Y. 45 (2007) 1558–1565. https://doi.org/10.1016/j.carbon.2007.02.034.

[128] M. Lian, J. Fan, Z. Shi, H. Li, J. Yin, Kevlar®-functionalized graphene nanoribbon for polymer reinforcement, Polymer (Guildf). 55 (2014) 2578–2587. https://doi.org/10.1016/j.polymer.2014.03.059.

[129] J.E. Baer, M. Carmack, The Ultraviolet Absorption Spectra of Aliphatic Sulfides and Polysulfides, J. Am. Chem. Soc. 71 (1949) 1215–1218. https://doi.org/10.1021/ja01172a022.

[130] J. Jung, H.A. Sodano, Aramid Nanofiber Reinforced Rubber Compounds for the Application of Tire Tread with High Abrasion Resistance and Fuel Saving Efficiency, ACS Appl. Polym. Mater. (2020). https://doi.org/10.1021/acsapm.0c00797.

[131] C.K. Hong, H. Kim, C. Ryu, C. Nah, Y. Il Huh, S. Kaang, Effects of particle size and structure of carbon blacks on the abrasion of filled elastomer compounds, J. Mater. Sci. 42 (2007) 8391–8399. https://doi.org/10.1007/s10853-007-1795-3.

[132] X. Cao, C. Xu, Y. Liu, Y. Chen, Preparation and properties of carboxylated styrene-butadiene rubber/cellulose nanocrystals composites, Carbohydr. Polym. 92 (2013) 69–76. https://doi.org/10.1016/j.carbpol.2012.09.054.

[133] C. Thulluri, R. Balasubramaniam, H.R. Velankar, Generation of highly amenable cellulose-Iβ via selective delignification of rice straw using a reusable cyclic ether-assisted deep eutectic solvent system, Sci. Rep. 11 (2021). https://doi.org/10.1038/s41598-020-80719-x.

[134] K.K. Sadasivuni, A. Kafy, L. Zhai, H.U. Ko, S. Mun, J. Kim, Transparent and flexible cellulose nanocrystal/reduced graphene oxide film for proximity sensing, Small. 11 (2015) 994–1002. https://doi.org/10.1002/smll.201402109.

[135] C. Chang, A. Lue, L. Zhang, Effects of crosslinking methods on structure and properties of cellulose/PVA hydrogels, Macromol. Chem. Phys. 209 (2008) 1266–1273. https://doi.org/10.1002/macp.200800161.

[136] B. Yang, L. Wang, M. Zhang, J. Luo, X. Ding, Timesaving, High-Efficiency Approaches To Fabricate Aramid Nanofibers, ACS Nano. (2019). https://doi.org/10.1021/acsnano.9b02258.

[137] M. Chen, J. Parot, V.A. Hackley, S. Zou, L.J. Johnston, AFM characterization of cellulose nanocrystal height and width using internal calibration standards, Cellulose. 0 (2021). https://doi.org/10.1007/s10570-021-03678-0.